EXCITON DIFFUSION AND ELECTRON TRANSFER OF PLATINUM- ACETYLIDE POLYMERS AND THEIR SOLID STATE PHOTOPHYSICS

By

HSIEN-YI HSU

A DISSERTATION PRESENTED TO THE GRADUATE SCHOOL
OF THE UNIVERSITY OF FLORIDA IN PARTIAL FULFILLMENT
OF THE REQUIREMENTS FOR THE DEGREE OF
DOCTOR OF PHILOSOPHY

UNIVERSITY OF FLORIDA

2014

To my beautiful wife Hsiao-Yu

ACKNOWLEDGEMENTS

I would like to thank my wife Hsiao-Yu for all of her love, support, and encouragement over the entirety of my graduate career. She has been overly supportive of every career and life choice I have made and I am certain I would not have made it through this program without her love and support.

I must express my deepest gratitude to my advisor, Prof. Kirk Schanze for the immeasurable amount of support and guidance he has provided throughout this study. He introduced me into this exciting research area and taught me from the design of materials to laser spectroscopic techniques and photophysics of molecules. His knowledge, insight, enthusiasm and dedication to scientific research have been a constant inspiration for me.

I would like to thank my committee members, Prof. Alexander Angerhofer, Prof. Valeria D. Kleiman, Prof. Gail E. Fanucci, and Prof. James F. Klausner, for their time and support. I would especially like to thank Prof. Kleiman for her teaching because I learned all the quantum mechanics from her lectures, as well as discussion with her outside the classroom. I extend my thankfulness to Prof. Omar F. Mohammed Abdelsaboor from King Abdullah University of Science and Technology (KAUST) for his contribution in the ultrafast laser spectroscopic measurements.

Lastly, I would like to thank all the former and current members of Schanze group who have helped and contributed to my projects. Especially, I appreciate helps from Dr. Randi Sue Price, including but not limited to teaching me the basics of photophyscs and operation of the spectrometers, and working with me side by side during the early stage of my research. I would like to take time to thank my collaborators who made many contributions to my thesis projects. Dr. Jarrett H. Vella conducted time-of-flight (TOF)

measurements. Dr. Zhuo Chen synthesized polymers and model compounds presented in Chapter 4. I would also like to warmly thank Dr. Anand Parthasarathy, Dr. Galyna Dubinina, Dr. Gyu Leem, Dr. Xiangli Meng, Subahdip Goswami, Ali Gundogan, Russ Winkel, Zhengxing Pan, Junlin Jiang, Shanshan Wang, Seda Cekli, Jiliang Wang, Yun Huang, Austin Jones, Yajing Yang and Bethy Kim for their valuable advice and friendship.

TABLE OF CONTENTS

LIST OF TABLES

LIST OF FIGURES

LIST OF ABBREVIATIONS

Acac	Acetoacetate
AFM	Atomic force microscopy
ATRP	Atom transfer radical polymerization
Ar	Argon
BHJ	Bulk heterojunctions
Bpy	Bypyridine
BTD	4,7-Dibromobenzothiadiazole
CCD	Charge-coupled device
$CDCl_3$	Deuterated chlorofo
CPs	Conjugated polymers
CuBr	Copper(I) boromide
CuI	Copper(I) iodide
Cz	3,6-Carbazole
DIPA	Diiospropylamine
DMF	Dimethyl fomamide
DNA	Deoxyribonucleic acid
DP	Degree of polymerization
DSB	Distyrylbenzene
DSSC	Dye-sensitized solar cell
EF-TEM	Energy filtered transmission electron microscopy
ESA	Excited-state absorption
EXAFS	extended X-ray absorption fine structure
FC	Frank-Condon
FRET	Förster resonance energy transfer

FTIR	Fourier transform infrared spectroscopy
FTO	Fluorine-doped tin(IV) oxide
GPC	Gel permeation chromatography
GSB	Ground-state bleaching
HPLC	High-performance liquid chromatography
HOMO	Highest occupied molecular orbital
IC	Internal coversion
IPCE	Internal photon to current efficiency
iPr_2NH	Diisopropylamine
ISI	Intersystem crossing
ITO	Indium tin oxide
LEDs	Light-emitting devices
LUMO	Lowest unoccupied molecular orbital
MD	Molecular dynamics
MLCT	Metal to ligand charge transfer
MMLCT	Metal–metal to ligand charge transfer
MP	Metallophorphyrins
MW	Molecular weight
MWD	Molecular weight distribution
NDI	Naphthalene diimides
NMR	Resonance
OLED	Organic light-emitting devices
OPE	Oligo(phenylene ethynylene)
OPVs	Organic photovoltaic cells
PAEs	Poly(arylene ethynylene)s

PCBM	Phenyl-C61-butyric acid methyl ester
P3HT	Poly(3-hexylthiophene)
PDA	Photodioide array
PDI	Polydispersity index
PET	Photoinduced electron transfer
PF	Polyfluorene
PFP	Petafluorephenyl
Ph	Phenylene
PL	Photoluminescence
PLEDs	Polymer light-emitting devices
PMDETA	N,N,N′,N″,N″-pentamethyldiethylenetriamine
PMMA	Poly(methyl methacrylate)
PMT	Photomultiplier tube
PPE	Poly(phenylacetylene)
PVBA	Poly(4-vinylbenzyl azide)
PVBC	Poly(4-vinylbenzyl chloride)
Py	Pyrene
RAFT	Reverse addition-fragmentation transfer
SDS	Dodecylsulfate
SE	Stimulated emission
SEM	Scanning electron microscopy
TA	Transient absorption
TBAF	Tetrabutyl ammonium fluoride
TCSPC	Time-correlated single photon counting
TFA	Trifluoroacetic acid

Th	Thiophene
THF	Tetrahydrofuran
TIPSA	Trisisopropylsilyl acetylene
TMS	Tetramethylsilane
XPS	X-ray photoelectron

Abstract of Dissertation Presented to the Graduate School
of the University of Florida in Partial Fulfillment of the
Requirements for the Degree of Doctor of Philosophy

EXCITON DIFFUSION AND ELECTRON TRANSFER OF PLATINUM- ACETYLIDE POLYMERS AND THEIR SOLID STATE PHOTOPHYSICS

By

Hsien-Yi Hsu

August 2014

Chair: Kirk S. Schanze
Major: Chemistry

Up till now, the photophysical properties of conjugated polymers have been studied extensively. However, there are relatively few reports about the similar properties of triplet states in these systems. Hence, we investigated the photophysics of triplet exciton in platinum containing PPEs, which are often called Pt-acetylides. The main target is to analyze the vital mechanisms, such as energy transfer and electron transfer. According to these fundamental photophysics, we can improve the performance of electronic and optoelectronic devices effectively.

First, a series of conjugated and conjugation-interrupted platinum acetylide polymers were studied. We find that the conjugated polymers absorbed at lower energies than the conjugation interrupted polymers. According to the experimental photophysical results of conjugated and conjugation-interrupted platinum phenyl-thiophene copolymers, the mechanisms of singlet energy transfer and triplet energy transfer take place at room temperature in the conjugated copolymers; the exciton may not transport to a lower energy trap effectively while the π-conjugation structure is interrupted with methylene spacer.

Second, a series of conjugated and conjugation-interrupted platinum acetylide polymer films were spin-coated and doped with varying amounts of acceptors. The thin film acceptor concentration was related to the donor exciton quenching rate constant, which is a manifestation of the triplet exciton diffusion coefficient. The estimated triplet exciton length of diffusion and diffusion coefficient, validated against literature-based time-of-flight measurements. Also, an enhanced triplet diffusion coefficient in the conjugated polymer is found as a result of lower activation energy.

Third, the graft copolymers with a polystyrene backbone and pedant poly-platinums were prepared. The different Pt acetylides in poly-platinums act as triplet energy donor and acceptor. Photoluminescence spectroscopy and transient absorption spectroscopy were applied to study the energy transfer in these macromolecular triplet donor-acceptor systems. The results indicate that triplet-triplet energy transfer between platinum acetylides is highly efficient.

Four, relatively efficient photovoltaic devices were fabricated using blends of a platinum–acetylide thiophene polymer and a fullerene (PCBM) because photoinduced charge transfer contributed to the device efficiency. In order to explore the photophysical behaviors in solid state, the platinum–acetylide thiophene polymer films are monitored by UV-Vis absorption, photoluminescence, time-resolved transient absorption and fluorescence upconversion.

CHAPTER 1
INTRODUCTION

Conjugated Polymers

The backbone of conjugated polymers consists of atoms with a continuous π orbital system. Polyacetylene, which was reported in 1977, can exhibit significant conductivity when oxidation or reduction occurs.[1] Generally, most electrically conducting polymers belong to the larger class of conjugated polymers (CPs). In conjugated polymers, the π-cloud of one monomer is in conjugation with all other repeat units around it. This extended conjugation lowers the energy necessary to promote an electron from the highest occupied molecular orbital (HOMO) to the lowest unoccupied molecular orbital (LUMO) of the conjugated units.

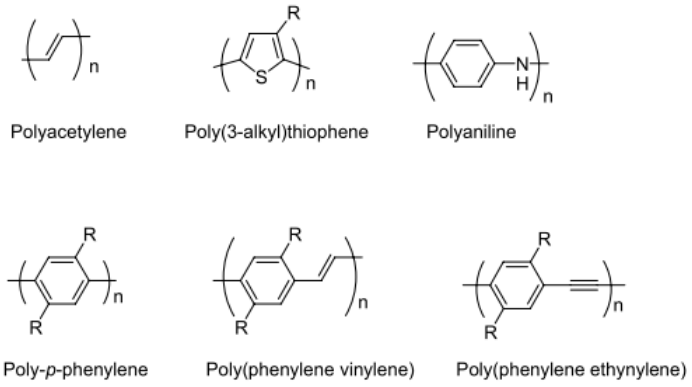

Figure 1-1. Examples of conjugated polymer structures.[1]

In 2000, when the leading inventors of conductive polymers, H[1]eeger, MacDiarmid, and Shirakawa, were awarded the Nobel Prize in Chemistry, they attracted extensive worldwide attention in this field. To date, conjugated polymers have been applied to a wide range of commercial needs, even since the incipience of this conductive property in 1977. A wide array of structures of conjugated polymers has

---

This Chapter is considered for publication in the Journal of the American Chemical Society.

been reported, and several of these are shown in Figure 1-1. These macromolecules feature aromatic or heteroaromatic rings that are connected either directly or via conjugated vinyl or ethynyl linkers, excluding polyacetylene.[1]

Poly(arylene ethynylene)s (PAEs) are one of the most valuable categories of conjugated polymers. PAEs feature aromatic or heteroaromatic rings containing ethynyl linkages.[2] Until now the most popular kind of PAEs are poly(phenylene ethynylene)s (PPEs), where the aromatic group is a benzene ring. Enormous benefits can be found in PPEs, which may bear a great variety of functional group substituents. Platinum polyynes are another considerable category of PPEs. Their photophysics is dominated by long-lived phosphorescent excited states.[3] This property makes them promising possible materials for the fabrication of electro-luminescent devices,[4] and for applications in optical limiting.[5] Platinum polyyne, which is presented in Figure 1-2, is the common structure. These materials comprise sp hybridized alkyne carbons which connect bis(trialkylphosphine)platinum (II) with phenylene rings. When the aromatic rings are not substituted, good solubility in organic solvents can be achieved by using butyl or longer alkyl groups.

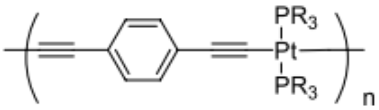

Figure 1-2. General structure of a platinum containing PPE.

The Hagihara coupling reaction, which was discovered in 1978, is applied to the synthesis of platinum polyyne.[6] In the presence of an amine, the chlorine on a bis(trialkyl-phosphine) platinum (II) chloride is substituted by Cu(I) catalyst. The acetylene, which forms a copper acetylide upon reaction with the Cu(I) catalyst, is

deprotonated by the amine. Then the activated acetylide substitutes chloride forming the platinum-carbon bond. The reaction can also be found without a catalyst, but the product is only mono-substituted in this situation.[7] Thus the polymers cannot be made under catalyst-free conditions, but these conditions are still workable for the synthesis of oligomeric platinum containing PPEs.[8]

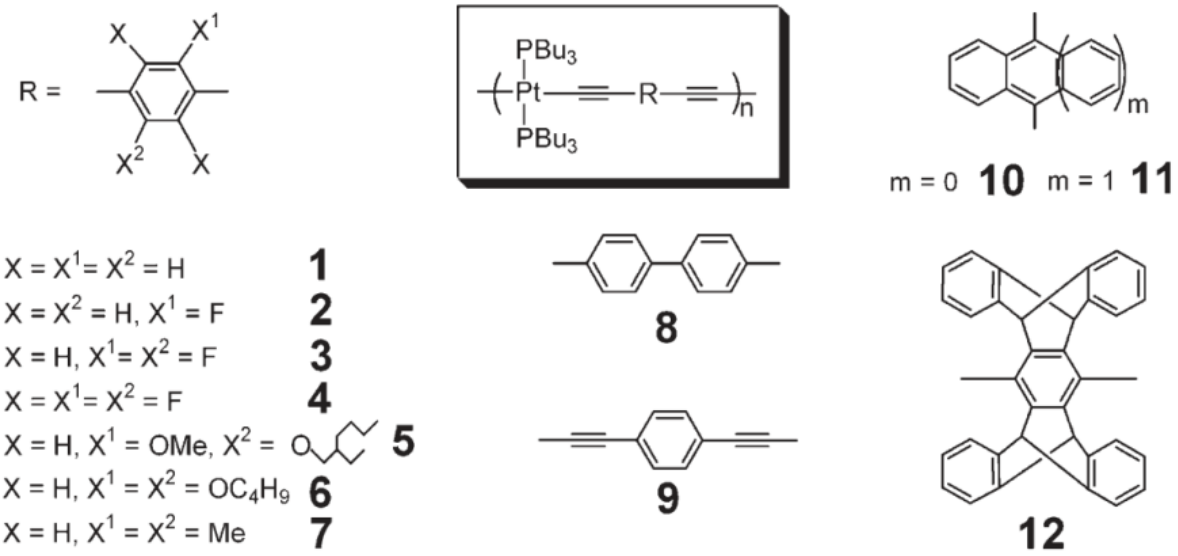

Figure 1-3. Structure of Pt-polyyne polymers with various aryl groups.[9-14]

The photophysical properties of platinum polyynes have been studied systematically. The common structure of the polymers is trans-(bis(trialkylphosphine) platinum (II)-R)$_n$ where R is a conjugated group, including phenylene, thiophene, biphenyl, fluorene, carbazole, quinone derivative, and metallopor-phyrin residue (Figure 1-3). The phosphine ligands are usually triethyl- or tri-n-butylphosphine groups. Polymers 1 –12 were investigated by different research groups (Figure 1-3). Lewis et. al. demonstrated that Pt polyyne 1 is a successful model system for the study of triplet excitons in conjugated polymers.[15] The heavy metal atom can promote spin-forbidden $S_0 \rightarrow T_1$ processes by mixing the singlet and triplet wave functions, thus making

radiative and nonradiative decay from the triplet excited states. The absolute ISC efficiency of 1, which is reported by Wittmann, is almost equal to 1 at about 16 K.[16] From the investigated results of transition energies' dependence on chain length, triplet excited state remains highly confined between two platinum moieties due to the invariance of the phosphorescence with respect to increasing chain length. It was confirmed that the singlet states are more delocalized than the triplet states. Organometallic Pt polyynes is also one of the most potential materials for nonlinear optics applications based on the studies of 1 and 7.[10]

Wong's group has studied the synthesis and optical and structural properties of another platinum (II) polyyne-containing biphenyl moiety 8.[11] They mentioned that the two phenyl rings are twisted slightly due to the intrachain rotation in the biphenyl structure. This phenomenon can be proved by the X-ray structure of its model complex, as shown in Figure 1-4. The conjugated structure may be partially destroyed by the twisted conformation ($\Theta = 21.5^{o}$).

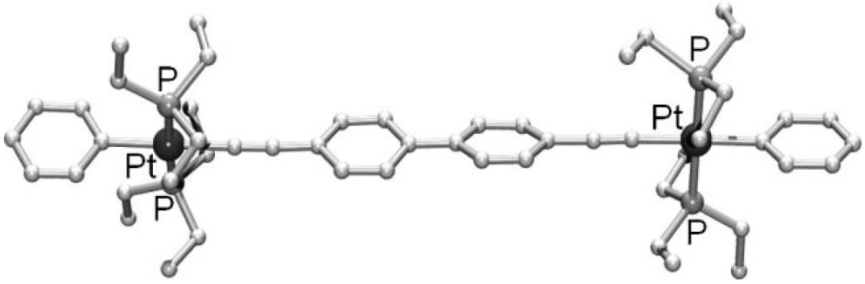

Figure 1-4. X-ray structure of the model complex of 8. This figure was adopted from Liu.[11]

Pt polyynes with substituted 1,4-diethynylbenzene derivatives 2, 3, and 4 were synthesized and studied with various optical spectroscopies.[12] Khan's group mentioned that the thermal stability is dependent on the degree of fluorination for Pt polyynes with fluorinated benzenes. The relative intensity of phosphorescence increases strongly with

the fluorine content. Pt polyyne 5 with alkoxy chains, which can favor stronger interchain van der Waals interactions, has a high thermal decomposition temperature.

In order to control the self-assembly into larger structures and develop the performance of these materials, we must consider the molecular orientation of the nanostructured metallopolymers as the materials are deposited on solid substrates. The surface morphologies of 6 and 8 were analyzed by scanning electron microscopy (SEM), energy filtered transmission electron microscopy (EF-TEM), X-ray photoelectron (XPS), and extended X-ray absorption fine structure (EXAFS) spectroscopies.[17,18] The results of their nanostructures revealed that the ropes were oriented on the solid surface of 8, but the chains of 6 tended to self-organize into columnar nanosized structures. Pt polyynes with the organic spacer naphthalene 10 and anthracene 11 are prepared and characterized. While the phosphorescence of 10 was weak, that of 11 was almost undetectable even at low temperature. And the phosphorescence of 11 thin films cannot be detected at all. As the delocalization in the aromatic group increases, the transition between HOMO–LUMO and the energy gap of $T_1 \rightarrow S_0$ decrease (1: 2.90 eV; 10: 2.80 eV; 11: 2.35 eV; Figure 1-5). This is in agreement with an increase in donor–acceptor interaction between the Pt center and the electron-rich conjugated ligand in going from benzene, through naphthalene to anthracene. The bands of absorption and emission were red-shifted when the number of C≡C units on each side of the benzene ring (i.e., 1 vs 9) was doubling. The effect of aggregation or interchain interaction on the triplet excited state in Pt-acetylide materials was also studied by Schanze's group. The photophysical properties of Pt polyyne 1 was compared to that of Pt polyyne 12 with the

pentiptycene unit.[14] They found low-lying excitations appeared from metal–metal to ligand charge transfer (MMLCT) because of interchain Pt–Pt interactions.

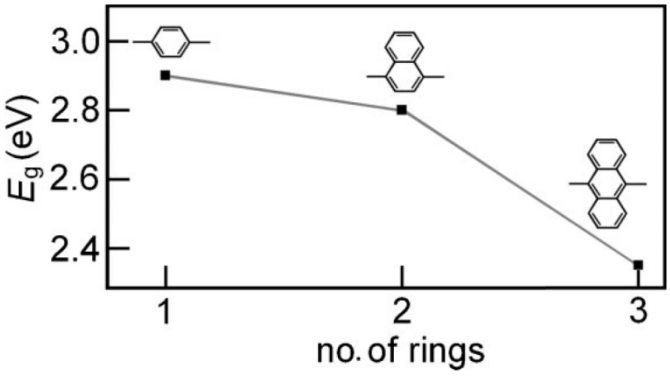

Figure 1-5. Effect of spacer ring size on E g in various metallopolyyne systems, 1, 10 and 11. This figure was adopted from Wong.[19]

Photophysical Processes of Conjugated Polymers

Conjugated polymers can interact with light from the near-UV region to the near-IR region since π electron clouds of the repeat units are extended in the polymer chain. It is possible that the photon will be absorbed by the material as an incident photon ($h\nu$) interacts with the polymer. Nevertheless, it will appear only when the reaction followed the second law of photochemistry, the Stark-Einstein law, which states that for every quantum of radiation that is absorbed, one molecule of the substance reacts. The Stark-Einstein law is also sometimes called the photochemical equivalence law. After photoexcitation from the ground state to a higher excited state, the excited state will stay in higher energy states until the relaxation processes happen. Molecules or parts of molecules that absorb light strongly in the UV-vis region are called chromophores, which is the part of a molecule responsible for its color, and the color arises when a molecule absorbs certain wavelengths of visible light and transmits or reflects others.

A compact working exemplar for the intermolecular photophysical processes related to the absorption of a photon by a chromophore are provided by a state energy diagram. This energy diagram is sometimes referred to as Jablonski diagram in honor of Aleksander Jablonski, a Polish physicist who used a schematic portrayal of the relative portions of the electronic and vibrational levels of R and *R without any attempt to indicate the relative nuclear geometries, as illustrated in Figure 1-6.[20] In the beginning, after the molecule absorbs a photon of appropriate energy, the vibronically excited level of electronic singlet state, S_1, is reached immediately from lowest vibronic level of electronic ground state, S_0. The absorption process is rapid, with rates typically in the range of 10^{14}-10^{16} s^{-1}. The molecule can be excited to one of several vibrational levels within the S_1 state, which is dependent on the photon's energy. The lowest vibronic level of electronic state S_1 is reached after the transfer of vibrational energy to the solvent and solvent reorganization. Chromophores can also be promoted to the vibronically excited level of higher energy electronic singlet states, S_2 -S_n. The higher excited states can be produced using a laser system, which is a device that emits light through a process of optical amplification based on the stimulated emission of electromagnetic radiation.

For the lowest singlet excited states, some possible pathways in the absence of external forces are described as following: decay to S_0 or intersystem crossing to vibronically excited level of first excited triplet state, T_1. Vibronically excited level of electronic ground state S_0 is reached by emission of fluorescence (process F in Figure 1-6), or nonradiatively by internal conversion. When fluorescence occurs, the singlet excited molecule relaxes to the vibronically excited level of the electronic ground state;

in this radiative process, the energy of the emitted photon is different from that of the absorbed photon. When the emitted photon has less energy than the absorbed photon, this energy difference is referred to as a Stokes shift. In addition to radiative fluorescence, the singlet state can also return to electronic ground state nonradiatively, usually with rates of 10^{10}-10^{11} s^{-1}. In this singlet nonradiaitve pathway, the singlet excited state, S_1, is losing its energy by the loss of heat energy. An alternative pathway for a molecular in the lowest singlet excited state is to cross over into the vibronically excited level of electronic triplet state, T_1; then the system relaxes rapidly into the lowest vibronic level of triplet excited state, T_1. This radiationless process is called intersystem crossing (ISC).

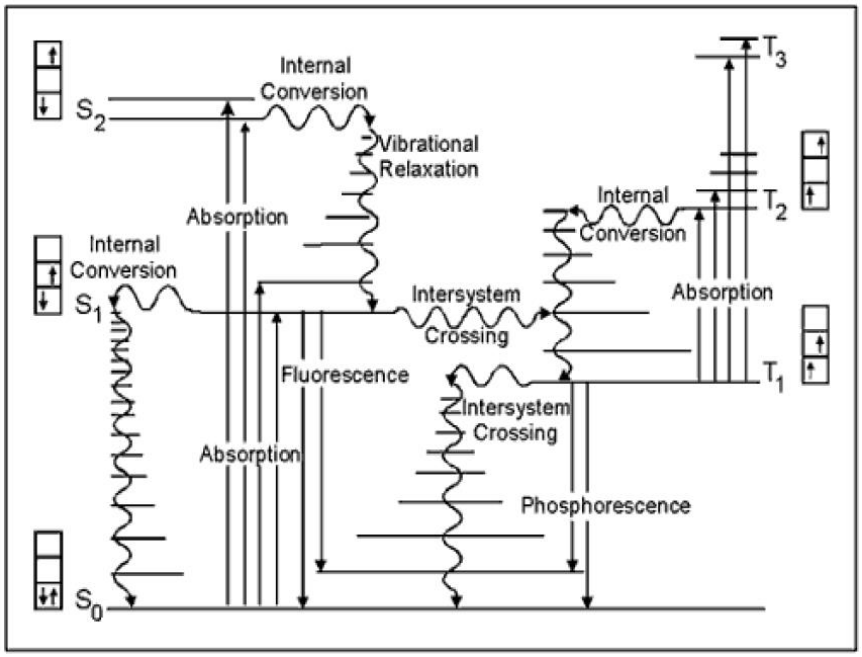

Figure 1-6. Jablonski diagram illustrating the electronic states of a molecule and the transitions between them. The photophysical processes include absorption, internal conversion, singlet decay, intersystem crossing, and triplet decay.[21]

The electron spins of a singlet exicted state electronic state are paired. The paired spin of the excited electron is still the same with the ground state electron due to

the Pauli exclusion principle, which states a pair of electrons in the same energy level must have opposite spins, as shown in Figure 1-7. The electron spins of a triplet excited state are parallel (same spin), as illustrated in Figure 1-7. Because excitation to a triplet state is a quantum mechanically forbidden process, it is less probable that a triplet state will form when the molecule absorbs radiation. The spin-flip process in the radiative process from T_1 to S_0 thus happens relatively slowly, with rates in the range of 10^6-10^8 s^{-1}.

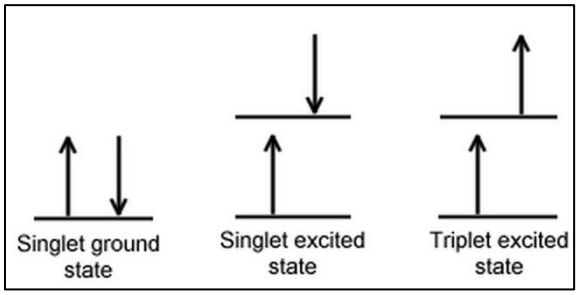

Figure 1-7. Singlet and triplet energy levels.

According to the classical theory of the interaction of light with molecules, the terms “spin-allowed” and “spin-forbidden can be clarified. The oscillator strength (f) to understand the “allowance” or strength of radiative transition are able to be measured. The relationships of f, ε and $\bar{\upsilon}$ in Equation (1-1) can be applied to estimate f.

$$f = \int \varepsilon \, d\bar{\upsilon} \sim \varepsilon_{max} \, \Delta\bar{\upsilon}_{1/2} \qquad (1\text{-}1)$$

In Equation (1-1), ε is the experimental extinction coefficient and $\bar{\upsilon}$ is the energy of the absorption, which is given in units of 1/λ, typically in reciprocal centimeters cm^{-1}, termed wavenumbers. ε_{max} is the value of ε at the absorption maximun and $\Delta\bar{\upsilon}_{1/2}$ is the width of the absorption band at a value of ½ ε_{max} in wavenumber units. Generally, the strongest “spin-allowed” transitions (f~1) correspond to the value of ε_{max} on the order

of 10^4–10^5. By contrast, the "spin-forbidden" transitions ($f \sim 10^{-7}$) correspond to value of ε_{max} on the order of 10^{-1}–10^{-2}.

For spin-allowed transition, the probability of absorption and emission can be affected by a certain degree of forbiddenness. If we consider a perfectly allowed transition as having an oscillator strength f_{max} = 1.0, then we consider an observed measured f_{obs} value in terms of the product of the individual "forbiddenness factors" f_i, which reduce the value of f_{max} from that of the ideal system, Equation (1-2):

$$f_{obs} = (f_e \times f_v \times f_s) f_{max} \tag{1-2}$$

where is $f_e$the prohibition due to electronic factors, f_v is the prohibition duo to vibrational factors, and f_s is the prohibition due to spin factors. For a spin-allowed transition, f_s = 1 , and for a spin-forbidden transition, f_s depends on the spin-orbit coupling during the transition.

With regard to the spin-orbit coupling, the matrix element for spin-orbit coupling in zero-order approximation is $\langle \psi_1 | \mathrm{H}_{SO} | \psi_2 \rangle$, where H_{SO} is the operator for spin-orbit coupling and $\psi_1$and ψ_2 are the initial and final orbitals involved, respectively. Spin-orbit coupling is the interaction between the magnetic moment (μ_S) due to the electron's spin angular momentum (S) and the magnetic moment (μ_L) due to the electron's orbital angular momentum (L), as shown in Equation (1-3). ζ_{SO} is the spin-orbit coupling constant and is related to nuclear charge. The magnitude of the spin-orbit coupling (E_{SO}) is represented by a matrix element, Equation (1-4). The magnitude of the spin-orbit coupling constant for organic compounds with light atoms (e. g., C, H and O) is much smaller (~ 0.01 – 0.1 kcal mol^{-1}), but the magnitude of the spin-orbit coupling constant for the compound with heavy atoms (e. g., Br, Hg and Pt) can be large. In general, the

dependence on spin-orbit coupling for atoms is proportional to Z^4.Thus, heavy atom effect can enhance spin-orbit coupling to accelerate the rate of intersystem crossing to ≥ 10^9 s^{-1}.[22]

$$\mathrm{H}_{SO} = \zeta_{SO}\, \mathrm{S}\, \mathrm{L} \sim \zeta_{SO}\, \mu_S\, \mu_L \tag{1-3}$$

$$E_{SO} = \langle \psi_1 | \mathrm{H}_{SO} | \psi_2 \rangle = \langle \psi_1 | \zeta_{SO}\, \mathrm{S}\, \mathrm{L}\, | \psi_2 \rangle \sim \langle \psi_1 | \zeta_{SO}\, \mu_S\, \mu_L\, | \psi_2 \rangle \tag{1-4}$$

The triplet excited states can be produced by undergoing intersystem crossing. In a similar way to singlets, the lowest vibrational state of the lowest energy triplet state, T_1, reached by internal conversion. Furthermore, higher triplet excited states (T_2-T_n) are also accessible, but they are not reached by common light sources. T_2-T_n states can be populated using a much intensive laser source. Also, the T_1 state can relax radiatively or nonradiatively. The radiative decay from an excited triplet state back to a singlet state is known as phosphorescence. The rate of phosphorescence is in the range of 10-10^6 s^{-1}, the slowest forms of relaxation, because of the occurrence of intersystem crossing again.[22]

Ground and Excited State Molecular Interactions

Ground state intermolecular interactions can be monitored by the spectral changes in the absorption spectra. Intermolecular and intramolecular excited state interactions indicate the energy and electron transfer in the excited states of systems, such as excimers, dimers or oligomers. Photoinduced energy and electron transfer can be investigated by the rate of the interactions. There are various deactivation pathways of the excited states, including fluorescence decay, phosphorescence decay, thermal deactivation processes, electron or energy transfer and photochemical relaxation pathways. The exciton will transfer from donor to acceptor in the vicinity of an excited

donor. The excited donor deactivates to the ground state and the acceptor activates to the excited states through the energy transfer relaxation pathways. With respect to the photoinduced electron transfer, we can use frontier molecular orbitals (FMOs) to understand these two important photophysical processes. The electron donor can be initiated after photoexcitation. An excited single electron in the lowest-unoccupied molecular orbital (LUMO) of the electron donor is transferred to the LUMO of the acceptor. The mechanisms of the energy and electron transfers are described as following:

Energy Transfer

The excited donor (D*) can be deactivated by energy transfer when a lower energy excited acceptor (A) exists. This process can be presented by the following equations, Equation (1-5) and Equation (1-6).

$$\mathrm{D} + h\nu \rightarrow \mathrm{D}^{*} \tag{1-5}$$

$$\mathrm{D}^{*} + \mathrm{A} \rightarrow \mathrm{D} + \mathrm{A}^{*} \tag{1-6}$$

There are two requirements for energy transfer. First of all, the energy level of the excited donor (D*) is higher than that of the excited acceptor (A*). Secondly, the lifetime of D* is longer than the time scale of the energy transfer process. There are two possible kinds of energy transfers, which are radiative and nonradiative energy transfer.

For radiative energy transfer, it appears by the two sequential steps of Equation (1-7) and Equation (1-8). Because the radiative transfer requires that D* emits photons that A is able to absorb, the photoluminescence spectrum of D* must overlap the absorption spectrum of A, as illustrated in Figure 1-8. The probability of radiative energy transfer from D* to produce A* is dependent on several important parameters, i.e., the quantum yield of D*, the concentration of A, the extinction coefficient of A and the

overlap integral (J) of the photoluminescence spectrum of D* and the absorption spectrum of A.

$$\mathrm{D}^{*} \rightarrow h\nu + \mathrm{D} \tag{1-7}$$

$$h\nu + \mathrm{A} \rightarrow \mathrm{A}^{*} \tag{1-8}$$

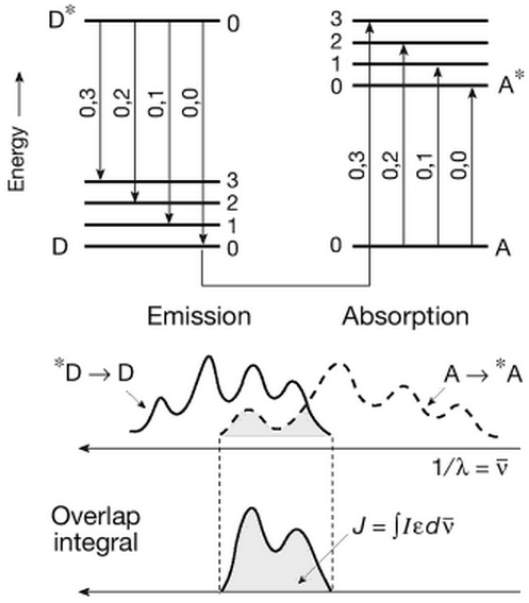

Figure 1-8. The requirements of radiative energy transfer. This figure was adopted from Turro.[22]

In addition, the other kind of energy transfer is nonradiative energy transfer, which is more efficient than radiative energy transfer. This kind of energy transfer consists of Förster and Dexter mechanisms. The Förster mechanism is also termed as the “Columbic” or “resonance” mechanism for electronic energy transfer. It was first developed by the German scientist Theodor Förster. This kind of energy transfer is rapid and appears without a photon emission. In Förster mechanism, the resonant coupling of electrical dipoles between an excited donor and an acceptor can induce the energy migration. This process can occur over long distances (30 – 100 Å). The Förster mechanism is illustrated in Figure 1-9. In this figure, an electron of the excited donor

relaxes from the LUMO state to the HOMO state, and the energy is transferred to the acceptor through columbic interactions. As a consequence, an electron of the acceptor molecular is promoted from the HOMO state to the LUMO state. This mechanism occurs in the singlet states of the donor and acceptor due to the strong dipole-dipole interaction of the multiplicity-conserving transitions.

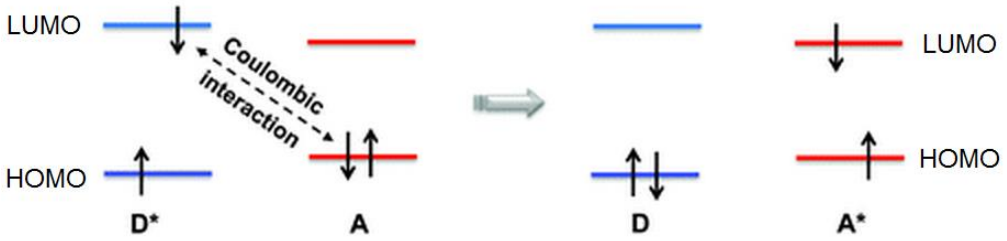

Figure 1-9. Mechanism of energy transfer action according to Förster. This figure was modified from Praveen.[23]

In the classical theory, the electrostatic interaction energy (E) between two electric dipoles is directly proportional to the magnitude of the two transition dipoles (μ_D and μ_A) and inversely proportional to the cube of the distance between the donor and acceptor(R_{DA}), as presented in Equation (1-9). In quantum mechanical principles, the golden rule can be used to compute the rate of energy transfer (k_{ET}) for dipole-dipole mechanism, as shown in Equation (1-10). The matrix element for this energy transfer process comprises the product of wave function $\Psi(D^*)\Psi(A)$for the initial state, the product of wave function $\Psi(D)\Psi(A^*)$ for the final state, and an operator $P_{D\rightarrow A^*}$ that represents dipole-dipole interaction, which mixes the wave functions $\Psi(D^*)$ and $\Psi(A)$ and causes transition to the wave function of $\Psi(D)$ and $\Psi(A^*)$. The value of the rate constant for energy transfer (k_{ET}) is dependent on the square of this matrix element in accordance with the golden rule. $\langle\chi_i|\chi_f\rangle^2$is the Frank-Condon (FC) factor, which is corresponding to the overlap for the vibrational wave function of the initial state (χ_i) and

the vibrational wave function of the final state (χ_f). Based on the analysis above, Turro[22] conclude that the magnitude will be directly related to the square of the interaction energy of the transition dipoles, as presented in Equation (1-11).

$$E(dipole-dipole) \propto \frac{\mu_D \mu_A}{R_{DA}^3} \tag{1-9}$$

$$k_{ET} \sim \langle \Psi(D^*)\Psi(A)|P_{D\rightarrow A^*}|\Psi(D)\Psi(A^*)\rangle^2 \langle \chi_i|\chi_f\rangle^2 \tag{1-10}$$

$$k_{ET}(dipole-dipole) \propto E^2 \approx \left(\frac{\mu_D \mu_A}{R_{DA}^3}\right)^2 = \frac{{\mu_D}^2 {\mu_A}^2}{R_{DA}^6} \tag{1-11}$$

The other important nonradiative energy transfer process is Dexter Mechanism, which consists of a double electron exchange between the donor and the acceptor, as illustrated in Figure 1-10. There is no charge separated state in this mechanism, although the two electrons exchange in this process. For Dexter mechanism, an electron moves from the LUMO state of the donor to the acceptor when an electron moves from the HOMO state of the acceptor to the donor. This process can be the electron tunneling. Both singlet-singlet energy transfer and triplet-triplet energy transfer can result from the electron exchange interaction. In contrast, dipole-dipole interaction cannot operate in the triplet states. For the Dexter energy transfer process, it requires the molecular orbital overlap between the excited donor and the acceptor molecule. Thus, this mechanism belongs to short-range interactions (~5-10 Å and shorter). The rate constant of Dexter mechanism decays exponentially with the intermolecular distance between the donor and the acceptor.[24] Thus the rate constant can be expressed by the following equation.

$$k_{ET}(exchange) = KJ \exp\left(\frac{-2\,R_{DA}}{R_{DA}^0}\right) \tag{1-12}$$

Where *K* is a parameter related to the specific orbital interactions, *J* is the normalized spectral overlap integral, and R_{DA}^{0} is the separation of *D and A when they are in van der Waals contact.

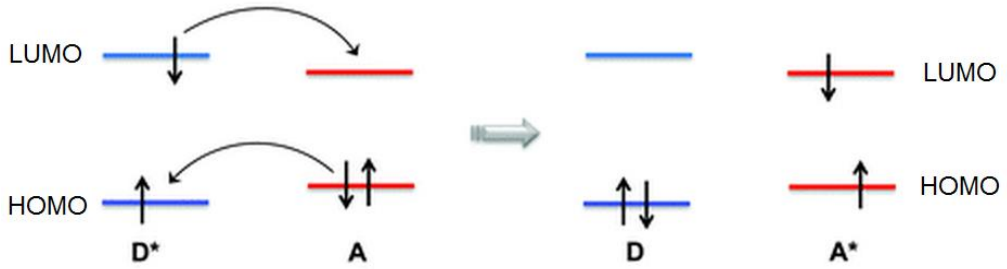

Figure 1-10. Mechanism of energy transfer action according to Dexter. This figure was modified from Praveen.[23]

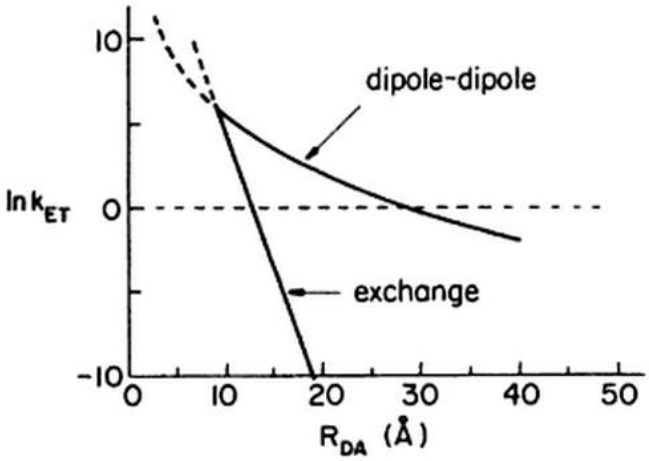

Figure 1-11. The plot of $\ln k_{ET}$ versus distance R_{DA} for both dipole-dipole energy transfer mechanism and electron exchange energy transfer mechanism. This figure was modified from Turro.[22]

The rates of dipole-dipole energy transfer and electron exchange energy transfer depend on the separation distance between the donor and the acceptor, shown qualitatively in Figure 1-11. The former decreases as the inverse sixth power of the distance, whereas the latter falls off exponentially as the distance increases. Hence, the dipole-dipole energy transfer can appear over very large distances, while electron

exchange energy transfer will produce much greater rate at short distances and close contacts.

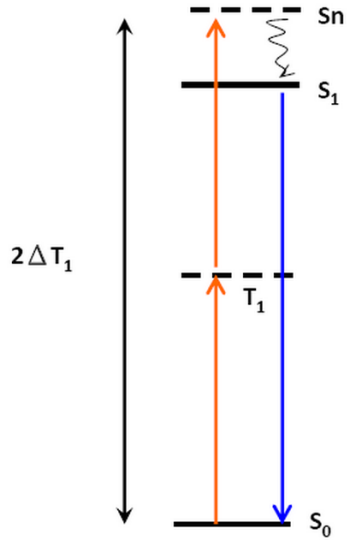

Figure 1-12. Energy diagram for triplet–triplet annihilation. This figure was adopted from http://chemwiki.ucdavis.edu/Theoretical_Chemistry/Fundamentals/Dexter_Energy_Transfer

A special mechanism of exchange energy transfer is triplet-triplet annihilation (TTA), as shown in Equation 1-13. In this case, the interaction of two triplets produces an excited singlet and a ground-state singlet. While the energy gap between the lowest excited triplet state (T_1) of a molecular and its ground state (S_0) is larger than the energy gap between the lowest excited singlet state (S_1) and the lowest excited triplet state (T_1) (Figure 1-12), the interaction of two triplets will acquire enough electronic excitation energy (2 X $\Delta \boldsymbol{E}_{\mathbf{T_1-S_0}}$), which can produce an excited singlet state (S_1) and a ground state (S_0).

$$\mathrm{D}^*(\mathrm{T}_1) + \mathrm{D}^*(\mathrm{T}_1) \rightarrow \mathrm{D}^*(\mathrm{S}_1) + \mathrm{D}(\mathrm{S}_0) \qquad (1\text{-}13)$$

Electron Transfer

In the mechanism of photoinduced electron transfer, an electron transfer occurs within an electron donor-acceptor pair, as illustrated in Figure 1-13. Photoinduced

electron transfer is a representative photophysical process and a prime method to convert light energy for other applications. In Figure 1-13, after excitation between a donor and an acceptor, it produces a charge separated state, which then deactivates to ground state through electron recombination. Marcus theory[25] was originally developed by Rudolph A. Marcus in 1956 for the explanation of photoinduced electron transfer. This theory treated the electron transfer reaction with transition state theory. The excited donor and acceptor is the reactant state, and the charge-separated state (D^+A^-) of the donor and acceptor is the product state, as shown in Figure 1-14.

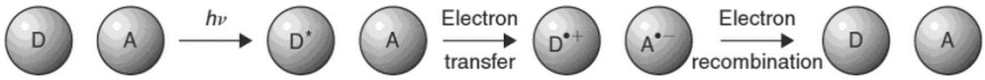

Figure 1-13. Photoinduced electron transfer process

In accordance to Frank-Condon principle, a vertical transition occurs from the ground state to the excited state after photoexcitation, and then a fast nuclear equilibrium takes place. If the donor is not excited, the electron transfer process will be too endothermic to occur. Nevertheless, electron transfer happens at the crossing of the equilibrated excited state surface and the product state after the excitation of the donor. The relationship between $\Delta G^{\#}$, $\Delta G^{0}$and λ was derived, as shown in Equation (1-14).

$$\Delta G^{\#} = \frac{(\Delta G^{0}+\lambda)^{2}}{4\lambda} \qquad (1\text{-}14)$$

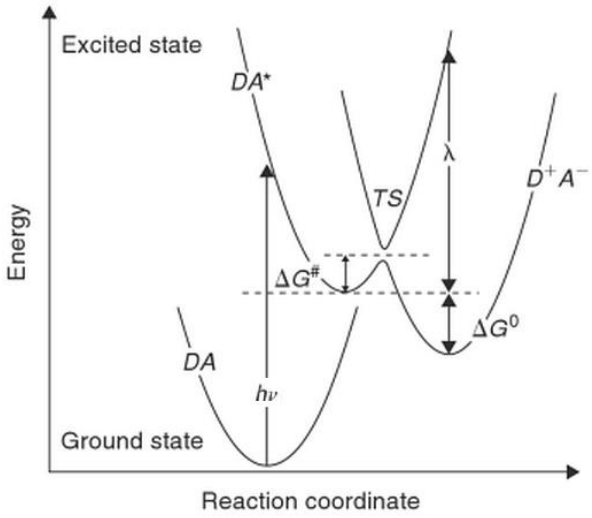

Figure 1-14. Potential energy surface for the ground state (DA), the excited state (DA*, reactant state), and the charge separated state (D^+A^-, product state). λ is reorganization energy; TS is transition state. This figure was modified from Marcus.[26]

The reorganization energy, λ, represents the vertical transition from the minimum of the excited-state parabola for the reactants (DA*) to the intersection with the parabola for the products (D^+A^-). λ is required to distort the reactant structure to the product structure without electron transfer, and it is the sum of the solvent (λ_s) of the internal (λ_i) component ($\lambda = \lambda_s + \lambda_i$). λ_s is from the reorganization of the solvent around the reactants and products. The value of λ_i can reflect any changes in bond orders and angles between the structures of the reactants and the products. The reaction free energy, ΔG^0, is the change of free energy between the equilibrium configuration of the reactant (DA*) and of the product states (D^+A^-). In the classical Marcus theory, the rate of electron transfer can be expressed by Equation (1-15)

$$k_{et} = \kappa_{et}\nu_n \exp\left(\frac{-\Delta G^{\#}}{k_B T}\right) \quad (1\text{-}15)$$

where ν_n is the effective frequency of motion along the reaction coordinate and κ_{et} is the electronic transmission factor. The transmission factor is proportional to the

transition probability (P_0) at the interaction of two potential energy surfaces, Equation (1-16), which is derived by Landau-Zener theory.[26]

$$\kappa_{et} = \frac{2P_0}{1+P_0} \tag{1-16}$$

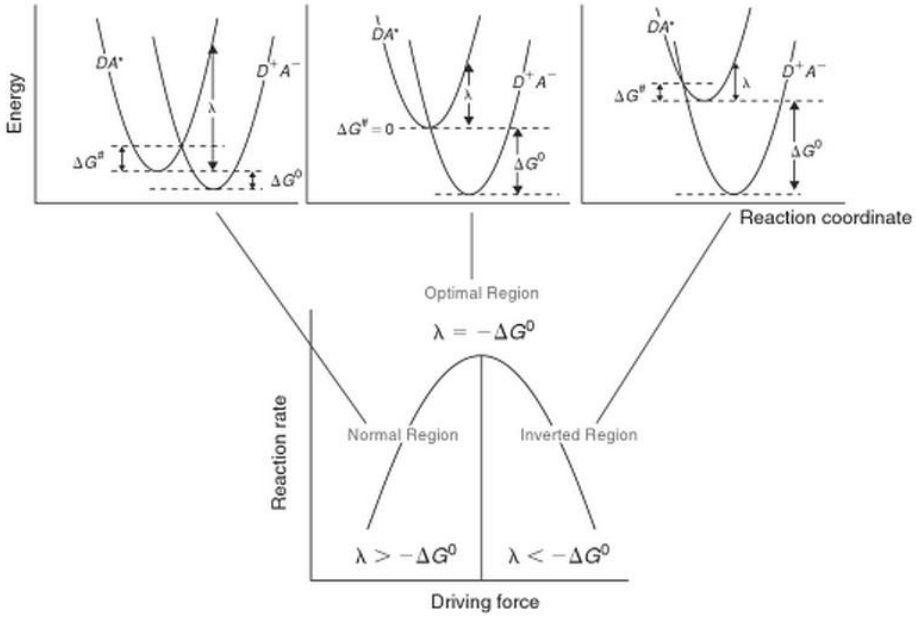

Figure 1-15. The free energy regimes for electron transfer (top) and the corresponding reaction rate dependence on the free energy (bottom; driving force is $\Delta G^0 - \lambda$). This figure was modified from Marcus.[26]

Figure 1-15 shows the reaction rate constant versus the change of the driving force for the electron transfer process, which is plotted from the Marcus theory. The electron transfer rate can be calculated using Equation (1-15). For the Marcus normal region ($\lambda > -\Delta G^0$), the electron transfer rate (k_{et}) increases as the free reaction energy (ΔG^0) decreases. For the optimal or the activationless region, the driving force of the electron transfer is equal to the reorganization energy ($\lambda = -\Delta G^0$). For the inverted Marcus region ($\lambda < -\Delta G^0$), the activation barrier ($\Delta G^{\#}$) reoccurs as ΔG^0 becomes even more negative. In this inverted region, the electron transfer rate (k_{et}) decreases as the free reaction energy (ΔG^0) decreases. The first successful approach, providing reliable

evidence for the inverted region, examined electron transfer between aromatic molecules in rigid organic systems and was developed by Closs and Miller.[27] All different Marcus regions are illustrated in Figure 1-15.

Photoprocesses in Macromolecules

Intermolecular energy transfer, intramolecular energy transfer, and energy migration are the major categories of energy transfer process in polymer systems. Energy transfer and energy migration have been systematically studied in many artificial polymers by Chen group.[28] Because the processes of energy transfer have not been clearly reported in various environments, they built schematic diagrams of the different occasions to describe how the excitation energy is transferred from one species to another, as illustrated in Figure 1-16. The energy can be harvested and then transferred sequentially, directionally, and efficiently in a photosynthesis multipigment array (a). Energy transfer may occur intramolecularly between different pendent chromophores of the polymer chain (b), or between the segments on the polymer backbone with the same chemical structures but different conjugation lengths (c). Because intramolecular or intermolecular aggregates sometimes occur in the polymers, the energy can transfer from the nonaggregated segments to the aggregates (d, e). The energy transfer occasionally happens from some pendant chromophores to the conjugated polymer backbone (f). Excited energy can also be transferred from the randomly oriented segments of the conjugated polymer to the isolated, aligned single chains in the channels of mesoporous silica (g). The aggregates may form in some conjugated polymer systems with various extents of interactions between chromophores. The energy transfer can thus occur sequentially from the individual conjugated segments, through the loose aggregates, finally to the most aligned, compact aggregates (h).

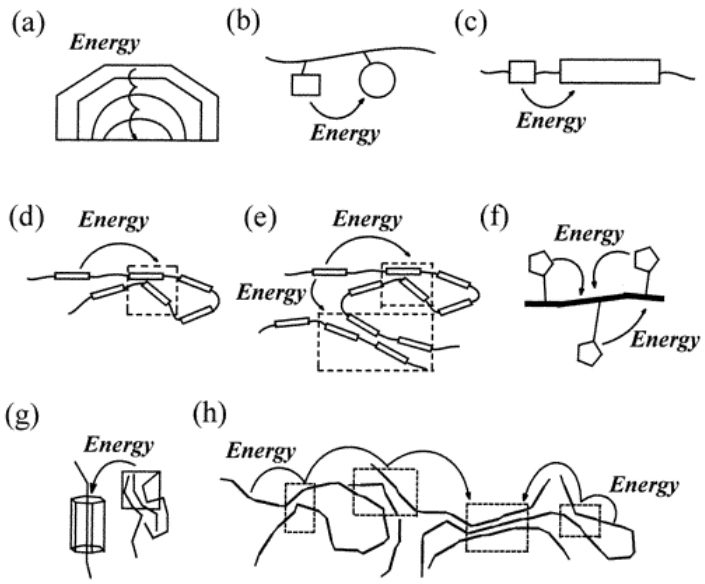

Figure 1-16. Scheme diagrams of the different environments for energy transfer. This figure was adopted from Chen. [28]

Figure 1-16 shows some energy transfer processes, which have been reported. But there are few direct observations of the energy process for conjugated polymers in the literature because the rate of energy transfer or energy migration may be too fast to observe these photophysical behaviors directly. Also, the energy transfer mechanisms are hard to distinguish due to the complicated and disordered structures of polymers. A series of polymers with the specific structures was designed by Chen and his co-workers to simplify the situation. They synthesized polymers of substituted distyrylbenzene (DSB) with well-defined conjugation length as repeating units linked by methylene and ethylene linkages, polymers I–IV, as shown in Figure 1-17. The conformational distortion and tetrahedron defects in the fully conjugated polymers result in the complexity of the photophysical mechanisms. The effects on the photophysical properties from the interactions between individual chromophores (DSB units) can be separated in the polymers I–IV. Additionally, the energy transfer process can be

decelerated to an observable extent by the saturated spacers between the chromophores on the polymer backbone.

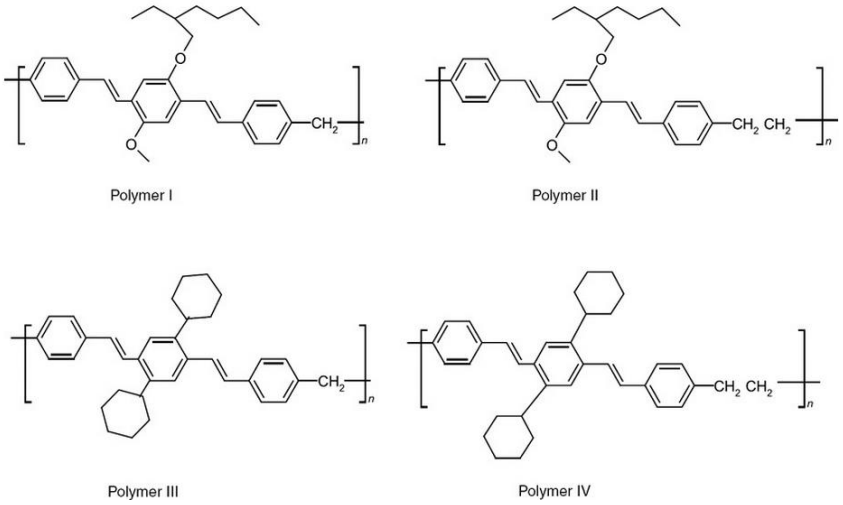

Figure 1-17. Structure of polydistyrylbenzene (PDSB) I–IV. This figure was adopted from Chen. [28]

In order to explore the energy transfer process, the polymers I–IV in the solution with various concentrations (0.01–10 mg/mL) and polymer films were studied using UV-vis absorption and excitation, steady-state, and time-resolved photoluminescence spectroscopy. They found that the interactions between neighboring chromophores are crucial to the energy transfer processes. There are aggregates besides the individual conjugated polymer chromophores in concentrated solutions and solid films. Various extents of interaction lead to different kinds of aggregates between the chromophores, such as loose, compact, and the most aligned aggregates. By using time-resolved photoluminescence spectroscopy, they can directly detect the sequential energy transfer from individual DSB units to their aggregates, and then from the loose aggregates to the relatively more compact aggregates. Thus, the emission of the concentrated solutions and films of PDSBs I-IV in the steady-state photoluminescence can be assigned to the aggregates of these polymers. Nevertheless, a sequential

energy transfer process cannot be detected at all in fully conjugated polymers at room temperature. The Chen group indicated that this kind of process can occur in the conjugated systems although it may be disguised by the ultrafast photophysical processes.[28]

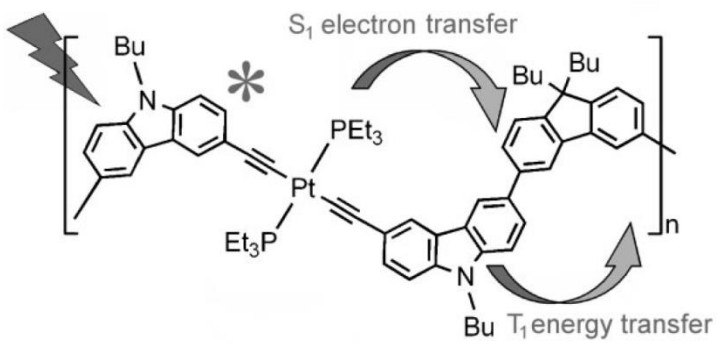

Figure 1-18. Drawing illustrating the two non-radiative processes inducing the quenching of the carbazole fluorescence and phosphorescence. The figure was adopted from Aly.[29]

The photoprocesses of multifunctional organometallic polyyne oligomers and polymers have been investigated since this kind of materials exhibits convenient structural variability as well as optical and electronic properties. Aly et al.[29] designed and synthesized a series of polymers, $(\text{-Cz-C}\equiv\text{C-PtL}_2\text{-C}\equiv\text{C-Cz-X-})_n$, along with the corresponding model compounds $(\text{Ph-PtL}'_2\text{-C}\equiv\text{C-Cz})_2\text{-X-}$, where Cz=3,3′-carbazole, X=nothing, Cz, or F (2,2′-fluorene), L=PBu_3, and L′=PEt_3. They found that the fluorescence of the 3,6-carbazole is totally quenched in the polymer, as illustrated in Figure 1-18.[29] From the results of wavelength dependence excitation and transient absorption spectra, intramolecular singlet electron and triplet energy transfer from the 3,6-carbazole chromophore to the 2,7-fluorene moiety are observed (Figure 1-18).

The photoluminescence lifetimes, quantum yields, and transient absorption lifetimes of the oligomers and polymers with organic spacers consisting of the

carbazole-fluorene hybrids were detected and analyzed, as shown in Figure 1-19.[30] They demonstrated that the rate of triplet–triplet energy transfer (ET) ($k_{ET} \approx 10^3\ s^{-1}$) is much slower than that of electron transfer (et) ($k_{et} > 4 \times 10^{11}\ s^{-1}$) at room temperature. In addition, the k_{ET} values of the model digold dyads are slower than those of the model diplatinum analogues and the platinum-containing polymers, as presented in Figure 1-19.[30] The k_{ET} of the diplatinum systems is faster than that of the digold congener since the triplet excitons of the diplatinum species have higher populations. With regard to the polymers, their k_{ET} are twice as fast as the dinuclear systems due to the presence of two fluorene units flanking the carbazole-containing chromophore, which provides two pathways to relaxation.

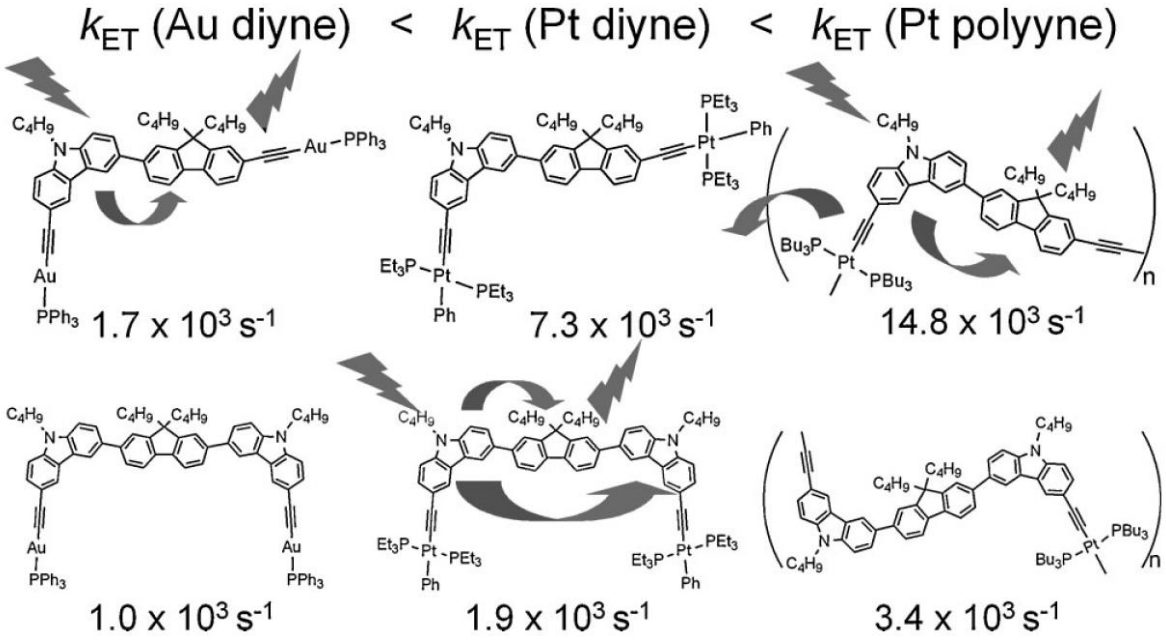

Figure 1-19. Comparison of the triplet ET for various model compounds and polymers. The figure was adopted from Aly.[30]

The development of the metallopolyynes with low E_g is desirable for the photovoltaic applications. The porphyrin monomers have a relatively low E_g with large absorption coefficients due to their large π conjugation. The porphyrin oligomers and

polymers bridged by ethylene,[31] butadiyne, [32,33] phenylenevinylene,[34] aryl acetylene[35] and so on have been studied. Nevertheless, there are very few reports in relation to conjugated porphyrin oligomers or polymers bridged by Pt(II) acetylides. Because insertion of Pt(II) in macromolecules also resulted in a large conduction bandwidth with a d^8 square-planar configuration in addition to the heavy metal effect,[36] Jiang et al. have reported the photophysical properties of Pt-Acetylides/Porphyrin Oligomers, as displayed in Figure 1-20. There are three main energy transfer processes in this mixed-metalloporphyrin trimer. First of all, a triplet energy transfer occurs from the trans-$C_6H_4C{\equiv}C–Pt(PEt_3)_2–C{\equiv}CC_6H_4$ unit to the metalloporphyrins with the excitation of 355 nm; i.e., within the absorption band of this chromophore.[37] Also, singlet (S_1) and triplet (T_1) energy transfer occur from the palladium to the zinc(porphyrin) macrocycle when this oligomer is excited in the Q-bands of the palladium part, which acts as the energy donor.

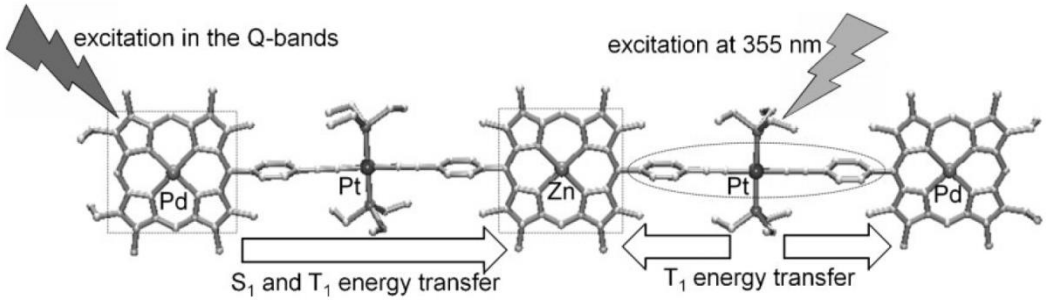

Figure 1-20. Various energy transfer processes within the small oligomers. The figure was adopted from Jiang.[37]

Liu et al. have prepared and investigated the (trans-$C_6H_4C{\equiv}C–Pt(PBu_3)_2–C{\equiv}CC_6H_4$–zinc(porphyrin))$_n$ oligomers with n = 3, 6, 9, as illustrated in Figure 1-21.[38] The triplet energy transfer occurs from the trans-$C_6H_4C{\equiv}C–Pt(PBu_3)_2–C{\equiv}CC_6H_4$ spacer to the zinc(II)porphyrin unit, and the rates vary from 2.4 X 10^4 to 1.3 X 10^6 s^{-1} as the

oligomer size (n) increases. This is because the back energy transfer (T_1(acceptor) → T_1(donor)) occurs along the zinc(II)porphyrin arrays (Figure 1-21). Therefore, the energy is transferred from the donor to the acceptor, and then back energy transfer may occur to decrease the overall rate of the photophysical process. In other words, the depopulation of the T_1 state of the acceptor leads to less back energy transfer. As a result, the overall rate will be faster. According to the photophysical model above, as the number of units, n, increases, the increasing probability of an excitonic process (depopulating the T_1 state of the acceptor) results in the higher overall rate for the energy transfer.

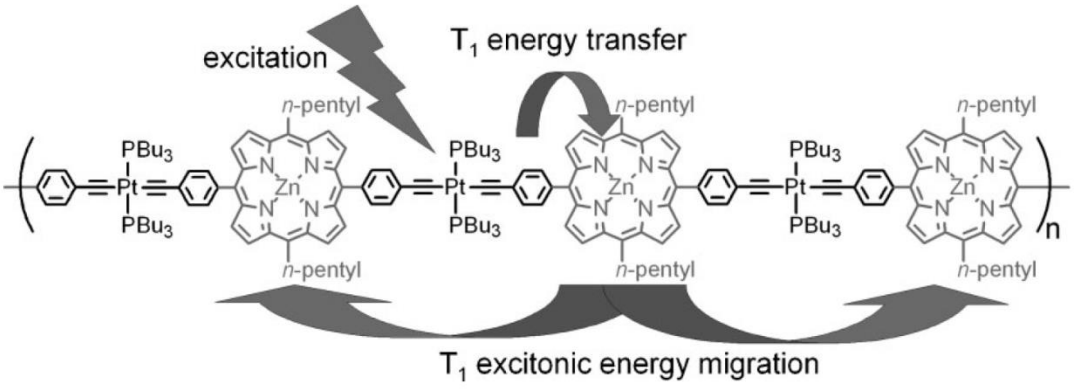

Figure 1-21. Non-radiative energy delocalization processes in the Pt-acetylides/zinc porphyrin oligomer. The figure was adopted from Liu.[38]

Photophysical Spectroscopy

Absorption and Emission

A photon is a fundamental particle of light. The energy of each photon is hc/λ; where h is Plank's constant, c is the speed of the light, and λ is the wavelength of the radiation. Light has wave and particle properties. The particle behavior is the ejection of electrons after the light collides with an atom. On the other hand, the wave properties can be observed by the light diffraction at gratings. There are different processes in the

interaction between light and molecules, such as excitation, fluorescence, phosphorescence, relaxation, quenching, energy transfer, internal conversion, and so forth. The change of physical and chemical properties can be initiated by the light absorption of the materials. The negative change is the needless changes in the structure of the material, such as a discolored response. By contrast, the absorption of light can produce positive changes as well. Polymer cross-linking and associated insolubilization can be made purposely with the absorption of light. This can be applied to coatings and negative-lithographic resists. Light-induced chain breakage can be applied to positive-lithographic resists. Photoconductivity can be applied to photocopying, and photovoltaic effects can be applied to diverse kinds of solar cells.

The first law of photochemistry, the Grotthuss-Draper law, states that photophysical and photochemical reactions take place only when a photon of light is absorbed. It can be described as follows, Equation (1-17).

$$M + h\nu \rightarrow M^* \tag{1-17}$$

where M^* is the excited materials after the light absorption of M.

Optical transmittance, T, is the fraction of incident light (electromagnetic radiation) at a specified wavelength that passes through a sample.

$$T = \frac{I}{I_0} \tag{1-18}$$

If there is no absorbed light, $I = I_0$. Thus, a low value of the transmittance means that much of the incident light is absorbed.

Most spectrophotometers reveal optical absorbance, *A*, which is defined as

$$A = \log\left(\frac{I_0}{I}\right) \tag{1-19}$$

so that

$$A = \log\left(\frac{1}{T}\right) = -logT \quad (1\text{-}20)$$

Beer's law states that the absorbance of the chromophores, *A*, is directly related to the concentration of the chromophores, where *k* is a constant, as shown in Equation (1-21)

$$A = kc \quad (1\text{-}21)$$

Beer's law can be used to determine the concentration of an unknown after acquiring a line of the known absorbance versus concentration by the relationships between absorbance and concentration (Beer's law). The optical path, l, is the distance the light travels through the sample. Lambert's law states that the absorbance is proportional to the optical path, where k' is another empirical constant, as presented in Equation (1-22).

$$A = k'l \quad (1\text{-}22)$$

Even if the c and l are the same, the absorbance may differ due to the molar absorption coefficient, ε. Generally, as the molar absorption coefficient is larger, the material absorbs more. Beer's law and Lambert's law combine to form Beer's-Lambert's law, which is expressed in Equation (1-23).

$$A = \varepsilon lc \quad (1\text{-}23)$$

The extinction coefficients of chromophores vary from forbidden transitions (<100 $M^{-1}cm^{-1}$) to fully allowed transitions (>10^5 $M^{-1}cm^{-1}$).

The fluorescence emission band is red-shifted relative to the absorption band. There are some overlaps between the shorter wavelength of fluorescence emission and the longer wavelength of the absorption band. When the spectra are plotted on a wavelength scale, the absorption and fluorescence spectra are the mirror-image of each

other. The Frank-Condon energy diagram can be applied to understand the relations between the photophysical processes, as illustrated in Figure 1-22. The absorption of a photon excites the molecule at the most probable internuclear radius to an excited vibrational level, and then the excited molecular experiences the vibrational relaxation by the quantum losses of vibrational energy. After the total excited lifetime on a time scale of ~ 10^{-8} s, fluorescence decay to the electronic ground singlet state (S_0) occurs. The wavelength of the maximum fluorescence intensity corresponds to decay from the most probable internuclear separation in the excited states to ground state.

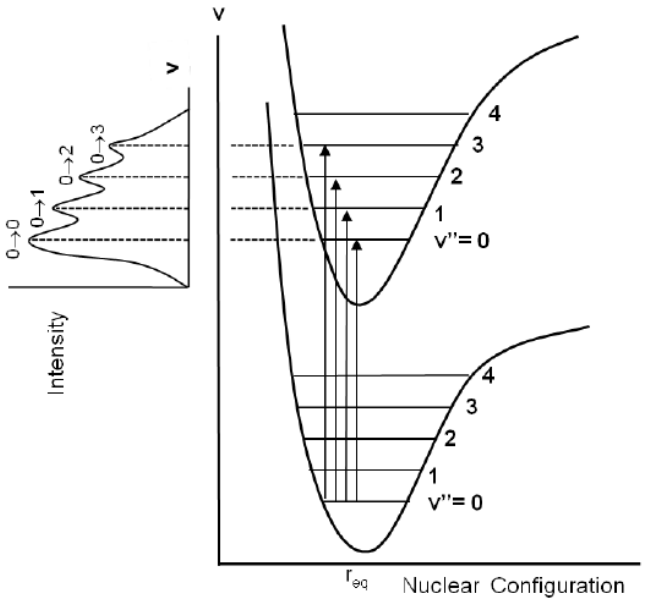

Figure 1-22. Frank-Condon diagram. This figure is adopted from Atkins.[39]

Phosphorescence photoluminescence occurs with the emissive lifetime from 10^{-3} s to many seconds (and even minutes). The wavelength of phosphorescence is longer than that of fluorescence. It is impossible that the molecule is excited to the excited triplet state directly by absorption of a photon if ground state is singlet. The energy levels of excited singlet states are often close to that of excited triplet states, so

processes of a transition may occur with a reasonable probability. The process of a transition between states of different multiplicity is known as intersystem crossing. Internal conversion between states of identical multiplicity occurs in a time scale of ~ 10^{-13} s. But Intersystem crossing occurs from 10^{-7} s to 10^{-8} s because this process is a spin-forbidden transition. The phosphorescence photoluminescence occurs at longer wavelength than fluorescence because the energy of triplet states is generally less than that of the corresponding singlets.

Time-Resolved Photoluminescence Spectroscopy

The photoluminescence lifetime is the average lifetime of the excited molecule before the emission of the photon. The definition of the lifetime is the rate of the depopulation of the excited states (singlet or triplet). Generally, the photoluminescence is first-order kinetics and can be expressed as,

$$[M^*] = [M^*]_0 e^{-kt} \tag{1-24}$$

where $[M^*]$ is the concentration of the excited state molecule at time t, $[M^*]_0$ is the initial concentration and k is the decay rate of the population of the excited state.

Because different kinds of radiative and nonradiative processes can decrease the excited state population, the overall decay rate is the summation of these rates, as shown in Equation (1-25).

$$k_{total} = k_r + k_{nr} \tag{1-25}$$

Both the steady-state and time-resolved photoluminescence are significant for the photophysical studies. Time-resolved photoluminescence can provide a lot of information concerning the rates and kinetics of the intermolecular and intramolecular processes.

A molecule is excited from ground state to the excited state. The excited molecule can then be deactivated to the ground state by the radiative and nonradiative pathways, as presented in Equation (1-26), (1-27) and (1-28)

$$A_0 + h\nu \rightarrow A^* \quad (1\text{-}26)$$

$$A^* \rightarrow A_0 + h\nu \quad \text{(radiative processes, } k_r\text{)} \quad (1\text{-}27)$$

$$A^* \rightarrow A_0 + heat \quad \text{(nonradiative processes, } k_{nr}\text{)} \quad (1\text{-}28)$$

Thus, we can write

$$-\frac{d[A^*]}{dt} = (k_r + k_{nr})[A^*]t \quad (1\text{-}29)$$

where $[A^*]$ is the concentration of the species A in the excited state at a given time t, and k_r and k_{nr} are the rate constants for the radiative and nonradiative processes, respectively.

The relative concentration of $[A^*]$ is given by Equation (1-30),

$$ln\frac{[A^*]_t}{[A^*]_{t=0}} = -(k_r + k_{nr})t = -\frac{t}{\tau} \quad (1\text{-}30)$$

Therefore, the lifetime (τ) of $[A^*]$ is

$$\tau = 1/(k_r + k_{nr}) \quad (1\text{-}31)$$

Thus, the measured unimolecular radiative lifetime is the reciprocal of the sum of the unimolecular rate constants for all the deactivation processes. The general equation can be expressed in Equation (1-32).

$$\tau = \frac{1}{\sum_i k_i} \quad (1\text{-}32)$$

where τ is the observed radiative lifetime and the rate constant k_i represents the unimolecular processes that deactivate $[A^*]$.[40]

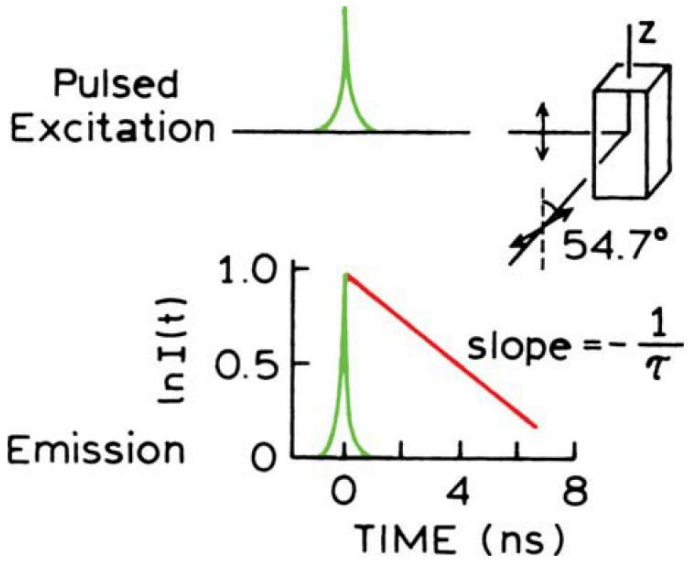

Figure 1-23. Time-domain lifetime measurement. This is adopted from Lakowicz.[41]

The lifetime can be recorded by a time-resolved measurement with a short pulsed excitation, as shown in Figure 1-23. The intensity decays often measured through a polarizer to avoid the effects of anisotropy on the intensity decay.[41] Then the log of the recorded intensity is plotted against time to obtain a straight line. The slope of this line is inversely proportional to the lifetime. If more than one species is emitting light at the excitation wavelength, there will be more than one lifetime in the kinetic traces.

Transient Absorption Spectroscopy

Norrish and Porter received the Nobel Prize in 1967 for studies of fast chemical reaction because they developed valuable techniques that enabled us to study reactions at the sub-millisecond timescale for the first time.[42] This technique, which allows the study of short-lived transient species, is transient absorption (TA) spectroscopy, also known as “pump-probe” spectroscopy. In transient absorption spectroscopy, a fraction of the molecules is excited to an electronically excited state with an excitation (or pump) pulse. This fraction generally varies from 0.1% to tens of

percents. There is a time delay (τ) between the pump pulse and the probe pulse, as shown in Figure 1-24.

With the weak probe pulse, we can calculate the absorption spectrum of the excited sample minus the absorption spectrum of the sample in the ground state to acquire a difference absorption spectrum (ΔA). A ΔA profile as a function of τ and wavelength λ can be collected by changing the time delay τ between the pump and the probe and recording a ΔA spectrum at each time delay. The $\Delta A(\lambda, \tau)$ can provide useful information about the dynamically photophysical processes, such as excited-state energy migration, electron and proton transfer processes, isomerization, and intersystem crossing. Time-resolved absorption spectroscopy is more comprehensive than time-resolved fluorescence, because the evolution of nonradiative states can be observed in the time-resolved absorption spectroscopy. This advantage is very essential since nonradiative decays play an important role for photophysical studies. Generally, there are some featured bands, which are corresponding to different processes, in transient absorption spectroscopy, as shown in Figure 1-25.

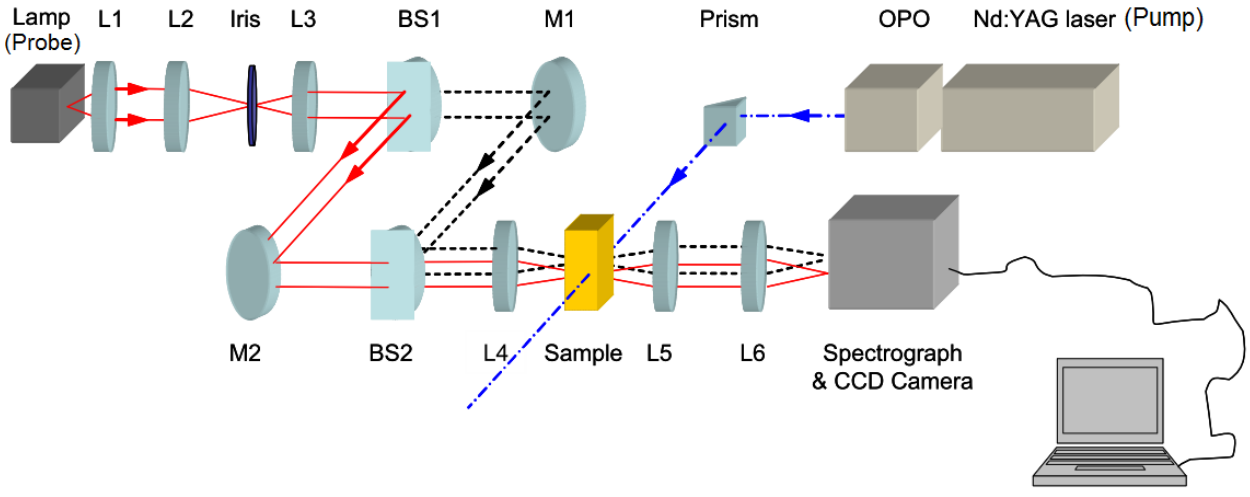

Figure 1-24. Scheme of the transient absorption spectroscopy principle.

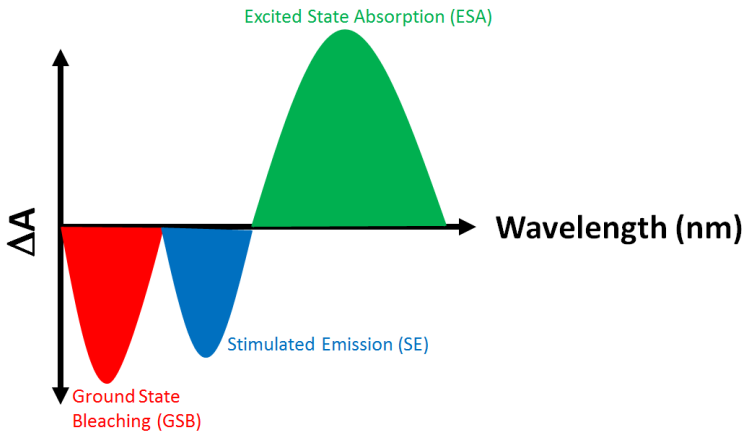

Figure 1-25. Contributions to a ΔA spectrum: ground- state bleach (GSB, red), stimulated emission (SE, blue), excited-state absorption (ESA, green).

The first one is ground-state bleaching (GSB) in Figure 1-25. Because a fraction of the molecules has been excited to the higher energy level by a pump pulse, the population of molecules in the ground state has been reduced. The ground-state absorption in the excited sample is thus weaker than that in the non-excited sample. As a result, the ground state bleaching (GSB) is observed as a negative band at the wavelengths of the UV-Vis absorption spectra, as illustrated in Figure 1-25 (red). In addition, the second one is stimulated emission (SE), which will occur from the excited molecule to the ground state as the probe pulse propagates through the excited sample. The photoluminescence spectrum of stimulated emission will follow the fluorescence spectrum of the excited molecule. Because the direction of the emissive photon is the same with that of the probe photon, both will be detected. Also, the intensity of the probe pulse is so weak that it cannot affect the population of the excited-states. A negative signal in the transient absorption spectrum is detected since stimulated emission (SE) increases intensity of the light on the detector, as illustrated in Figure 1-25 (blue). For numerous molecules, the Stokes shift may be so small that the band of stimulated emission overlaps with that of ground-state bleach. The third one is excited-

state absorption (ESA). The populated excited states of a molecule may be promoted to higher excited states in certain wavelength regions. Hence, this photophysical process will result in a positive signal in the wavelength region of excited-state absorption (ESA), as indicated in Figure 1-25 (green).

This Study

The background of conjugated polymers and platinum containing poly(phenylene ethynylene)s is described. The chemical structures and photophysical processes of conjugated polymers are discussed. The mechanisms of energy transfer, including Förster energy transfer, Dexter energy transfer, intermolecular energy transfer and intramolecular energy transfer, are also introduced and illustrated in detail to utilize these photophysical concepts for the designation and application of conjugated polymers.

Chapter 2 contains a photophysical study in platinum containing conjugated and conjugation interrupted polymers. The polymers to be investigated are a series of platinum acetylides in this chapter. The first polymer, which is called Ph_{100}, is 1,4-phenylene-based conjugated platinum acetylide homo-polymer; the name of 1,4-phenylene-based homo-polymer interrupted with methylene (CH_2) is $Ph_{100}(CH_2)$; the conjugated copolymer with 2,5-thienylene(Th) and 1,4-phenylene(Ph) units at Th:Ph=1:19 is denominated $Ph_{95}Th_5$; the final polymer $Ph_{95}Th_5(CH_2)$ is the conjugation interrupted 2,5-thienylene and 1,4-phenylene co-polymer with methylene (CH_2) linked spacer at Th:Ph=1:19, which means x is equal to 0.05. This investigation is to compare intrachain energy transfer of conjugation interrupted Pt-acetylides with that of conjugated Pt-acetylides. As we expected, the conjugation-interrupted structure is less effective.

Chapter 3 describes triplet exciton diffusion in platinum acetylide thin films. To enhance the efficiency of the organic photovoltaic cells (OPVs) and organic light-emitting diodes (LEDs), it is necessary to estimate the triplet exciton diffusion and understand what conducts triplet exciton transport through the organic electronics. Here, we have evaluated triplet exciton diffusion coefficient and length of diffusion using a concentration-based exciton quenching method, and explored triplet diffusion using a model compound that has the structure of 1,4-phenylene-based homo-polymer interrupted with methylene (CH_2). We conclude that the triplet diffusion coefficient in the conjugated polymer is higher than that in the conjugation-interrupted structure is found due to lower activation energy of the conjugated structure.

Chapter 4 details triplet-triplet energy transfer in polystyrene-based platinum acetylide arrays. Multichromophoric light-harvesting polymers have been targeted for solar energy applications. A polystyrene based copolymer of donor (PE2-Pt) and acceptor (Py-Pt) pendants was designed and studied. Steady-state emission spectroscopy, time-resolved photoluminescence and time-resolved transient absorption spectroscopy were applied to study the efficiency and dynamics of energy transfer in these macromolecular triplet donor-acceptor systems. We find that triplet-triplet energy transfer between different platinum acetylides in these polymers is much more efficient. For only 3% of Py-Pt loaded onto the copolymer, the phosphorescence from the PE2-Pt chromophore at 527 nm is quenched ~ 85%, and its energy transfer efficiency is ~ 86%.

Chapter 5 investigates ultrafast photophysics in platinum acetylide thiophene polymers. In this chapter, we would like to understand and control the photophysical behaviors of platinum–acetylide thiophene polymer (*p*-PtTh) in solution and the solid

state. By applying UV-Vis ground state absorption, steady-state photoluminescence, time-resolved transient absorption and fluorescence upconversion, the ultrafast photophysical properties and dynamics of the p-PtTh can be monitored for fundamental photophysical studies and photovoltaic applications. Chapter 6 will summarize all the work I have done and the scientific value of this dissertation.

CHAPTER 2
PHOTOPHYSICS IN PLATINUM CONTAINING CONJUGATED AND CONJUGATION INTERRUPTED POLYMERS

Introductory Remark

Up to the present, a great deal of investigation has focused on the study of carrier properties of singlet excitons in single chain conjugated polymers.[43-50] Despite these efforts, relatively little is known regarding the analogous properties of triplet excitons in these systems. Hence, the photophysical properties and dynamics of triplet transport in platinum containing PPEs, which are often called Pt-acetylides, were studied.[51,52] The major purpose of this investigation is to find out whether intrachain energy transfer in conjugation interrupted Pt-acetylides is an inefficient process. Another target is to build a model for photophysical explanation of exciton transport in these materials.

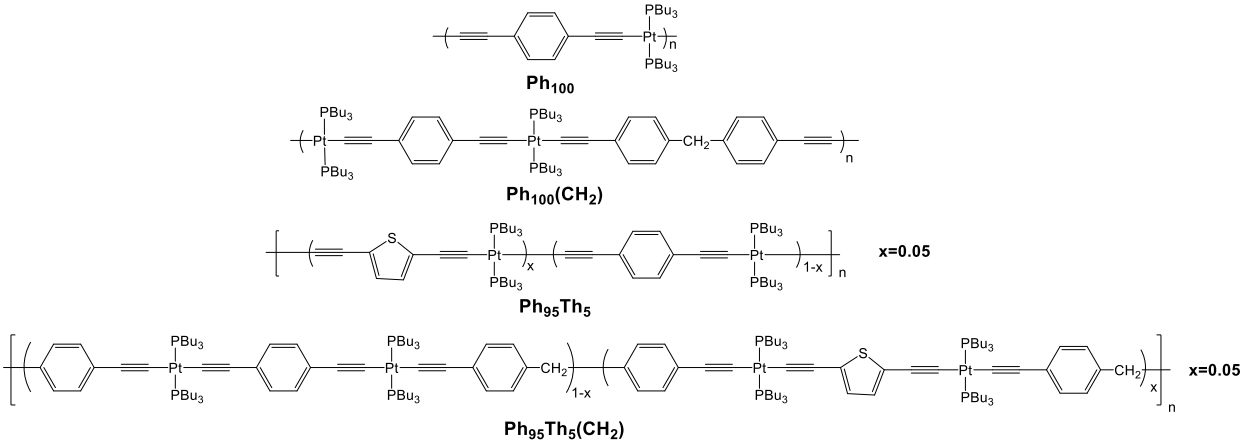

Figure 2-1. Structures of Ph_{100}, $Ph_{100}(CH_2)$, $Ph_{95}Th_5$ and $Ph_{95}Th_5(CH_2)$.

Due to their efficient phosphorescence, which can be monitored by photoluminescence spectroscopy, platinum acetylides were chosen in this research.[15,53] In addition, this series of polymers is easily made by use of copper iodide catalyzed

This Chapter is considered for publication in the Journal of the American Chemical Society.

Hagihara condensation polymerization.[51,54] For realizing the exciton transport in these materials, thiophene was designed as a triplet energy trap, which means its triplet state energy is lower than that of the polymer main chain. In this study, the triplet energies of the thiophene and phenylene part are 2.05 eV and 2.40 eV individually.[55]

The polymers to be studied are a series of platinum acetylides, as depicted in Figure 2-1. These polymers are labeled as Ph_{100}, $Ph_{100}(CH_2)$, $Ph_{95}Th_5$ and $Ph_{95}Th_5(CH_2)$. The first polymer, which is called Ph_{100}, is 1,4-phenylene-based conjugated platinum acetylide homo-polymer; the name of 1,4-phenylene-based homo-polymer interrupted with methylene (CH_2) is $Ph_{100}(CH_2)$; the conjugated co-polymer with 2,5-thienylene(Th) and 1,4-phenylene(Ph) units at Th:Ph=1:19 is denominated $Ph_{95}Th_5$; the final polymer $Ph_{95}Th_5(CH_2)$ is the conjugation interrupted 2,5-thienylene and 1,4-phenylene co-polymer with methylene (CH_2) linked spacer at Th:Ph=1:19, which means x is equal to 0.05.

Synthesis

For the first platinum acetylide homo-polymer, Ph_{100}, a great deal of information can be found from the literature. It is worth noting that the AA + BB co-polymerization has a great influence on the butadiyne defect present in the polymer backbone. Therefore, in order to avoid this fault, the strategy preferred is the self-polymerization of an asymmetric AB monomer.[56,57] Figure 2-2 illustrates this strategy for Ph_{100} synthesis. In the beginning, diiodobenzene, 1, was subjected to a one pot Sonogashira coupling between propargyl alcohol 2 and (triisopropylsilyl) acetylene (TIPS-acetylene), 3, giving asymmetrically protected diethynylbenzene, 4, in 35% yield. The propargyl alcohol protecting group was selectively removed through reaction with manganese dioxide and potassium hydroxide to give 5 in 86% yield. Following a Hagihara reaction with

platinum complex 6, the TIPS-protected monomer 7 was then deprotected in situ with TBAF and polymerized overnight to give polymer, Ph_{100}, in 64% yield.

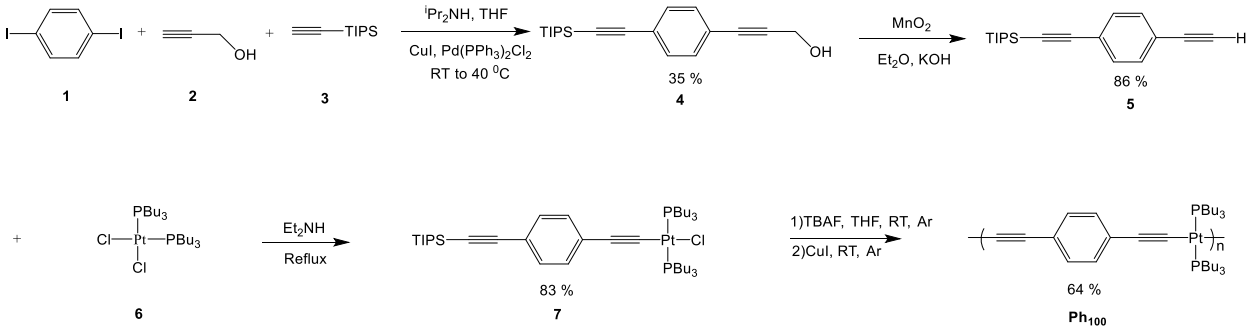

Figure 2-2. Synthesis of Ph_{100} using an AB asymmetric monomer.

The synthesis of conjugation interrupted homo-polymer, $Ph_{100}(CH_2)$, is shown in Figure 2-3. Through Sonogashira coupling reaction, diiodobenzene, 1, was reacted with (trimethylsilyl)-acetylene (TMS-acetylene), 8, giving symmetrically protected diethynyl-benzene, 9, in 80% yield. The TMS protecting group was removed through reaction with potassium hydroxide in the mixture of methanol (MeOH) and dichloromethane (DCM) at room temperature to give 10 in 80% yield. Following a Hagihara reaction with platinum complex 6 in diethylamine, the platinum acetylide monomer 11 was polymerized with organic compound 12 by copper iodide catalysts at room temperature. The conjugation interrupted polymer, $Ph_{100}(CH_2)$, was synthesized in 53% yield.

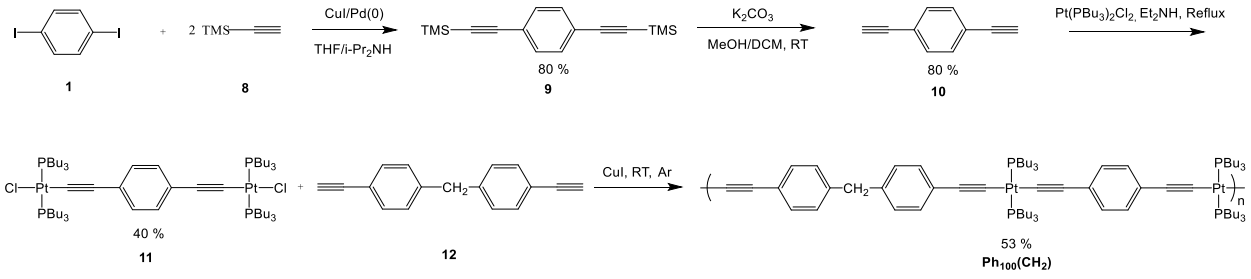

Figure 2-3. The synthesis of conjugation interrupted homo-polymer $Ph_{100}(CH_2)$.

For the synthesis of $Ph_{95}Th_5$, there are two synthetic methods which can greatly affect the defects present in the polymer backbone, i. e. butadiyne defects. In the first method, two symmetric monomers were reacted in an AA + BB co-polymerization to make $Ph_{95}Th_5$.[58] In the second method, an asymmetric AB monomer was self-polymerized. The butadiyne defects are produced in the first method. In order to prevent this defect, the method which we prefer is the polymerization of asymmetric AB monomers. Figure 2-4 illustrates this method for $Ph_{95}Th_5$ synthesis. In the beginning, 2,5-dibromothiophene, 13, was subjected to a one pot Sonogashira coupling between (trimethylsilyl)-acetylene (TMS-acetylene) 8 and (triisopropylsilyl) acetylene (TIPS-acetylene), 3, giving asymmetrically protected triisopropyl((5-((trimethylsilyl)ethynyl)-thiophen-2-yl)ethynyl)silane, 14, in a 80% yield. The TMS-acetylene protecting group was selectively removed through reaction with potassium hydroxide in the mixture of methanol (MeOH) and dichloromethane (DCM) at room temperature to give 15 in a 95% yield. Following a Hagihara reaction with platinum complex 6, the TIPS-protected monomer 16 and TIPS-protected monomer 7 were then deprotected in situ with TBAF and polymerized overnight to give conjugated co-polymers, $Ph_{95}Th_5$, in a 70% yield.

The conjugation interrupted co-polymer with methylene spacers, $Ph_{95}Th_5(CH_2)$, was synthesized, as depicted in Figure 2-5. 2,5-Diiodothiophene, 17, reacted with trimethylsilylacetylene in the use of copper iodide and palladium complex as catalysts. Because 2,5-diethynyl thiophene, 19, is unstable, the very stable bis(trimethylsilyl-ethynyl) thiophene, 18, was deprotected with tetrabutyl ammonium fluoride rapidly, and then intermediate 19 would afford monomer 20 in the presence of CuI and an excess of $Pt(PBu_3)_2Cl_2$ (Figure 2-6), which is very stable and can be easily purified by

chromatography. Following the three component A-A + A'-A' + B-B polymerization manner, 20 was synthesized with suitable amount of another platinum acetylide monomer 11, organic compound 12 and CuI gives $Ph_{95}Th_5(CH_2)$, as shown in Figure 2-5.

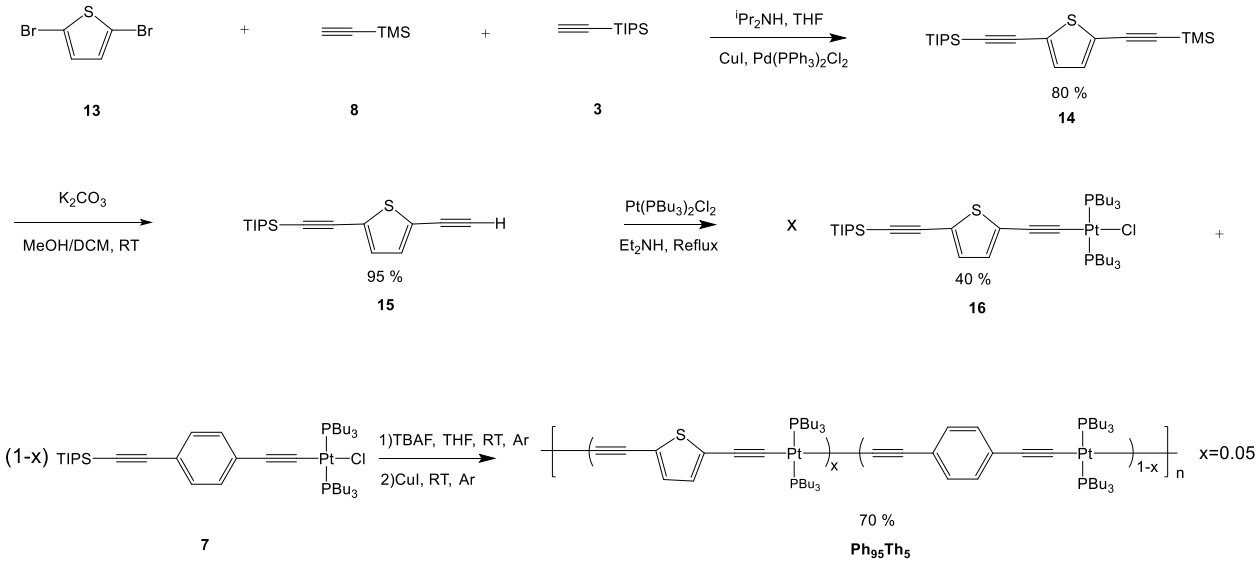

Figure 2-4. Synthesis of $Ph_{95}Th_5$ using AB asymmetric monomers.

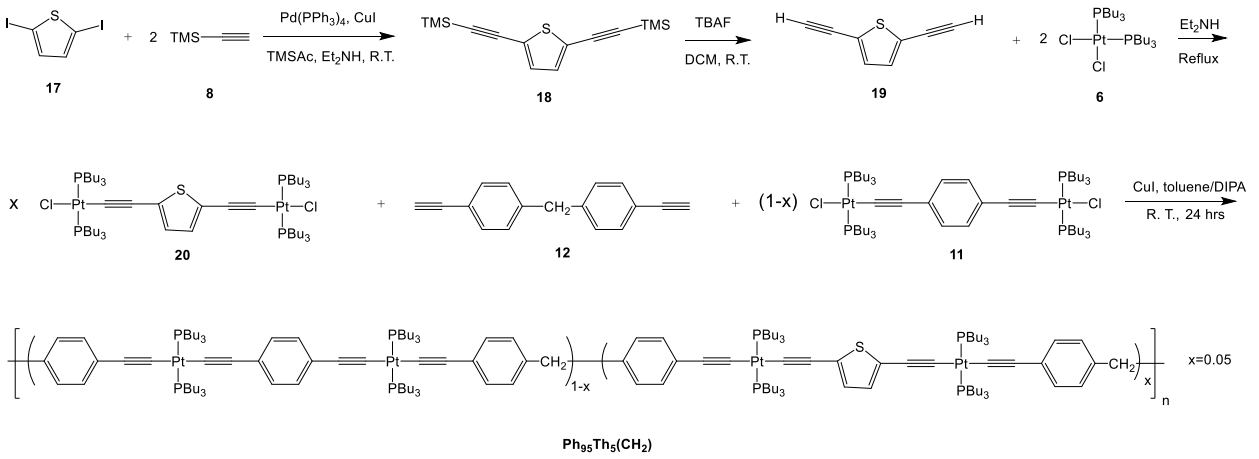

Figure 2-5. Synthesis of conjugation interrupted platinum acetylide co-polymers $Ph_{95}Th_5(CH_2)$.

Results and Discussion

UV-Visible Absorption and Steady-State Photoluminescence

The absorption and photoluminescence spectra of the series of polymers are illustrated below. First, the spectra of the conjugated phenylene-based homo-polymers, Ph_{100}, are considered, whose absorption spectrum exhibits one broad, featureless band with λ_{max} at 375 nm (Figure 2-6, dashed lines). This band is assigned to the long-axis polarized absorption of Ph_{100}.[59] The emission spectrum of Ph_{100} exhibits weaker peaks from 390 nm to 450 nm, which are assigned as fluorescence in view of previous studies.[59] The emission of this polymer at 516 nm is completely quenched in the presence of oxygen, and this peak is similar to the spectra of the same polymer reported in earlier investigations.[59] Therefore, the emission centered at 516 nm is assigned as phosphorescence.

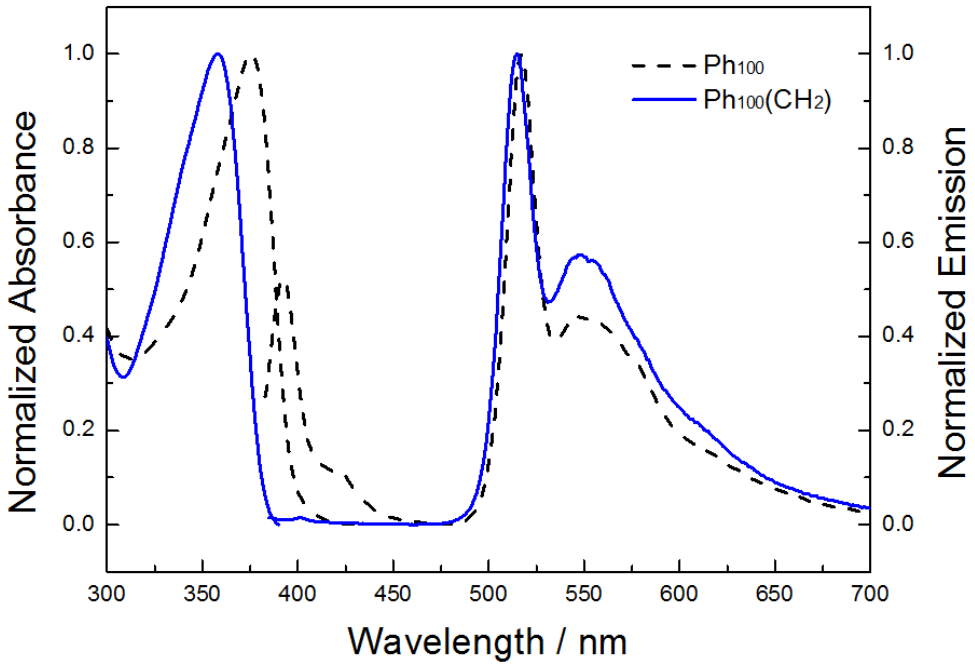

Figure 2-6. Normalized absorption and emission spectra of Ph_{100} (dashed lines) and $Ph_{100}(CH_2)$ (solid lines) in Ar-saturated THF. Excitation wavelengths: 365 nm for Ph_{100} and $Ph_{100}(CH_2)$.

The absorption spectrum observed for the conjugation interrupted phenylene-based homo-polymer, $Ph_{100}(CH_2)$, features a broad absorption with λ_{max} ~ 358 nm. $Ph_{100}(CH_2)$ exhibits much weaker fluorescence than Ph_{100} at around 390 nm due to the conjugation interrupted structure of $Ph_{100}(CH_2)$ (Figure 2-6, solid lines). The heavy atom effect can enhance intersystem crossing due to spin-orbit coupling, and the intersystem crossing rate becomes a fast process and competes favorably with higher singlet excitation and fluorescence or other relaxation pathways. Hence, this polymer shows prominent phosphorescence emission centered at 516 nm which is also completely quenched in the presence of oxygen.

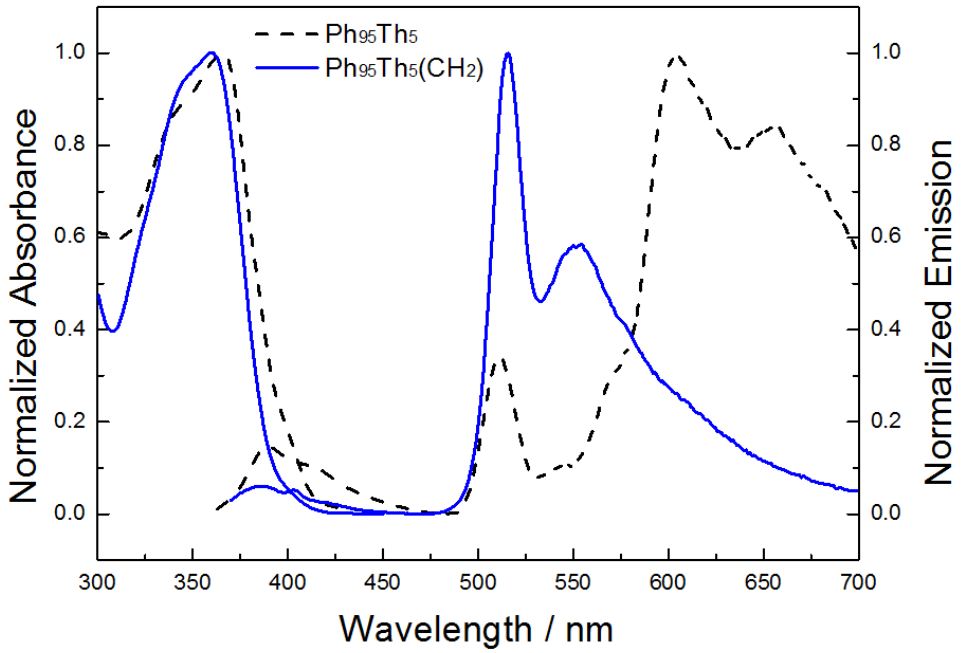

Figure 2-7. Normalized absorption and emission spectra of $Ph_{95}Th_5$ (dashed lines) and $Ph_{95}Th_5(CH_2)$ (solid lines) in Ar-saturated THF. Excitation wavelengths: 365 nm for $Ph_{95}Th_5$ and $Ph_{95}Th_5(CH_2)$.

A more complicated spectrum is found in the co-polymers. The absorption of conjugated phenylyne-thiophene co-polymer, $Ph_{95}Th_5$, is dominated by a broad band with λ_{max} at 365 nm, as depicted in Figure 2-7 (dashed lines). Based on our previous

research, $Ph_{95}Th_5$ exhibits a very weak emission band at 390 nm that is not quenched by oxygen.[58] This band is assigned to the mixture of phenylene-based and thiophene-based fluorescence. A band at 516 nm, corresponding to phenylene-based phosphorescence, is also apparent. However, this band is quite weaker than the phenylene-based phosphorescence in Ph_{100}, as displayed in Figure 2-8. Instead, a band distributed from 600 to 800 nm, corresponding to thiophene phosphorescence, dominates the spectrum. It is evident that from this observation that energy transfer occurs from phenylene moieties to thiophene moieties.

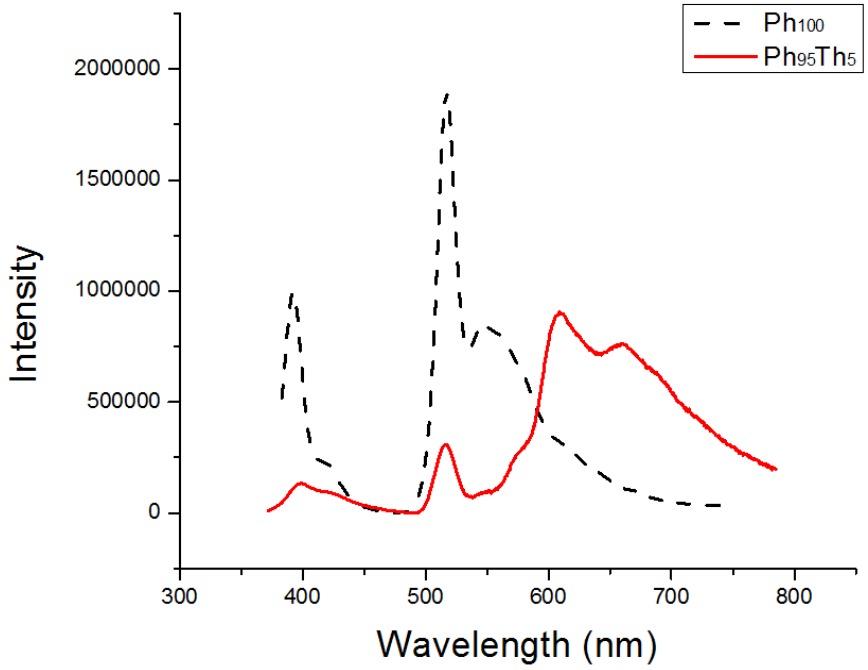

Figure 2-8. Emission spectra of Ph_{100} and $Ph_{95}Th_5$ (samples have matched absorbance = 0.3 O.D. @365 nm) in Ar-saturated THF. Intensities are absolute and reflect the relative quantum yields. Excitation wavelengths: 365 nm for Ph_{100} and $Ph_{95}Th_5$.

For the phenylene-thiophene conjugation interrupted co-polymer, $Ph_{95}Th_5(CH_2)$, its absorption is dominated by a broad band with λ_{max} at 361 nm. The emission spectrum of $Ph_{95}Th_5(CH_2)$ exhibits a weaker band at 390 nm that is not quenched by

oxygen. Because the fluorescence lifetime of both Ph_{100} and $Ph_{95}Th_5(CH_2)$ are approximately 1.1 ns, this band is assigned to phenylene-based fluorescence. Additionally, due to conjugation interrupted structure, the fluorescence intensity of $Ph_{95}Th_5(CH_2)$ is less than that of $Ph_{95}Th_5$. The band is at 516 nm which is nearly identical in shape and wavelength to the emission of the all-phenylene polymer, and as such it is assigned to emission of the phenylene based chromophore. It is interesting to note that as the conjugation structure of $Ph_{95}Th_5$ is interrupted, the thiophene-based phosphorescence is almost replaced by the phenylene-based phosphorescence, as shown in Figure 2-7 (solid lines). As expected, the energy transfer efficiency in conjugation interrupted co-polymers is more incomplete.

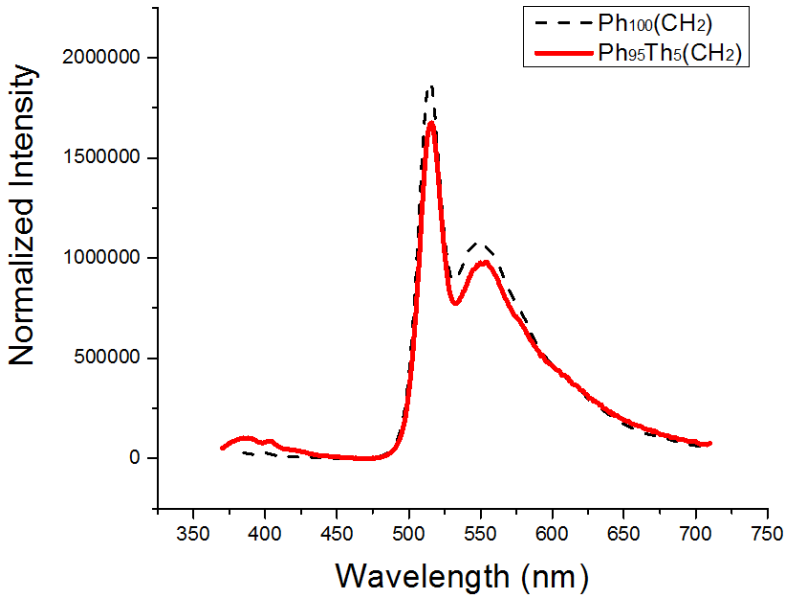

Figure 2-9. Emission spectra of $Ph_{100}(CH_2)$ and $Ph_{95}Th_5(CH_2)$ (samples have matched absorbance = 0.3 O.D. @365 nm) in Ar-saturated THF. Intensities are absolute and reflect the relative quantum yields. Excitation wavelengths: 365 nm for $Ph_{100}(CH_2)$ and $Ph_{95}Th_5(CH_2)$.

The emission spectrum of $Ph_{100}(CH_2)$ is compared with that of $Ph_{95}Th_5(CH_2)$, as depicted in Figure 2-9. The intensity of $Ph_{95}Th_5(CH_2)$ at 604 nm is slightly enhanced due

to very weak triplet energy transfer. The quantum yields of phenylene-based phosphorescence decreased sharply from Ph_{100} to $Ph_{95}Th_5$ (from 0.043 to 0.008), but only slightly from $Ph_{100}(CH_2)$ to $Ph_{95}Th_5(CH_2)$ (from 0.077 to 0.073). On the other hand, the quantum yields of thiophene-based emission increased from Th_{100} to $Ph_{95}Th_5$ (from 0.037 to 0.050). The quantum yields of the series of conjugated and conjugation interrupted polymers are tabulated in Table 2-1.

Table 2-1. Photophysical properties of these polymers in THF[a]

	Abs			Emission[b]			
Polymer	λ_{max}/nm	λ_{max}^F/nm	λ_{max}^P/nm	Φ^F	Φ^P (Ph^c) (500-575 nm)	Φ^P(Th^c) (575-800 nm)	Φ^P(Total[c]) (500-800 nm)
Ph_{100}	375	390	516	0.0016	-	-	0.043
$Ph_{100}(CH_2)$	358	-	516	0.0000	-	-	0.077
$Ph_{95}Th_5$	365	390	604	0.0008	0.008	0.050	0.058
$Ph_{95}Th_5(CH_2)$	361	390	516	0.0001	-	-	0.073
Th_{100}	400	425	604	0.0030	-	-	0.037

[a]Measurements for THF solutions at ambient temperature (argon outgassed for lifetime and quantum yield measurements). [b]F and P superscripts indicate fluorescence and phosphorescence, respectively. Φis emission quantum yield relative to $Ru(bpy)_3$ in degassed water for which quantum yield = 0.055. [c] Ph and Th indicate phenylene-based and thiophene-based phosphorescence, respectively.

Table 2-2. The kinetics of these polymers in THF

Polymer	τ_1/μs (A_1) (520 nm)	τ_2/μs (A_2) (520 nm)	τ_{median} (μs)[a] (520 nm)	τ_1/μs (A_1) (600 nm)	τ_2/μs (A_2) (600 nm)	τ_{median} (μs)[b] (600 nm)
Ph_{100}	18.30 (30.5%)	2.82 (69.5%)	7.50	-	-	-
$Ph_{100}(CH_2)$	16.70 (100.0%)	-	16.7	-	-	-
$Ph_{95}Th_5$	5.75 (21.2%)	1.08 (78.8%)	2.10	9.90 (23.0%)	5.20 (77.0%)	6.3
$Ph_{95}Th_5(CH_2)$	15.6 (100.0%)	-	15.9	7.26 (46.6%)	3.43 (53.4%)	5.2
Th_{100}	-	-	-	6.91 (50.7%)	3.09 (49.3%)	5.0

[a] The median lifetime was measured at phenylene-based phosphorescence emission maximum . [b] The median lifetime was measured at thiophene-based phosphorescence emission maximum .

In addition to the photophysical studies in solution, we were interested in understanding the photophysical mechanisms and exciton diffusion for this series of polymers in the solid state. Spin coated films were used for these experiments. The absorption spectra of the conjugated and conjugation interrupted homo-polymer films, Ph_{100} and $Ph_{100}(CH_2)$, were recorded and the results are presented in Figure 2-10. Ph_{100} and $Ph_{100}(CH_2)$ display a strong absorption band at λ_{max} = 376 nm and 357 nm respectively which correspond with the absorption spectra of Ph_{100} and $Ph_{100}(CH_2)$ in THF. The red-shifting of the Ph_{100} thin film absorption is consistent with the idea that the increasing conjugation length of the polymer leads to greater stabilization of the singlet excited state.

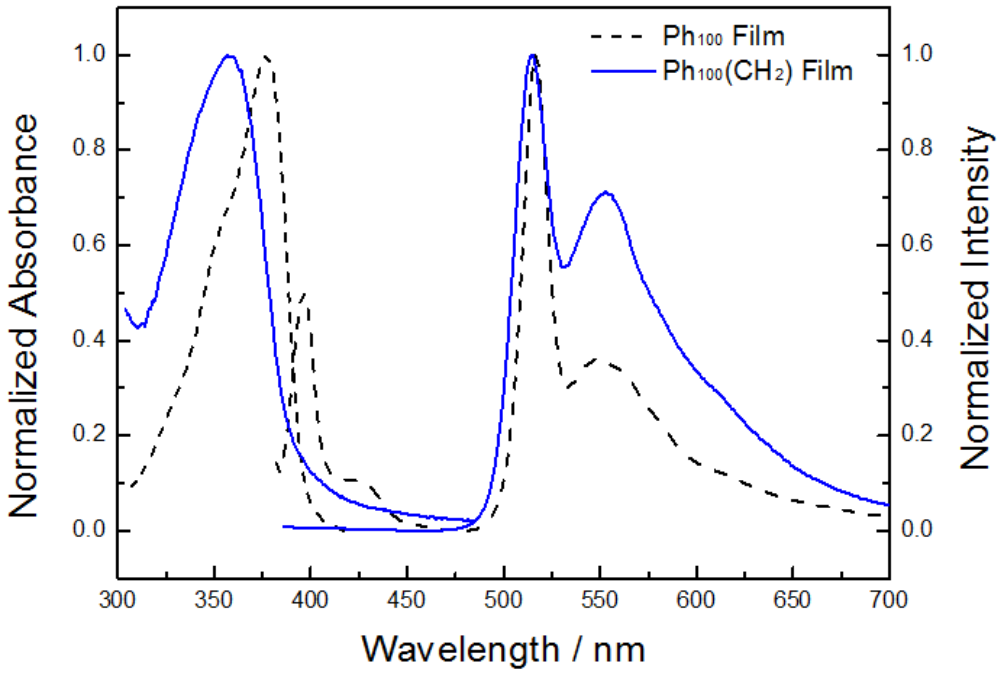

Figure 2-10. Normalized absorption and emission spectra of Ph_{100} (dashed lines) and $Ph_{100}(CH_2)$ (solid lines) thin films. Excitation wavelengths: 365 nm for Ph_{100} and $Ph_{100}(CH_2)$ thin films.

The photoluminescence of Ph_{100} and $Ph_{100}(CH_2)$ films was recorded with the excitation wavelength λ = 365 nm and the spectra are also shown in Figure 2-10. The fluorescence emission band for Ph_{100} thin film is located at 390 nm and the phosphorescence band is centered at λ = 516 nm and it arises from the relaxation of a well-studied triplet excited state.[60] Very little fluorescence for the $Ph_{100}(CH_2)$ thin film is seen in the spectrum, implying that intersystem crossing is very efficient. The phosphorescence emission band of $Ph_{100}(CH_2)$ appears similar to that of Ph_{100}, which is also dominated by a sharp band with a maximum at λ = 516 nm. This sharp band was proved to originate from a phenylene-based triplet excited state.

For the conjugated and conjugation interrupted co-polymers, $Ph_{95}Th_5$ and $Ph_{95}Th_5(CH_2)$, the absorption spectra were measured, as depicted in Figure 2-11. The strong absorption bands of $Ph_{95}Th_5$ and $Ph_{95}Th_5(CH_2)$ are located at λ_{max} = 366 nm and 360 nm respectively, which are very similar with the absorption spectra of $Ph_{95}Th_5$ and $Ph_{95}Th_5(CH_2)$ in THF. The interruption of the conjugation structure by the methylene spacer results in the blue-shifting of the $Ph_{95}Th_5(CH_2)$ thin film absorption.

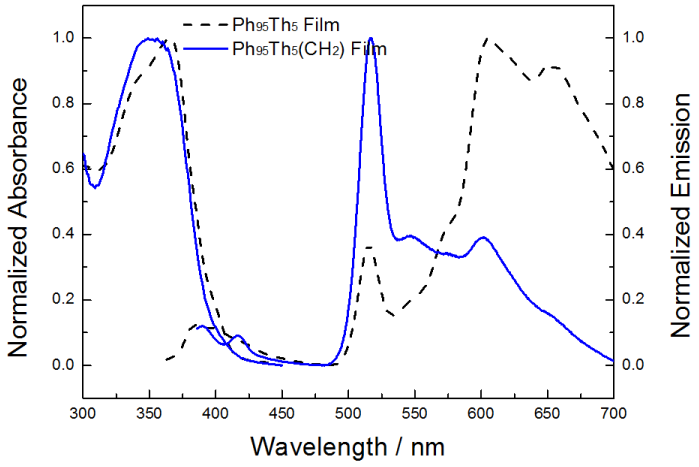

Figure 2-11. Normalized absorption and emission spectra of $Ph_{95}Th_5$ (dashed lines) and $Ph_{95}Th_5(CH_2)$ (solid lines) thin films. Excitation wavelengths: 365 nm for $Ph_{95}Th_5$ and $Ph_{95}Th_5(CH_2)$ thin films.

In Ar-saturated cuvette, the photoluminescence of $Ph_{95}Th_5$ and $Ph_{95}Th_5(CH_2)$ thin films was detected with the excitation wavelength λ = 365 nm and the spectra are also presented in Figure 2-11. The spectrum of $Ph_{95}Th_5$ thin film is dominated by a broad band with a maximum at λ = 604 nm, while the phosphorescence band at λ =516 nm observed in $Ph_{95}Th_5$ is relatively weak. This broad band is believed to originate from the thiophene-based triplet excited state. This assignment is made by comparison with the broad phosphorescence observed around λ = 604 nm in a platinum acetylide polymer with a thiophene unit as a spacer.[55] Some broad fluorescence is also seen in this spectrum (λ = 390 nm) and it is believed to originate from the mixtures of phenylene-based and thiophene-based singlet excited state.[60] $Ph_{95}Th_5(CH_2)$ thin film also displays the mixtures of phenylene-base and thiophene-based fluorescence emission at 390 nm. The band is centered at λ = 516 nm which represents the phenylene-based phosphorescence.[60] The weaker band of $Ph_{95}Th_5(CH_2)$ at λ = 604 nm is ascribed to the thiophene-based phosphorescence emission.[55] Thus, the triplet energy transfer in conjugation interrupted co-polymer, $Ph_{95}Th_5(CH_2)$, occurs weakly because of the conjugation interrupted structure.

Time-Resolved Photoluminescence

In order to understand the photophysical dynamics of the conjugated and conjugation interrupted polymers, Ph_{100}, $Ph_{100}(CH_2)$, $Ph_{95}Th_5$ and $Ph_{95}Th_5(CH_2)$, the time-resolved photoluminescence were carried out on this series of polymers. The triplet excitons which were produced by the phenylene-based chromophores in conjugated co-polymer, $Ph_{95}Th_5$, was quenched by the thienylene repeats, which act as a triplet energy trap, as presented in Figure 2-12a. The median phosphorescence lifetime monitored at 516 nm for Ph_{100} and $Ph_{95}Th_5$ decreases from 7.5 μs to 2.1 μs (Table 2-2).

The median phosphorescence lifetime monitored at 604 for $Ph_{95}Th_5$ is 6.3 μs, which corresponds closely to the phosphorescence lifetime of the conjugated thiophene-based homopolymer, Th_{100}, as listed in Table 2-1. By contrast, the triplet excitons in the conjugation interrupted co-polymer, $Ph_{95}Th_5(CH_2)$, were quenched only slightly by triplet energy traps, as displayed in Figure 2-12b. The phosphorescence kinetic decays were detected at 520 for $Ph_{100}(CH_2)$ and $Ph_{95}Th_5(CH_2)$. The phosphorescence lifetime of $Ph_{100}(CH_2)$ and $Ph_{95}Th_5(CH_2)$ deceases from 16.7 μs to 15.6 μs (Table-2-1).

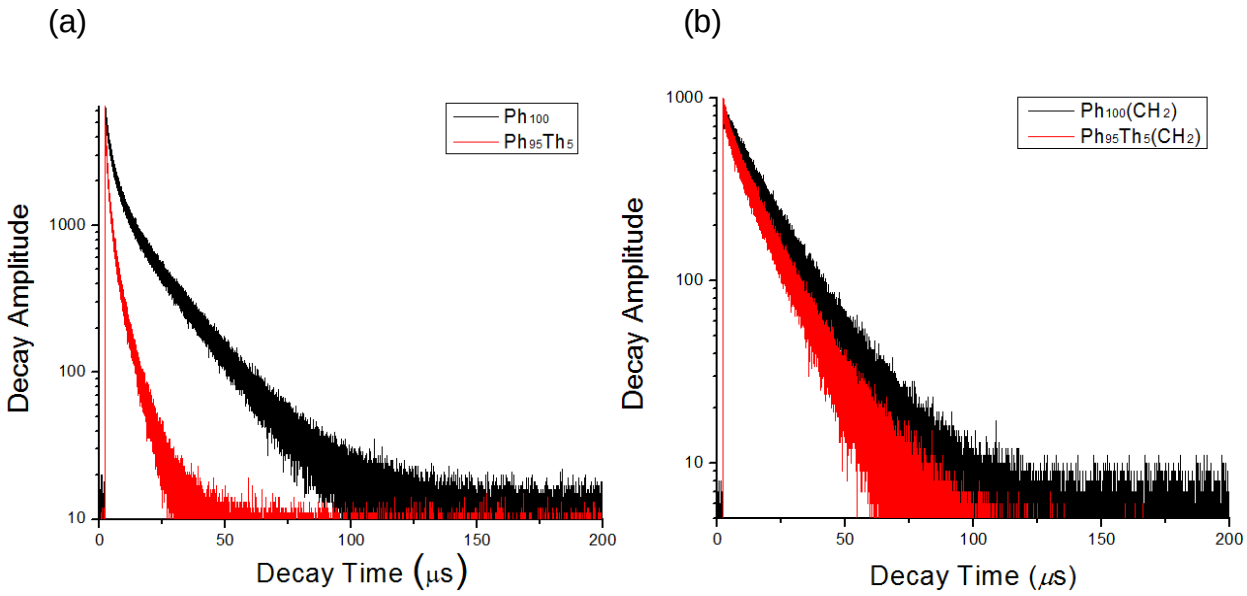

Figure 2-12. Time-resolved photoluminescence spectra of (a) Ph_{100} and $Ph_{95}Th_5$ in Ar-saturated THF (b) $Ph_{100}(CH_2)$ and $Ph_{95}Th_5(CH_2)$ in Ar-saturated THF. The phosphorescence lifetime monitored at 520 nm with 375 nm excitation wavelengths for Ph_{100}, $Ph_{100}(CH_2)$, $Ph_{95}Th_5$ and $Ph_{95}Th_5(CH_2)$.

The photophysical dynamics of the conjugated and conjugation interrupted polymer thin films were investigated with time-resolved photoluminescence to explore the photophysics in solid state. Similarly, the triplet excited states in conjugated co-polymer thin films, $Ph_{95}Th_5$, were quenched by the thienylene repeats, as shown in Figure 2-13a. The phosphorescence lifetime recorded at 516 nm for Ph_{100} and $Ph_{95}Th_5$ thin films deceases from 1.16 μs to 0.30 μs (Table 2-3). The phosphorescence lifetime

recorded at 600 for $Ph_{95}Th_5$ thin film is 0.92 μs, which is ascribed to the phosphorescence emission of conjugated thiophene-based homopolymer thin film, Th_{100} (Table 2-1). In contrast with conjugated polymers, the triplets in the conjugation interrupted co-polymer, $Ph_{95}Th_5(CH_2)$, were quenched slightly by thiophene repeats due to the interrupted structure in this co-polymer (Figure 2-13b).

The photoluminescence kinetics were collected at 516 nm with Nanoquant for $Ph_{100}(CH_2)$ and $Ph_{95}Th_5(CH_2)$ thin films. The phosphorescence lifetime of $Ph_{100}(CH_2)$ and $Ph_{95}Th_5(CH_2)$ films measured at 516 nm deceases from 2.15 μs to 1.78 μs (Table 2-3). The time-resolved photoluminescence of $Ph_{95}Th_5(CH_2)$ at 604 nm was measured, and its lifetime is 0.83 μs, which is corresponding to the lifetime of Th_{100} (τ = 0.77 μs) (Table 2-3). This indicates that the weak triplet energy transfer occurs in the conjugation interrupted systems in solution and the solid state.

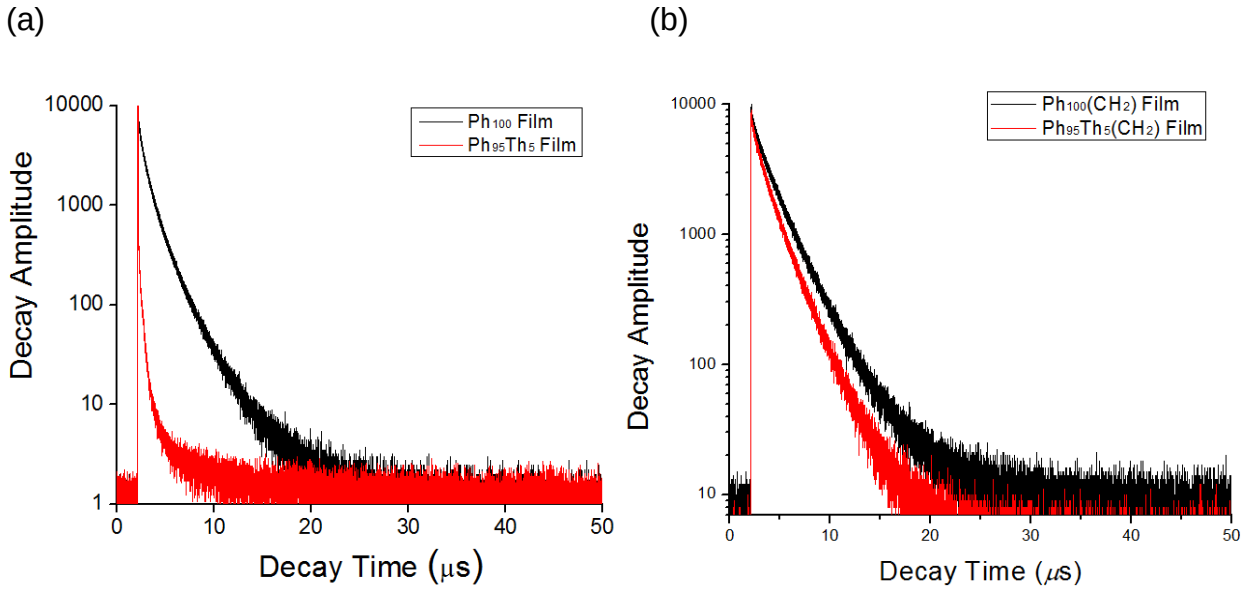

Figure 2-13. Time-resolved photoluminescence spectra of (a) Ph_{100} and $Ph_{95}Th_5$ thin films (b) $Ph_{100}(CH_2)$ and $Ph_{95}Th_5(CH_2)$ thin films. The phosphorescence lifetime monitored at 520 nm with 375 nm excitation wavelengths for Ph_{100}, $Ph_{100}(CH_2)$, $Ph_{95}Th_5$ and $Ph_{95}Th_5(CH_2)$ films.

Table 2-3. Photophysical properties of these polymer thin films[a]

	absorption	emission[b]	
Polymer	λ_{max}/nm	λ_{max}^{F}/nm	λ_{max}^{P}/nm
Ph_{100}	376	390	516
$Ph_{100}(CH_2)$	357	-	516
$Ph_{95}Th_5$	366	390	604
$Ph_{95}Th_5(CH_2)$	360	390	516
Th_{100}	400	425	604

[a] Measurements for polymer thin films at ambient temperature (argon-saturated for emission and lifetime measurements). [b] F and P superscripts indicate fluorescence and phosphorescence, respectively.

Table 2-4. The kinetics of these polymers thin films

Polymer	τ_1/μs (A_1) (520 nm)	τ_2/μs (A_2) (520 nm)	τ_{median} (μs)[a] (520 nm)	τ_1/μs (A_1) (600 nm)	τ_2/μs (A_2) (600 nm)	τ_{median} (μs)[b] (600 nm)
Ph_{100}	2.35 (25.0%)	0.76 (75.0%)	1.16	-	-	-
$Ph_{100}(CH_2)$	2.15 (100.0%)	-	2.15	-	-	-
$Ph_{95}Th_5$	0.81 (22.7%)	0.15 (77.3%)	0.30	5.21 (9.8%)	0.46 (90.2%)	0.92
$Ph_{95}Th_5(CH_2)$	1.78 (100.0%)	-	1.78	4.80 (9.4%)	0.42 (90.6%)	0.83
Th_{100}	-	-	-	4.78 (8.7%)	0.39 (91.3%)	0.77

[a] The median lifetime was measured at phenylene-based phosphorescence emission maximum . [b] The median lifetime was measured at thiophene-based phosphorescence emission maximum .

Transient Absorption

A solution of Ph_{100} in THF was prepared to measure nanosecond transient absorption spectrum. The TA spectrum was collected from 350 nm to 850 nm and data processing was done with Matlab. One hundred averages were taken at each time. The solution showed a broad transient absorption peak over the wavelength range 350 nm to acquisition end, with ΔA_{max} at approximately 650 nm (Figure 2-14). After this measured Ph_{100} solution was saturated by air, the triplet state absorption was decayed completely. Thus these bands are assigned to the triplet-triplet ($T_1 \rightarrow T_n$) absorption of

the polymers. For TA measurement of $Ph_{100}(CH_2)$ in degassed THF, the same experimental process mentioned above was used.

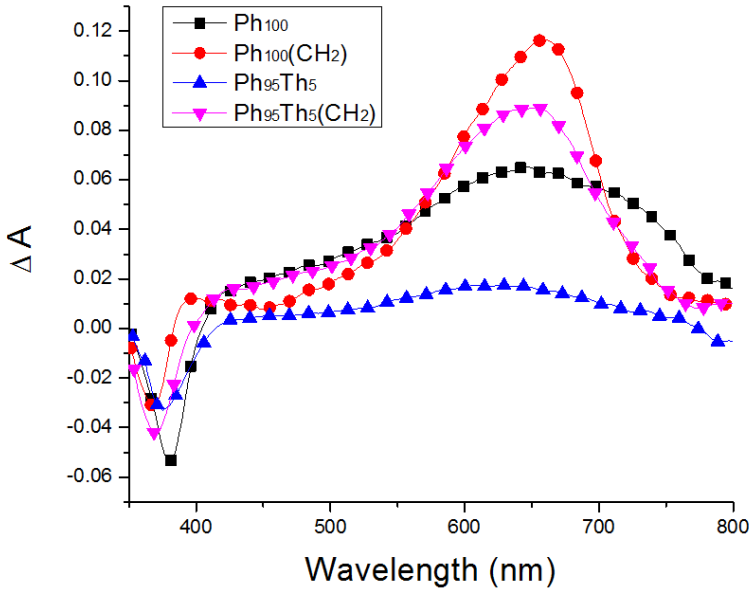

Figure 2-14. Nanosecond transient absorption spectra of Ar-saturated polymers in THF. (samples have matched absorbance = 0.7 O.D. @355 nm). The spectrum was obtained at 50 ns delay after photoexcitation with a 10 mJ, 355 nm laser with a 10 ns pulse width.

The TA spectra are characterized by strong bleaching in the near-UV region due to ground-state depletion, along with broad, moderately intense excited-state absorption extending throughout the visible region with a maximum between 400 and 800 nm (Figure 2-14). The absorbance of the triplet excited states of the $Ph_{100}(CH_2)$ is four times higher than that of Ph_{100} for the equivalent bleaching values. From the transient absorption of $Ph_{95}Th_5$, It was found that phenylene-based triplet excited states at 650 nm were quenched effectively by thiophene-based chomophores in $Ph_{95}Th_5$ co-polymers, giving rise to considerably reduced transient absorption intensity. In contrast, the quenching of the conjugation interrupted co-polymer, $Ph_{95}Th_5(CH_2)$, is more inefficient in comparison with conjugated co-polymer, $Ph_{95}Th_5$. Transient absorption

spectra reveal that energy transfer efficiency of conjugated polymers is faster than that of conjugation interrupted polymer.

Reversible Energy Transfer

Based on the phosphorescence energies for Ph_{100} and Th_{100} (2.40 and 2.05 eV, respectively), it is obvious that the energy of the $^3\pi,\pi^*$ state localized on a Pt - Th repeat unit is ca. 0.35 eV lower in energy than that localized on a Pt - Ph repeat, as shown in Figure 2-18 (a). So intrachain triplet energy transfer occurs in the $Ph_{95}Th_5$ copolymer.[58] In the emission spectrum of $Ph_{95}Th_5$ thin film (Figure 2-11), we observe that there is a small fraction of phenylene-based phosphorescence (λ = 520 nm). Uoyama[61] and Dias[62] groups reported that reverse energy transfer in a molecule is efficient as the energy gap is very small (ΔE < 0.5 eV). Thus, we think the weak phenylene-based phosphorescence is from the reversible energy transfer because the energy gap between a ^{3}Pt - Th repeat and a ^{3}Pt - Ph repeat unit is 0.35 eV.

In order to prove this viewpoint, the similar conjugated copolymer with 4,7-benzothiadiazole (BTD) and 1,4-phenylene (Ph) units at BTD:Ph = 1:19 ($Ph_{95}BTD_5$) is designed and synthesized, as shown in Figure 2-15. The absorption spectrum of the $Ph_{95}BTD_5$ copolymer in Ar-saturated THF is shown in Figure 2-16. First, the spectrum of $Ph_{95}BTD_5$ is dominated by abroad band with λ_{max} = 375 nm, with a weak band on the low-energy side at ca. 500 nm. The primary absorption band is very similar in shape and energy compared to that of Ph_{100}, and on this basis it is assigned to the phenylene-based repeat units (Pt-Ph) in the Pt - acetylide backbone. The weak band at 500 nm appears at a similar wavelength compared to the absorption of the BTD_{100} homopolymer,[63] and on this basis it assigned to chromophores in the chain that contain the benzothiadiazole unit (Pt-BTD). The photoluminescence spectra of the $Ph_{95}BTD_5$

copolymer and the Ph_{100} homopolymer thin films are shown together in Figure 2-17. The emission spectra were obtained with 375 nm excitation, which corresponds to excitation into the dominant absorption band. For $Ph_{95}BTD_5$, the emission at 298 K is dominated by a band with λ_{max} = 580 nm that corresponds to Pt-BTD fluorescence.[63] The phenylene-based phosphorescence of the $Ph_{95}BTD_5$ copolymer at 520 nm was almost completely quenched due to the 4,7-benzothiadiazole unit functions as a "trap". According to the phosphorescence energies for Ph_{100} and BTD_{100} (2.40 and 1.50 eV[63], respectively), the energy gap between a ^{3}Pt - Th repeat and a ^{3}Pt - BTD repeat is 0.9 eV, as displayed in Figure 2-18 (b). In the emission spectra of Ph_{100} and $Ph_{95}BTD_5$ thin films (Figure 2-17), there is almost no phenylene-based phosphorescence (520 nm) in the $Ph_{95}BTD_5$ copolymer because reversible energy transfer is quiet inefficient due to the large energy gap ($\Delta E = 0.9$ eV).

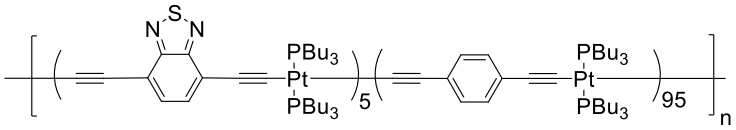

Figure 2-15. The structure of $Ph_{95}BTD_5$.

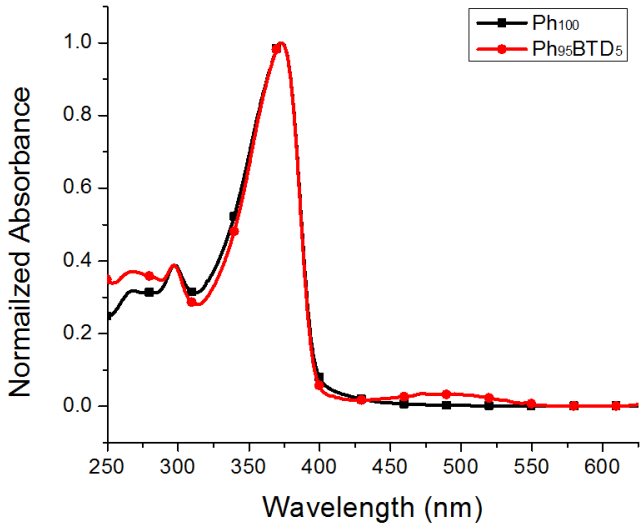

Figure 2-16. Absorption spectra of Ph_{100} and $Ph_{95}BTD_5$ in THF.

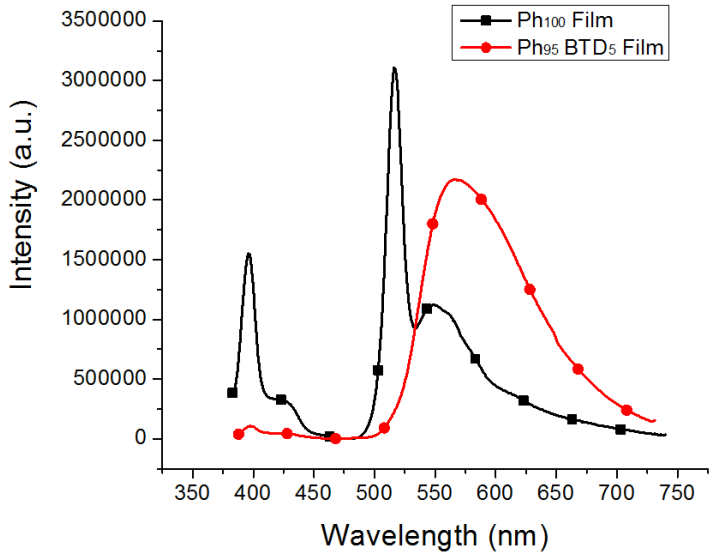

Figure 2-17. Emission spectra of Ph_{100} and $Ph_{95}BTD_5$ thin films. Excitation wavelengths: 365 nm for Ph_{100} and $Ph_{95}BTD_5$ thin films. Excitation wavelengths: 375 nm for Ph_{100} and $Ph_{95}BTD_5$ thin films.

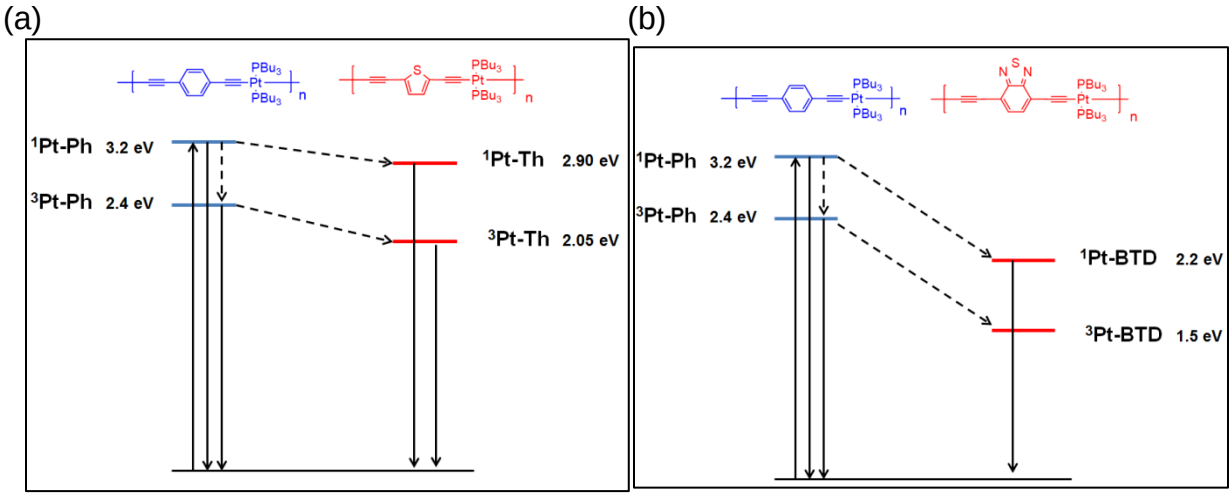

Figure 2-18. Jablonski diagrams for (a) $Ph_{95}Th_5$ and (b) $Ph_{95}BTD_5$ copolymers. These figure were modified from Schanze.[58]

Zimmerman[64] group has built a model relating the reversible energy transfer of donor-acceptor systems. This model can be applied to the $Ph_{95}Th_5$ copolymer because of the same photophysical processes. The excitation of the Phenylene moiety led to energy transfer to the thiophene moiety, with decay of the two chromophores to ground

state. This decay is both radiative and radiationless. The mechanism in the $Ph_{95}Th_5$ copolymer can be described by using the kinetic picture in Equation 2-1.

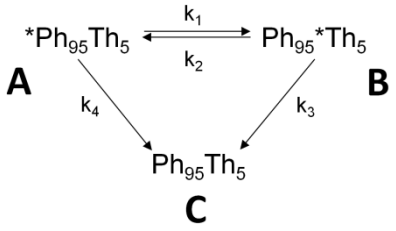

(2-1)

Here Ph is the phenylene moiety, Th is the thienylene moiety and the asterisk indicates electronic excitation. Because A is produced momentarily by the excitation of phenylene moiety, we do not need to consider processes leading to A other than those in Equation 2-1. Theory suggested a decay of the form of Equation 2-2 and Equation 2-3.

$$[\mathrm{A}] = L_1 e^{-m_1 t} + L_2 e^{-m_2 t} \quad (2\text{-}2)$$

$$[\mathrm{B}] = L_3 (e^{-m_2 t} - e^{-m_1 t}) \quad (2\text{-}3)$$

where A and B are defined above in Equation 2-1 and L_1, L_2 and L_3 are positive constants.

It is notable that the experimentally observed rate constants, m_1 and m_2, do not correspond directly to the rates of energy transfer and decay (i.e., k_1, k_2, k_3, and k_4). For a kinetic scheme of the type in Equation 2-1, Evans[65] has derived the dependence of [A] and [B] as a function of time. The operational rate constants m_1 and m_2 are given by Equation 2-4 and Equation 2-5.

$$m_1 = \left(\frac{1}{2}\right)\{(k_1 + k_2 + k_3 + k_4) + [(k_1 + k_2 + k_3 + k_4)^2 - 4(k_2 k_4 + k_1 k_3 + k_3 k_4)^{\frac{1}{2}}\} \quad (2\text{-}4)$$

$$m_2 = \left(\frac{1}{2}\right)\{(k_1 + k_2 + k_3 + k_4) - [(k_1 + k_2 + k_3 + k_4)^2 - 4(k_2 k_4 + k_1 k_3 + k_3 k_4)^{\frac{1}{2}}\} \quad (2\text{-}5)$$

Two useful expressions, Equation 2-6 and Equation 2-7, can be derived from Equation 2-2 and Equation 2-3.

$$m_1 + m_2 = (k_1 + k_2 + k_3 + k_4) \quad (2\text{-}6)$$

$$m_1 m_2 = k_2 k_4 + k_1 k_3 + k_3 k_4 \quad (2\text{-}7)$$

Zimmerman[64] suggested to use the decay rates of model Ph_{100} and Th_{100} monochromophoric systems to get k_4 and k_3, respectively (Table 2-4). Then we use Equation 2-6 and Equation 2-7 to obtain the two remaining unknown rates k_1 and k_2. These results are given in Table 2-5. The reverse rate constant, k_2, is much lower than the forward rate constant, k_1. This result demonstrates that the intensity of phenylene-based phosphorescence of $Ph_{95}Th_5$ thin films is feeble.

Table 2-5. Rate of energy transfer and decay to ground state of $Ph_{95}Th_5$ thin film

Polymer	k_1, s^{-1}	k_2, s^{-1}	k_3, s^{-1}	k_4, s^{-1}
$Ph_{95}Th_5$	5.1×10^6	8.8×10^5	1.3×10^6	5.1×10^6

Closing Remark

In this chapter, a series of conjugated and conjugation interrupted polymers were designed and prepared for the photophysical studies. Conjugated polymers, Ph_{100} and $Ph_{95}Th_5$ and conjugation interrupted polymers, $Ph_{100}(CH_2)$ and $Ph_{95}Th_5(CH_2)$, absorb around 300-400 nm. A red-shift of absorbance was observed from conjugation interrupted polymers to conjugated polymers due to increasing conjugation length.[66] This result indicates the ground state of conjugated polymers is more highly delocalized than the corresponding conjugation interrupted polymers. In addition, there is no change in the phosphorescence spectra (500-600 nm) of conjugated polymers and conjugation interrupted polymers. This shows that a highly localized T_1 state is confined between two Pt centers. Hence, we find that the conjugated polymers absorbed at lower energies

than the conjugation interrupted polymers, but the phenylene-base phosphorescence of all polymers are located at 520 nm.

According to the experimental photophysical results, triplet energy transfer mechanisms take place at room temperature in the conjugated copolymers; the exciton can transport to a lower energy trap more ineffectively while the π-conjugation structure is interrupted with methylene spacer. Additionally, in comparison to emission spectrum of the $Ph_{95}BTD_5$ copolymer thin film, relatively low phenylene-base phosphorescence still exists in the $Ph_{95}Th_5$ thin films. Thus, we think that the reversible energy transfer occurs between excited phenylene moieties and excited thienylene moieties due to a small energy gap between a ^{3}Pt - Th repeat and a ^{3}Pt - Ph repeat in the $Ph_{95}Th_5$ thin films. According to a kinetic model built by Zimmerman[64] group, the $Ph_{95}Th_5$ copolymer is treated kinetically as A⇄B→C processes. The result can confirm that the slower reverse energy transfer rate results in weaker phenylene-base phosphorescence.

Experimental

Materials

Starting materials 1, 2, 3, 8, 13, 17 were obtained from commercial sources. Compounds 4-7[67] 6[68], 9-11[69], 12[55], 14-20[70] were synthesized according to the literature procedures. All reactions were performed under nitrogen atmosphere in anhydrous solvents, which were dried prior to use following standard procedures. Merck silica gel 60 (particle size 0.04−0.063 mm) was employed for flash chromatography.

^{1}H NMR, ^{13}C NMR, ^{31}P NMR spectra were obtained on a VXR-300 instrument using deuterated chloroform ($CDCl_3$) as the solvent and tetramethylsilane (TMS) as the internal reference. Gel permeation chromatography (GPC) was performed by eluting a tetrahydrofuran (THF) solution of the polymer through two PL-Gel 5 Mixed D columns

pressurized by a Rainin Dynamax SD-200 solvent pump. Polymer elution was spectroscopically monitored using a UV detector set to a wavelength where the polymer absorbs, and molecular weight calculations were performed using Polymer Laboratories PL software against a polystyrene standard. All solvents used were of HPLC grade.

Synthesis

3-{4-[(Triisopropylsilyl)-ethynyl]-phenyl}-prop-2-yn-1-ol (4). 1,4-Diiodobenzene (5.0 g, 15.16 mmol) was dissolved in THF (60 mL) and *i*-Pr_2NH (40 mL) in a Schlenk flask and the solution was degassed with argon for 30 min. Then, tri-iso-propylsilylacetylene (2.76 g, 15.16 mmol), propargyl alcohol (0.85g, 15.16 mmol), $Pd(PPh_3)_2Cl_2$ (12 mg, 1.6 mmol) and CuI (0.346 g, 1.8 mmol) were added. The mixture was stirred at 70˚C for 3 hours. After cooling down, the mixture was passed through a bed of Celite, washed with 10% NH_4OH (3 x 50 mL) and water (3 x 50 mL), the organic phase dried on $MgSO_4$, filtered and the solvents were removed. Chromatography on silica (hexane first, then 9:1 hexane/CH_2Cl_2) gave the desired product 4 as a red oil (1.65 g, 35 %). ^{1}H NMR ($CDCl_3$, 300 MHz): δ (ppm) 1.20 (s, 21H), 4.40 (br, 1H), 4.58 (s, 2H), 7.40 (m, 4H); ^{13}C NMR ($CDCl_3$, 75 MHz): δ (ppm) 11.4, 18.7, 51.1, 85.1, 89.3, 92.5, 106.7, 122.7, 123.6, 131.5, 131.9.

1-Ethynyl-4-(tri-iso-propylsilylethynyl)-benzene (5). 3-{4-[(Tri-iso-propylsilyl)-ethynyl]-phenyl}-prop-2-yn-1-ol (1.43 g, 4.58 mmol) was dissolved in Et_2O (80 mL) and degassed with nitrogen for 15min. Then, activated MnO_2 (6.37 g, 73.3 mmol) and KOH (2.05 g, 36.6 mmol) were added in four fractions every hour and mixture was stirred at room temperature for 4 hours protected from light. After this time, mixture was washed with 5% HCl (3 x 50 mL), water (3 x 50 mL), dried on $MgSO_4$, filtered and the solvent was removed. Chromatography (silica gel, hexane) gave the desired product 5 as a red

oil (0.99 g, 86 %). ^{1}H NMR ($CDCl_3$,300 MHz): δ (ppm) 0.98 (s, 21H), 2.98 (s, 1H), 7.22 (s, 4H); ^{13}C NMR ($CDCl_3$, 75 MHz): δ (ppm) 11.3, 18.6, 78.8, 83.2, 92.9, 106.4, 121.9, 124.0, 131.9.

trans-Bis(tributylphosphine)chloro{(4-Ethynyl-phenylethynyl)-triisopropyl-silane}platinum(II) (7). 1-Ethynyl-4-(tri-iso-propylsilylethynyl)-benzene (0.36 g, 1.28 mmol) and Et_2NH (30 mL) were added to a round bottom flask with a stir bar. The mixture was stirred and degassed with argon for 10 min, follow by the addition of cis-$Pt(PBu_3)_2Cl_2$ (0.95 g, 1.41 mmol). The reaction was stirred at reflux under argon overnight, then cooled and diluted with CH_2Cl_2. The organic solution was washed with both d.i. water and brine then dried over $NaSO_{4(s)}$. TLC in 5:1 hexane/CH_2Cl_2 gave 4 spots (spot 3 was product). Solvent was evaporated to give a crude solid that was purified by flash chromatography (silica gel, 9:1 to 3:1 hexane/CH_2Cl_2). Fraction 3 solvent was evaporated to afford a yellow crystalline solid that did not phosphoresce under a long wave UV lamp. Yield 0.97 g (82.6%). M.p. 65-67 ℃. ^{1}H NMR (300 MHz, $CDCl_3$): δ (ppm) 0.89 (t, 18H), 1.18 (s, 21H), 1.3-1.6 (br m, 24H), 1.98 (br m, 12H), 7.14 (d, 2H), 7.31 (d, 2H). ^{31}P NMR ($CDCl_3$): δ (ppm) 8.0 (J = 2356 Hz).

Ph_{100}. Monomer 7 (250 mg, 0.272 mmol) was dissolved in a 7:2 mixture of diisopropy-amine:THF (9 mL) in a Schlenk flask. The solution was degassed over 5 freeze-pump-thaw cycles. The flask was backfilled with dry argon and tetrabutylammonium fluoride (0.144 g, 0.54 mmol) was added via syringe. A white precipitate immediately formed from the yellow-colored solution. The reaction was stirred at room temperature for about 40 min, at which time a TLC with 1:4 hexanes:DCM revealed total consumption of 7. Copper (I) iodide (2.8 mg, 0.015 mmol)

was then added and the reaction heated to 44 ℃. After stirring overnight, it was noticed that the polymerization reaction formed a neon-yellow suspension. The reaction was poured into an excess of methanol, precipitating the polymer as yellow fibers. The precipitate was filtered using a 2.5 µm glass fiber filter pad and redisolved in THF. The solution was reprecipitated into an excess of methanol and filtered using a glass fiber filter pad. The yellow fibers were once again redissolved in THF, precipitated from methanol, and filtered for a third and final time. After the final precipitation, the polymer was dried under a vacuum at room temperature overnight to give Ph_{100} (126 mg, 64%). The polymer was characterized by GPC, UV-VIS/emission and by NMR. ^{1}H NMR ($CDCl_3$, 300 MHz): δ (ppm) 0.91 (t, 18H), 1.44 (q, 24H), 2.12 (m, 8H), 7.09 (s, 4H). ^{31}P NMR ($CDCl_3$, 120 MHz): δ (ppm) 3.96 (t, 2360 Hz). GPC: Mn = 55,100; Mw = 163,200, PDI= 2.96.

1,4-Bis(trimethylsilylethynyl)benzene (9). To a flask charged with THF and diiospropylamine (DIPA) (8 mL, 1:1) was added 1,4-diodobenzene (660 mg, 2.0 mmol). The resulting solution was degassed for 30 min by purging with argon. This solution was added trimethylsilylacetylene (491 mg, 5 mmol), $Pd(PPh_3)_4$ (12 mg, 1.6 mmol), and copper iodide (4 mg, 2 mmol). The reaction was then stirred at room temperature for 24 hours. After this time the solvent was removed under reduced pressure. Flash chromatography of the residue with hexanes gave the desired product as a yellow solid. (yield 440 mg, 80%). ^{1}H NMR ($CDCl_3$, 300MHz): δ (ppm) 0.24 (s, 18H), 7.32 (s, 4H); ^{13}C NMR ($CDCl_3$, 300 MHz): δ (ppm) -0.23, 78.86, 84.90, 122.47, 131.29.

1,4-Diethynyl-benzene (10). 1,4-Bis(trimethylsilylethynyl)benzene 9 (73.5 mg, 0.272 mmol) was dissolved in a 1:1 mixture of methanol:DCM (9 mL) in a round flask.

The solution was purged by dry argon for 15 min and potassium carbonate (75.6 mg, 0.54 mmol) was added instantly. And then the reaction was stirred at room temperature for about 3 hours, at which time a TLC with 2:1 hexanes:DCM revealed total consumption of 9. (yield 61 mg, 80%). ^{1}H NMR ($CDCl_3$, 300MHz): δ (ppm) 3.06 (s, 2H), 7.39 (d, 2H); ^{13}C NMR ($CDCl_3$, 300 MHz): δ (ppm) 78.23, 84.12, 123.43, 131.08.

Complex (11). 1,4-Diethynylbenzene (46.2 mg, 0.373 mmol) and cis-dichloro-bis-(tri-n-butylphosphine) platinum(II) 6 (500.1 mg, 0.75 mmol) were dissolved in Et_2NH (15 mL) and the solution was degassed with nitrogen. The mixture was stirred under reflux for 8 hours. The solvent was removed and the crude product purified by flash chromatography (silica gel, hexane then 7:3 hexane/CH_2Cl_2) giving the desired product 11 as a yellow solid (210 mg, 40 %). ^{1}H NMR ($CDCl_3$, 300 MHz): δ (ppm) 0.85-1.0 (t, 36H), 1.40-1.63 (m, 48H), 1.9-2.0 (m, 24H), 7.05 (s, 4H); ^{13}C NMR ($CDCl_3$, 75 MHz): δ (ppm) 14.0, 22.1, 24.5, 26.3, 101.6, 125.3, 130.5; ^{31}P NMR ($CDCl_3$, 121 MHz): δ (ppm) 7.89 ($J_{Pt\text{-}P}$ = 2390.8 Hz).

$Ph_{100}(CH_2)$. Complex 11 (250 mg, 0.272 mmol) was added with compound 12 (58.8 mg, 0.272 mmol) and Copper (I) iodide (2.8 mg, 0.015 mmol) in a 7:2 mixture of diisopropyamine:THF (9 mL) in a Schlenk flask. The solution was degassed over 5 freeze-pump-thaw cycles. The flask was backfilled with dry argon. After stirring overnight at room temperature, it was noticed that the polymerization reaction formed a white suspension. The reaction was poured into an excess of methanol, precipitating the polymer as white fibers. The precipitate was filtered using a 2.5 µm glass fiber filter pad and redisolved in THF. The solution was reprecipitated into an excess of methanol and filtered using a glass fiber filter pad. The white fibers were once again redissolved

in THF, precipitated from methanol, and filtered for a third and final time. After the final precipitation, the polymer was dried under a vacuum at room temperature overnight to give $Ph_{100}(CH_2)$ (102 mg, 53%). The polymer was characterized by GPC, UV-VIS/ emission and by NMR. ^{1}H NMR ($CDCl_3$, 300 MHz): δ (ppm) 0.91 (t, 18H), 1.44 (q, 24H), 2.07 (m, 8H), 3.81 (s, 1H), 7.09 (s, 4H). ^{31}P NMR ($CDCl_3$, 120 MHz): δ (ppm) 3.96 (t, 2390 Hz). GPC: Mn = 24,400; Mw = 73,800, PDI= 3.03.

Triisopropyl((5-((trimethylsilyl)ethynyl)thiophen-2-yl)ethynyl)silane (14). To a flask charged with THF and diiospropylamine (DIPA) (8 mL, 1:1) was added 2,5-dibromo thiophene (480 mg, 2.0 mmol). The resulting solution was degassed for 30 min by purging with argon. This solution was added trimethylsilylacetylene (196 mg, 2 mmol), triisopropylsilylacetylene (364 mg, 2 mmol), $Pd(PPh_3)_4$ (12 mg, 1.6 mmol), and copper iodide (4 mg, 2 mmol). The reaction was then stirred at room temperature for 24 hours. After this time the solvent was removed under reduced pressure. Flash chromatography of the residue with hexanes gave the desired product as a yellow solid. (yield 580 mg, 80%). ^{1}H NMR ($CDCl_3$, 300MHz): δ (ppm) 0.33 (s, 9H), 1.19 (s, 21H), 7.03 (m, 2H). ^{13}C NMR ($CDCl_3$, 300 MHz): δ (ppm) 0.22, 11.3, 18.7, 96.6, 96.9, 98.8, 99.9, 124.5, 124.9, 131.8, 132.3.

((5-Ethynylthiophen-2-yl)ethynyl)triisopropylsilane (15). To a deoxygenated solution of 14 (720 mg, 2.0 mmol) in dichloromethane (DCM, 30 mL) and methanol (MeOH, 30 mL), potassium carbonate (KOH, 0.34 g, 6.0 mmol) was added under argon flow. The mixture was stirring at room temperature for 1 hour. Then deionized water (100 mL) was added to extract unreacted KOH. The organic layer was separated and washed 3 times with brine and deionized water, and was dried over sodium sulfate.

The solvent was evaporated to obtain colorless oil. The crude product was purified by column chromate-graphy on silica gel using hexane as the eluent (Rf = 0.47) to yield colorless liquid. Yield: 550 mg (95%). ^{1}H NMR (300 MHz, $CDCl_3$): δ (ppm) 1.12 (m, 21H), 3.33 (s, 1H) and 7.05 (m, 2H). ^{13}C NMR (75 MHz, $CDCl_3$): δ (ppm) 11.2, 18.6, 81.8, 96.8, 98.4, 114.0, 122.9, 125.2, 131.8, 132.6.

Complex (16). ((5-Ethynylthiophen-2-yl)ethynyl)triisopropylsilane (15) (107.4 mg, 0.373 mmol) and cis-dichloro-bis-(tri-n-butylphosphine) platinum(II) 6 (250.1 mg, 0.375 mmol) were dissolved in Et_2NH (15 mL) and the solution was degassed with nitrogen. The mixture was stirred under reflux for 8 hours. The solvent was removed and the crude product purified by flash chromatography (silica gel, hexane then 7:3 hexane/ CH_2Cl_2) giving the desired product 16 as a yellow solid (136 mg, 40 %). ^{1}H-NMR ($CDCl_3$, 300 MHz): δ (ppm) 0.93 (t, 18H), 1.11 (s, 21H), 1.46 (br m, 12H), 1.56 (br m, 12H), 1.99 (br m, 12H), 6.63 (d, 1H), 6.97 (d, 1H). ^{13}C NMR ($CDCl_3$, 75 MHz): δ (ppm) 11.3, 13.8, 18.7, 22.0, 24.3, 26.1, 92.0, 93.2, 94.2, 100.1, 120.0, 126.8, 131.3, 132.1. ^{31}P NMR ($CDCl_3$, 121 MHz): δ (ppm) 7.95 (J_{Pt-P} = 2360 Hz).

$Ph_{95}Th_5$. Compound 16 (9 mg, 0.01 mmol), compound 7 (175 mg, 0.19 mmol) were dissolved in a 7:2 mixture of diisopropy-amine:THF (9 mL) in a Schlenk flask. The solution was degassed over 5 freeze-pump-thaw cycles. The flask was backfilled with dry argon and tetrabutylammonium fluoride (0.120 g, 0.45 mmol) was added via syringe. A white precipitate immediately formed from the yellow-colored solution. The reaction was stirred at room temperature for about 80 min, at which time a TLC with 1:1 hexanes:DCM revealed total consumption of 7 and 16. Copper (I) iodide (2.8 mg, 0.015 mmol) was then added and reacted at room temperature. After stirring for 24 hours, it

was noticed that the polymerization reaction formed a yellowish suspension. The reaction was poured into an excess of methanol, precipitating the polymer as yellow fibers. The precipitate was filtered using a 2.5 µm glass fiber filter pad and redisolved in THF. The solution was reprecipitated into an excess of methanol and filtered using a glass fiber filter pad. The yellow fibers were once again redissolved in THF, precipitated from methanol, and filtered for a third and final time. After the final precipitation, the polymer was dried under a vacuum at room temperature overnight to give $Ph_{95}Th_5$ a yellow solid (yield 96 mg, 70%). ^{1}H NMR ($CDCl_3$, 300 MHz): δ (ppm) 0.77-1.03 (br, 72H), 1.30-1.72 (br, 96H), 1.86-2.25 (br, 48H), 6.57-6.61 (s, 0.48H), 7.03-7.11 (d, 3.15H), 7.14-7.32 (m, 11.19H). GPC: Mn = 10,900; Mw = 19,000, PDI= 1.76.

2,5-Bis(trimethylsilylethynyl)thiophene (18). 2,5-Diodothiophene (668 mg, 2.0 mmol) was dissolved into a flask charged with THF and diiospropylamine (DIPA) (8 mL, 1:1). The resulting solution was degassed for 30 min by purging with argon. And then trimethylsilylacetylene (491 mg, 5 mmol), $Pd(PPh_3)_4$ (12 mg, 1.6 mmol), and copper iodide (4 mg, 2 mmol) were added into this solution. The reaction was then stirred at room temperature for 24 hours. After this time the solvent was removed under reduced pressure. Flash chromatography of the residue with hexanes gave the desired product as a yellow solid. (yield 440 mg, 80%). ^{1}H NMR ($CDCl_3$, 300MHz): δ (ppm) 0.24 (s, 18H), 7.04 (s, 2H); ^{13}C NMR ($CDCl_3$, 300 MHz): δ (ppm) -0.23, 96.86, 99.90, 124.47, 132.29.

2,5-Diethynyl-thiophene (19). 2,5-Bis(trimethylsilylethynyl)thiophene 18 (75.2 mg, 0.272 mmol) was dissolved in a round flask with 1:1 mixture of methanol:DCM (9 mL). The solution was purged by dry argon for 15 min and tetrabutylammonium fluoride

(0.144 g, 0.54 mmol) was added instantly. And then the reaction was stirred at room temperature for about 2 hours, at which time a TLC with 1:3 hexanes:DCM revealed total consumption of 18. (yield 54 mg, 80%). ^{1}H NMR ($CDCl_3$, 300MHz): δ (ppm) 3.05 (s, 2H), 7.04 (d, 2H); ^{13}C NMR ($CDCl_3$, 300 MHz): δ (ppm) 72.86, 74.90, 126.47, 127.29.

Compound (20). To a flask charged with $Pt(PBu_3)_2Cl_2$ (501 mg, 0.75 mmol) and 19 (69 mg, 0.25 mmol) in a mixture of toluene and diethylamine (12 mL, 3:1) was added CuI (3 mg). The reaction mixture was deoxygenated with argon purging for 15 min. After stirring for 2 days at room temperature, the solvent was removed under reduced pressure. The resulting residue was stirred in dichloromethane, and the resulting suspension filtered. The soluble portion was collected and purified by flash chromatography with hexanes as the eluent to yield 20 as a yellow solid. (yield 224 mg, 64%). ^{1}H NMR ($CDCl_3$, 300MHz): δ (ppm) 0.93 (t, J = 7.20Hz, 36H), 1.38-1.62 (m, 48H), 1.90-2.80 (m, 24H), 7.04 (d, 2H); ^{13}C NMR ($CDCl_3$, 300 MHz): δ (ppm) 13.76, 21.90(t, J = 66.30 Hz), 24.24(t, J = 27.9 Hz), 26.01, 88.26, 93.77, 126.84. ^{31}P NMR ($CDCl_3$, 300 MHz): δ (ppm) -1.68, 8.04, 17.77.

$Ph_{95}Th_5(CH_2)$. A mixture of diisopropylamine and toluene (3 mL, 1:5) with a small magnetic stirring bar in a Schlenk flask was purged with argon for five minutes. This flask was then subjected to vacuum for one minute by inserting a needle connected by hoses to a water aspirator into the septum. This process was repeated twice, ending with argon-purging. To the flask compound 20 (14 mg, 0.01 mmol) was rapidly added complex 11 (253 mg, 0.18 mmol), compound 12 (41 mg, 0.19 mmol) and CuI (2 mg, 0.01 mmol). The solution was degassed by three more argon-vacuum cycles, sealed

under vacuum, and stirred at room temperature for 24 hours. After this time, the solution was poured into 50 mL of methanol to induce precipitation of the polymer as a pale yellow solid. The desired polymer was collected by filtration and washed with methanol and then water. This solid was dissolved in a minimal amount of chloroform, precipitated again into methanol, and collected by filtration to yield the desired polymer as a yellow solid (yield 86 mg, 65%). ^{1}H NMR ($CDCl_3$, 300 MHz): δ (ppm) 0.77-1.03 (br, 72H), 1.30-1.72 (br, 96H), 1.86-2.25 (br, 48H), 3.86 (s, 0.86H), 6.57-6.61 (s, 0.48H), 7.03-7.11 (d, 3.15H), 7.14-7.32 (m, 11.19H). GPC: Mn = 27,259; Mw = 91,622, PDI= 3.36.

Photophysical Measurements

Photophysical properties for solutions were measured using a 1-cm pathlength quartz or borosilicate cuvette in spectroscopic solvents. Solutions were deoxygenated by purging with argon or oxygen-saturated by purging with oxygen for transient absorption measurements. Ground state absorption spectra were collected on a Shimadzu UV-1800 dual-beam spectrophotometer with the appropriate solvent as the instrument baseline blank. Corrected steady-state emission measurements were collected by the QuantaMaster 300 of Photon Technology International (PTI) photon counting fluorescence spectrophotometer.

Phosphorescence decay kinetic was obtained with a multichannel scaler/photon counter system with a NanoQuant FluoTime 100 compact phosphorescence lifetime spectrophotometer (PicoQuant Photonics North America, Inc., http://www.picoquant-usa.com/). A CUBE diode laser provided the excitation at 375 nm (< 16 mW). The 100 ns pulsed laser was generated by SRS DG353 Digital Delay/Pulse Generator. The specific narrow bandpass filter was used for each measurements followed by global fit

processing (FluoroFit software). Decays were obtained using the biexponential fitting parameters (FluoroFit software, PicoQuant).

For the nanosecond transient absorption spectroscopy, the third harmonic of a Continuum Surelite series Nd:YAG laser (λ=355 nm, 10ns fwhm, 10 mJ pulse^{-1}) was used as the excitation source. Probe light was produced by a xenon flash lamp and the transient absorption signal was detected with a gated-intensified CCD mounted on a 0.18 M spectrograph (Princeton PiMax/Acton Pro 180). Sample concentrations are adjusted to approximately 0.6-0.8 absorbance at 355 nm and were degassed with argon for 30 min. A flow cell holding a volume of 10ml was used and continuously circulated at the pump-probe region during the measurements.

Polymer film photophysics were measured freestanding, open to the atmosphere. Absorption spectra were measured on a Varian Cary 100 dual-beam spectrophotometer with a clean glass slide as the instrument blank. Emission spectra were obtained by a front-face alignment on a Fluorolog 3 spectrophotometer.

CHAPTER 3
TRIPLET EXCITON DIFFUSION IN PLATINUM ACETYLIDE THIN FILMS

Introductory Remark

Exciton transport plays a significant role in the design and performance of optoelectronic devices including polymer light emitting devices (PLEDs) and organic photovoltaic cells (OPVs). The luminescence efficiency of PLEDs decreases when the excited state is quenched by intermolecular interactions,[71,72] exciton interactions,[72,73] and excited state annihilation.[74,75] These quenching processes have an important influence on phosphorescent PLEDs since the triplet excitons have much longer lifetime than singlet excitons. Nevertheless, internal quantum efficiencies close to unity are reached for PLEDs containing phosphorescent emitter materials because the light is generated from both triplet and singlet excitons due to strong spin-orbit interaction.[76-78] In OPVs, the singlet excited state is produced by photoexcitation. The excitons must diffuse to an interface for exciton dissociation. Because the lifetime of singlet exciton is too short, its dissociation efficiency is lower. Samiullah et al. found that the presence of heavy metal in the polymer chain results in enhanced photovoltaic cell efficiency due to the formation of triplet excitons.[79-81]

Concerning the exciton transport, singlets diffuse through Förster transfer, which is a coupling of electronic transition dipoles that can occur over hundreds of nanometers, allowing them to diffuse over a relatively large volume before they decay. Unfortunately, the lifetime of a singlet exciton lies in the picosecond-nanosecond range, decreasing the ability of exciton diffusion. Triplet exciton diffusion occurs through Dexter

---

This Chapter is considered for publication in the Journal of the American Chemical Society.

transfer, a concerted exchange of electrons that occurs at distances less than 1 nm, limiting the diffusion coefficient; however, these excitons have microsecond lifetimes that increase exciton migration efficiency.[40] At present, several methods have been established to determine the diffusion length of singlet excitons, e.g., photocurrent measurements,[82-85] photoluminescence quenching experiments[86-90] and singlet-singlet annihilation.[91] Despite these efforts, relatively little is known regarding convenient and practical methods for measuring the exciton diffusion parameters. There is therefore great interest to clarify the effective estimation for studying the triplet exciton diffusion in solid-state polymeric materials.

Here, we develop a method for determining the triplet exciton diffusion length utilizing time-resolved photoluminescence spectroscopy. To investigate this method, the conjugated platinum acetylide polymer as the donor, Ph_{100}, is spin-coated along with varying amounts of either phenyl[C61]butyric acid methyl ester (PCBM, an electron acceptor), platinum (II) octaethylporphyrin (PtOEP, a triplet energy acceptor) or conjugated copolymer with 4,7- benzothiadiazole (BTD) and 1,4-phenylene (Ph) units at BTD:Ph = 1:19 ($Ph_{95}BTD_5$), a homogeneous quencher), as shown in Figure 3-1. Our method is based on the quenching of the triplet exciton by acceptor molecules, where the dynamics of the triplet exciton depends on the concentration of the acceptor molecules. The method is more generally applicable since the photoluminescence decay of polymer thin films are thickness-independent. We further show that the classical models, such as the Stern-Volmer model and Hindered-Access model, are applied to deduce the quenching rate constant (kq). This rate constant is shown to be equal to the exciton-acceptor collision frequency, enabling the calculation of D and L_D.

These results are then compared with those obtained using conventional time-of-flight (TOF) techniques. The diffusion coefficients and lengths of diffusion are relatively consistent for the proposed and literature-based methods.

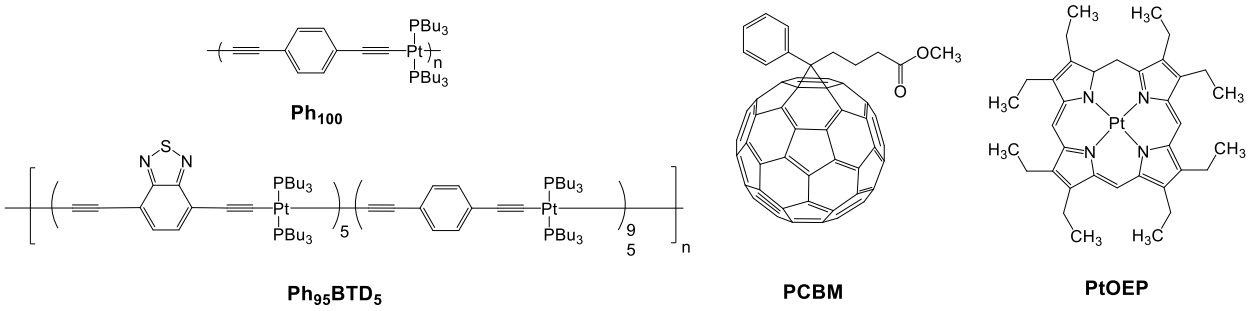

Figure 3-1. Structures of the platinum acetylide polymer, Ph_{100}, and three quenchers, PtOEP, PCBM and $Ph_{95}BTD_5$.

Synthesis

In order to avoid defects present in the polymer backbone, the strategy which we prefer is the polymerization of asymmetric AB monomers.[56,57] Figure 3-2 illustrates this strategy for $Ph_{95}BTD_5$ synthesis. In the beginning, 4,7-dibromobenzothiadiazole, 1, was subjected to a one pot Sonogashira coupling between (trimethylsilyl)-acetylene (TMS-acetylene) 2 and (triisopropylsilyl) acetylene (TIPS-acetylene), 3, giving asymmetrically protected triisopropyl((5-((trimethylsilyl)ethynyl)thiophen-2-yl)ethynyl)-silane, 4, in a 80% yield. The TMS-acetylene protecting group was selectively removed through reaction with potassium hydroxide in the mixture of methanol (MeOH) and dichloromethane (DCM) at room temperature to give 5 in a 95% yield. Following a Hagihara reaction with platinum complex 6, the TIPS-protected monomer 7 was synthesized. The TIPS-

protected monomer 9 were then deprotected in situ with TBAF and polymerized with monomer 8 overnight to give conjugated co-polymers, $Ph_{95}BTD_5$, in a 65% yield.

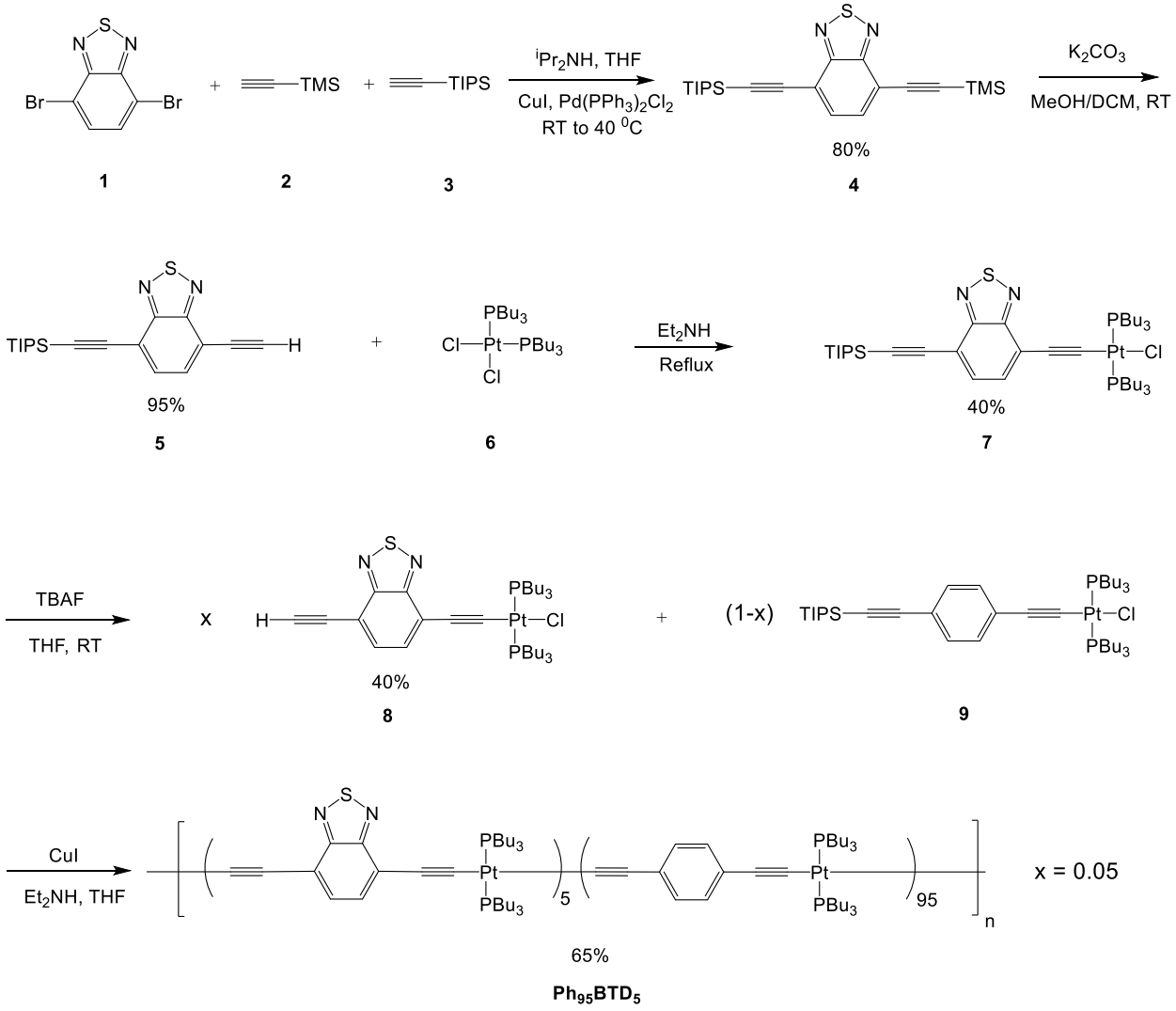

Figure 3-2. Synthesis of Ph95BTD5 using AB asymmetric monomers.

For the application of the newly-developed model and the studies of temperature-dependent dynamics, a series of polymers will be discussed below. Thus, another conjugated polymer, pPtBP, was synthesized. The self-polymerization of an asymmetric AB monomer can be applied to prevent defects in the polymers. [56,57] Figure 3-3 illustrates this strategy for pPtBP synthesis. In the beginning, 4,4'-diiodo-1,1'-biphenyl,

10, was subjected to a one pot Sonogashira coupling between 2-methylbut-3-yn-2-ol 11 and (trimethylsilyl)-acetylene (TMS-acetylene), 2, giving asymmetrically protected compound, 12, in a 65% yield. The TMS-acetylene protecting group was selectively removed through reaction with potassium hydroxide in the mixture of methanol (MeOH) and dichloromethane (DCM) at room temperature to give 13 in a 86% yield. Following a Hagihara reaction with platinum complex 6, the 2-methylbut-3-yn-2-ol protected monomer 14 was then deprotected in situ with NaOH and polymerized overnight to give polymer, pPtBP, in a 50% yield.

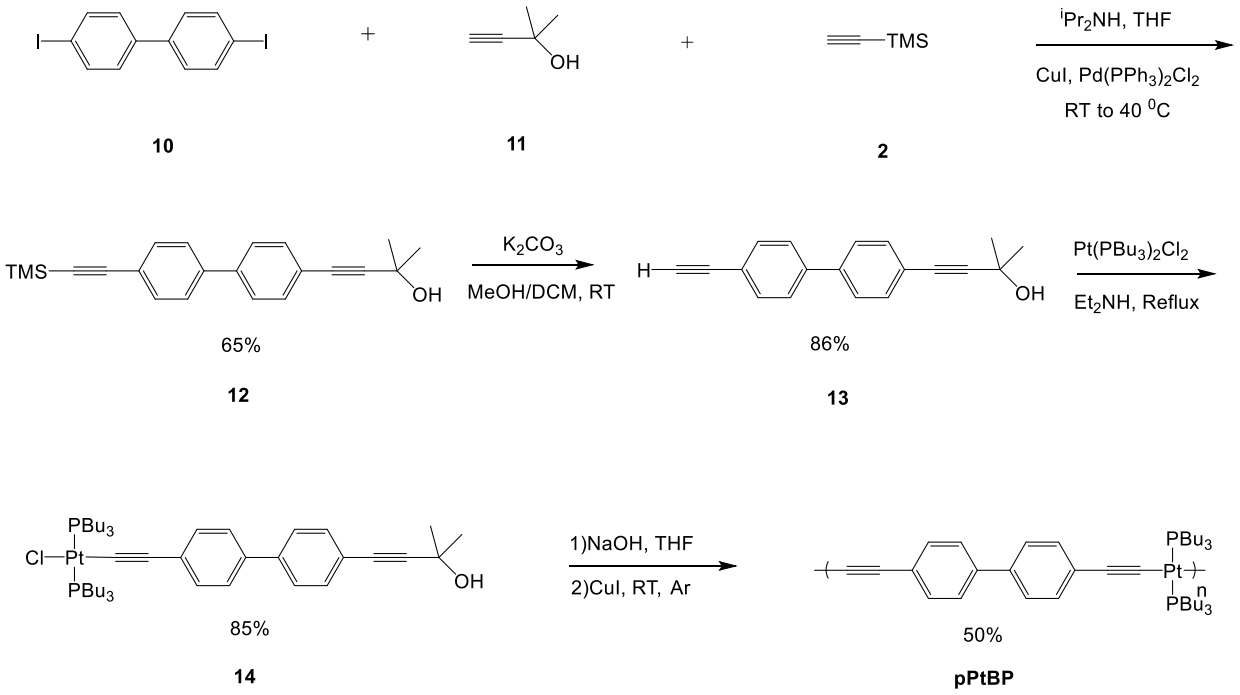

Figure 3-3. Synthesis of pPtBP using AB asymmetric monomers.

Results and Discussion

Photophysical Properties and Quenching Studies

The absorption and emission spectra of the conjugated phenylene-based homo-polymer thin film, Ph_{100}, was recorded, the absorption spectrum exhibits one broad, featureless band with λ_{max} at 375 nm, as shown in Figure 3-4.[92] This band corresponds

to the long-axis polarized absorption of Ph_{100}. The emission spectrum of Ph_{100} exhibits weaker peaks from 390 nm to 450 nm which are assigned as fluorescence according to previous investigations.[59] Additionally, the emission of this polymer at 520 nm is similar to the spectra of analogous materials in earlier studies.[59] Hence, the emission centered at 520 nm is assigned as phosphorescence.

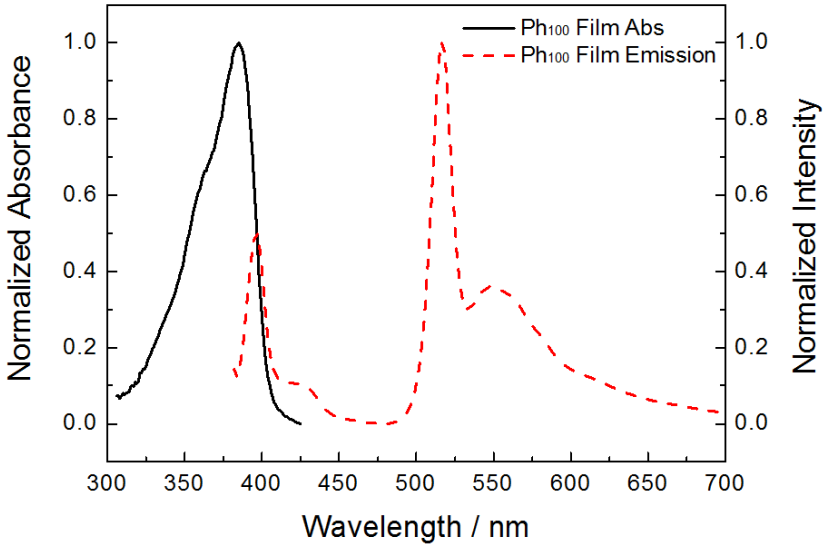

Figure 3-4. Normalized absorption and emission spectra of Ph_{100} thin film.

The absorption spectrum of the $Ph_{95}BTD_5$ copolymer thin film is displayed in Figure 3-5a. First, the spectrum of $Ph_{95}BTD_5$ is dominated by abroad band with λ_{max} = 375 nm, with a weak band on the low-energy side at ca. 500 nm. The primary absorption band is very similar in shape and energy compared to that of Ph_{100}, and on this basis it is assigned to the phenylene-based repeat units (Pt-Ph) in the Pt - acetylide backbone. The weak band at 500 nm appears at a similar wavelength compared to the absorption of the BTD_{100} homopolymer,[63] and on this basis it assigned to chromophores in the chain that contain the benzothiadiazole unit (Pt-BTD). The photoluminescence spectra of the $Ph_{95}BTD_5$ copolymer and the Ph_{100} homopolymer thin films are shown

together in Figure 3-5b. The emission spectra were obtained with 375 nm excitation, which corresponds to excitation into the dominant absorption band. For $Ph_{95}BTD_5$, the emission at 298 K is dominated by a band with λ_{max} = 580 nm that corresponds to Pt-BTD fluorescence.[63] The phenylene-based phosphorescence of the $Ph_{95}BTD_5$ copolymer at 520 nm was almost completely quenched due to the 4,7-benzothiadiazole unit functions as a "trap". The $Ph_{95}BTD_5$ copolymer can thus be one of the efficient triplet quenchers of the Ph_{100} homopolymer.

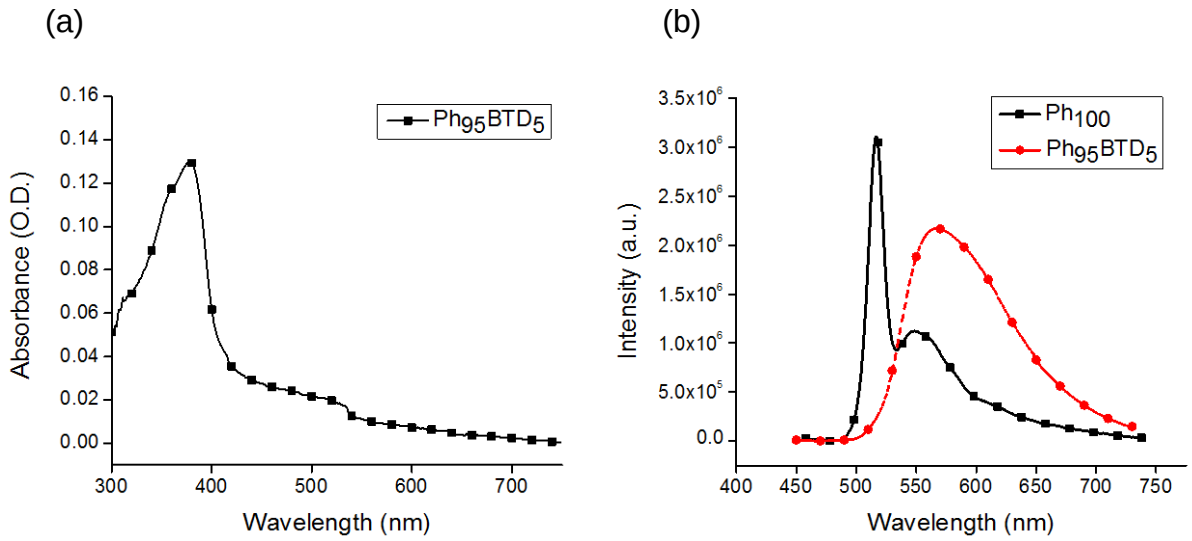

Figure 3-5. (a) Absorption spectrum of the $Ph_{95}BTD_5$ thin film. (b) Emission spectra of $Ph_{95}BTD_5$ and Ph_{100} thin films.

The phosphorescence of Ph_{100} thin films, blended with different amounts of PCBM, PtOEP or $Ph_{95}BTD_5$, decays faster, indicative of the luminescence quenching by energy and charge transfer from the platinum acetylide polymer to the acceptor, shown in Figure 3-6. In this time-resolved measurement the emission at 520 nm, corresponding to the phosphorescence maximum of Ph_{100}, was monitored. As the weight percent of PCBM, PtOEP or $Ph_{95}BTD_5$ in Ph_{100} film increases from 0.05-0.525

wt%, the lifetime of the Ph_{100} decreases due to triplet exciton quenching in the presence of acceptor molecules.

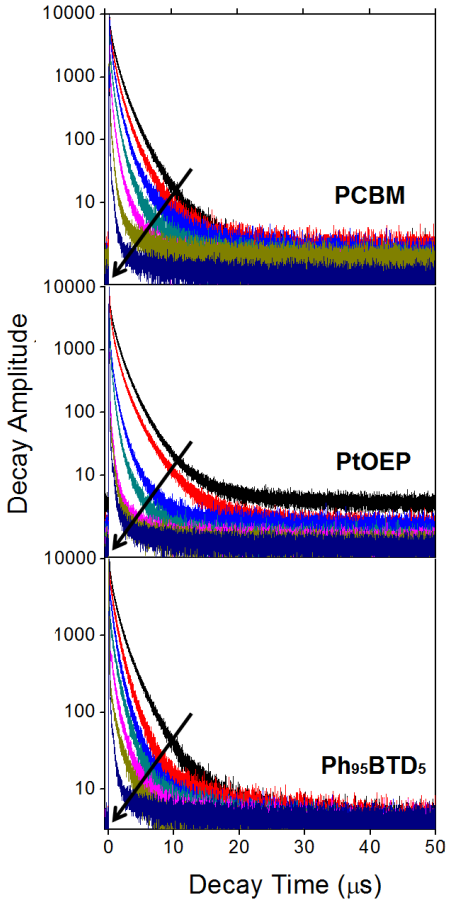

Figure 3-6. Photoluminescence Decay monitored at 520 nm for a) Ph_{100}/PCBM blended films; b) Ph_{100}/PtOEP blended films; c) Ph_{100}/$Ph_{95}BTD_5$ blended films , in order of decreasing decay lifetime: 0.00 wt%, , 0.05 wt%, 0.075 wt%, 0.100 wt%, 0.125 wt%, 0.225 wt%, and 0.525 wt% quenchers, i.e., PCBM, PtOEP and $Ph_{95}BTD_5$.

The effect of PCBM concentration on Ph_{100} lifetime for spin-coated Ph_{100} /PCBM films is shown in Figure 3-7a. At PCBM concentrations less than 0.225 weight percent (wt%), there is a pronounced effect on the Ph_{100} lifetime. When the PCBM concentration is larger than 0.225 wt%, there is a little effect of acceptor concentration on donor lifetime. As discussed below, we ascribe this to the onset of phase separation of the PCBM from the donor polymer.[93-95] When a set of Ph_{100} films

are spin-coated with varying amounts of PtOEP, the results of Figure 3-7b are obtained. A pattern similar to Ph_{100} / PCBM was observed for these films : as acceptor concentration increases, the lifetime decreases; at higher PtOEP concentrations, there is little change in donor lifetime, suggesting the onset of phase separation. The Ph_{100} is

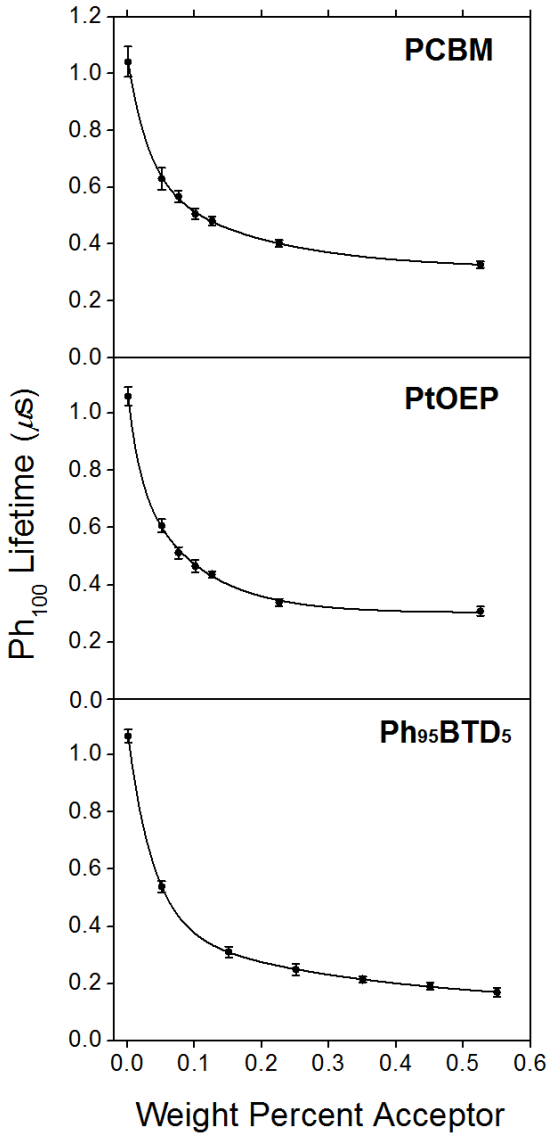

Figure 3-7. Lifetimes for a) Ph_{100}/PCBM blended films; b) Ph_{100}/PtOEP blended films; c) Ph_{100}/$Ph_{95}BTD_5$ blended films. Lines are included to guide the eye. The error bars represent the standard deviation of the average pPtPh triplet lifetime.

quenched with increasing $Ph_{95}BTD_5$ concentration, depicted in Figure 3-6c. As the $Ph_{95}BTD_5$ concentration increases, the donor lifetime deceases gradually due to the impact of acceptor concentration (Figure 3-7c). The pattern for Ph_{100} with $Ph_{95}BTD_5$ is different from Ph_{100} with PCBM or PtOEP. The lifetime of Ph_{100} decreases quickly up to 0.150 wt% $Ph_{95}BTD_5$. When the $Ph_{95}BTD_5$ concentration exceeds 0.250 wt%, the acceptor concentration still has an influence on donor lifetime. The quenching efficiency is more effective for $Ph_{95}BTD_5$ than for PCBM and PtOEP because $Ph_{95}BTD_5$ is the homogeneous quencher. Accordingly, all films, both pristine and quenched, were prepared in triplicate. Three separate lifetimes were thus obtained for three separate films at each quencher concentration. The lifetimes were averaged and are summarized in Figure 3-7. The error bars represent the range of lifetimes measured for each quencher concentration.

Quenching Model and Exciton Diffusion

In the present study we assume that the phosphorescence of the Ph_{100} films is quenched by quencher molecules that are dissolved within the polymer phase. When a film is spin-coated, the casting solution contains a known amount of donor and a known amount of acceptor, and this ratio is assumed to remain unchanged in the spin-coated film. Also, we are able to determine the diffusion kinetics for triplet states of Ph_{100} utilizing time-resolved photoluminescence because the exciton quenching efficiency depends on the concentration of the quencher sites. Then the diffusion parameters are estimated by the standard quenching methods.

Stern-Volmer (SV) analysis of emission quenching for a system comprising a luminophore and a quencher in fluid solution is based on a well-established kinetics model that assumes the quenching occurs within an encounter complex. When

quenching occurs with unit efficiency within the encounter complex the quenching rate constant extracted from SV analysis is equivalent to the diffusion controlled bimolecular rate constant, k_q. In the present study, we adopt a model which assumes that when the quencher is well-dispersed in the Ph_{100} phase that the SV model holds and the quenching is rate limited by diffusion of the triplet exciton in the polymer phase.

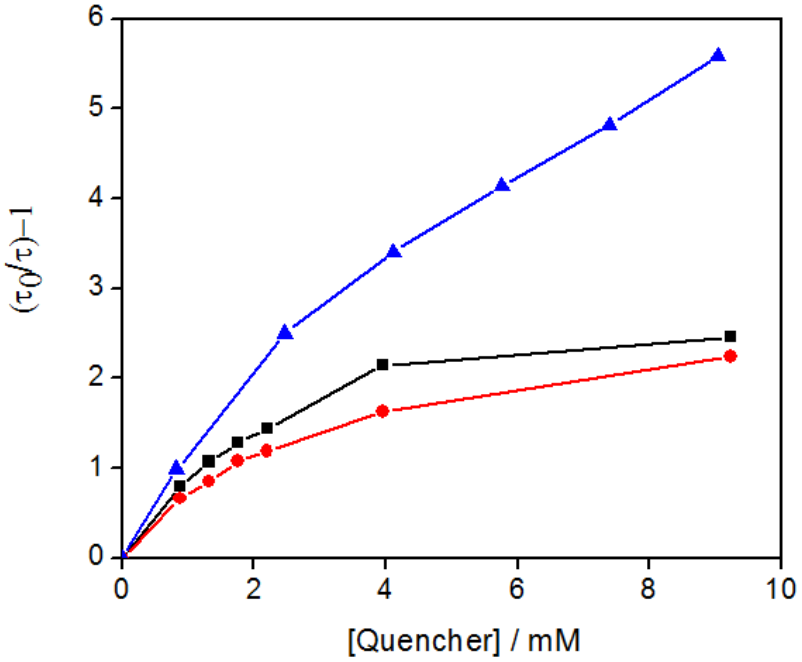

Figure 3-8. Stern-Volmer plots for Ph_{100}/PCBM (circles), Ph_{100}/PtOEP (squares) and $Ph_{100}/Ph_{95}BTD_5$ (triangles) blended films. Error bars have been omitted for clarity. Lines are added to guide the eye.

Given this assumption, we apply a standard SV analysis to the emission decay data, Equation 3-1, where τ_o is the lifetime of unquenched P_{100}, τ is the quenched donor lifetime, and [Q] is the quencher concentration. The quencher concentration was determined based on the amount of polymer and quencher present in each sample, along with the density of the polymer that was estimated by the method of Albert and Malone.[96-101] When applied to the quenching data, Figure 3-8 is obtained. For PCBM and PtOEP, The donor-acceptor phase separation in the spin-coated films results in a

poor fit. By contrast, the fit of Ph_{100} with $Ph_{95}BTD_5$ is more linear since there is almost no phase separation in this blended polymeric film.

$$\frac{\tau_o}{\tau} = 1 + (k_q \tau_o)[Q] \quad (3\text{-}1)$$

To compensate for the donor-acceptor phase separation, the Hindered Access model, Equation 3-2, was applied to the data.[102] This model still assumes that the donor diffuses to the acceptor before quenching occurs, but it also accounts for f_a, the fraction of donor able to be quenched by the acceptor.

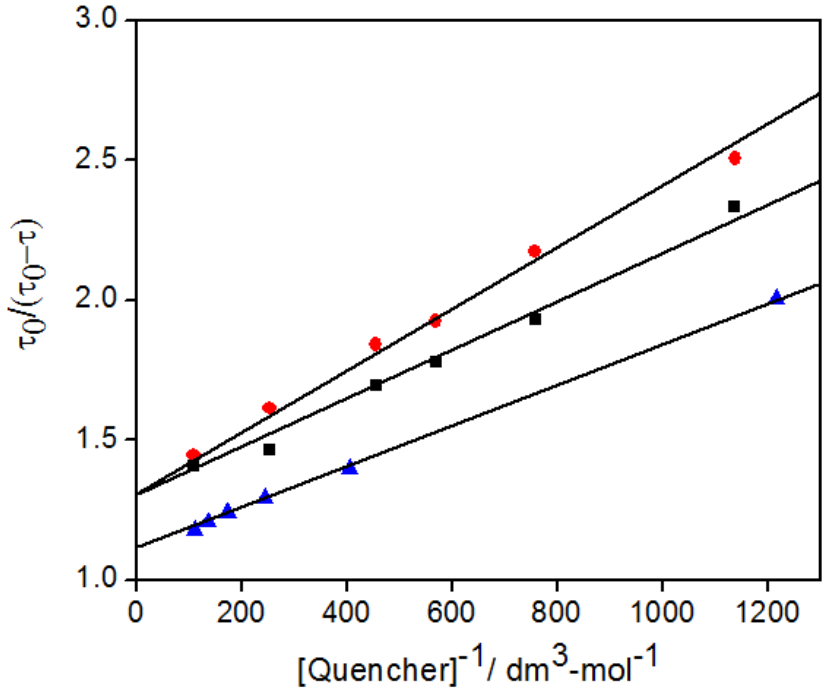

Figure 3-9. Hindered-Access plots for Ph_{100}/PCBM (circles), Ph_{100}/PtOEP (squares) and $Ph_{100}/Ph_{95}BTD_5$ (triangles) blended films. Error bars have been omitted for clarity.

As the spin-coated donor-acceptor films begin to phase separate, the amount of dispersed acceptor molecules remains constant: we assume that the addition of more acceptor molecules results in the growth of pure acceptor domains. This limits the amount of Ph_{100} that can be quenched by the acceptor. As shown in Figure 3-9, the

model produces a good linear fit to the PCBM, PtOEP and $Ph_{95}BTD_5$ quenching data. The trend for Ph_{100} blended with PCBM is similar to that of Ph_{100} blended with PtOEP. Hence, the quenching efficiencies of PCBM and PtOEP for this platinum acetylide polymer, Ph_{100}, are very close to each other. The quenching rate constants (k_q) of Ph_{100}/PCBM, Ph_{100}/PtOEP and $Ph_{100}/Ph_{95}BTD_5$ are 1.26×10^9 M^{-1}-s^{-1}, 1.31×10^9 M^{-1}-s^{-1} and 1.41×10^9 M^{-1}-s^{-1} respectively, which have the same order of magnitude (Table 1).

$$\frac{\tau_o}{\tau_o - \tau} = \frac{1}{f_a} + \frac{1}{(k_q \tau_o) f_a [Q]} \tag{3-2}$$

The rate of exciton quenching is the product of the probability, P, that a quenching reaction will occur when exciton-acceptor collisions occur at frequency Z (Equation 3-3). The collision frequency[103] is given by Equation 3-4, where r_{AB} is the reactive radius of the two colliding species. For reactions proceeding through the Dexter mechanism, r_{AB} is assumed to be 4 Å. Assuming every exciton diffusing to an acceptor is quenched, P = 1, in which case $k_q = Z$; through a rearrangement of Equation 3-4, D can be calculated.[103] Once D is known, the exciton diffusion length, L_D, can be calculated by Equation 3-5. Using this procedure, the values for D and L_D given in Table 3-1 are obtained. The exciton diffusion constants are relatively high for triplets, ~10^{-6} cm^2-s^{-1}, giving a diffusion length of approximately 21.5 nm for Ph_{100}. All of the values calculated using the concentration-based quenching procedure are reproducible regardless of the quencher used, indicating the assumptions and application of the method are valid.

$$k_q = PZ \tag{3-3}$$

$$Z'_{AB}\left(\frac{1}{MS}\right) = \frac{4\pi r_{AB} D_{AB} N_{AV}}{1000} \tag{3-4}$$

$$L_D = \sqrt{D\tau} \tag{3-5}$$

In a similar manner, the diffusion coefficients (D) of Ph_{100} with an acceptor (PCBM, PtOEP or $Ph_{95}BTD_5$) are approximately 4×10^{-6} cm^2-s^{-1}. Interestingly, the diffusion length (L_D) for Ph_{100} with $Ph_{95}BTD_5$ is slightly longer than L_D of Ph_{100} with PCBM or PtOEP since the quenching for Ph_{100}/ $Ph_{95}BTD_5$ is more efficient. With regard to fraction of donor able to be quenched by the acceptor (f_a) for Ph_{100} with PCBM, PtOEP or $Ph_{95}BTD_5$, the f_a of Ph_{100}/$Ph_{95}BTD_5$ is higher than that of Ph_{100}/PCBM and Ph_{100}/PtOEP since the blended film of Ph_{100}/$Ph_{95}BTD_5$ is much more homogeneous than that of Ph_{100}/PCBM and Ph_{100}/PtOEP.

Time of Flight Quenching

In order to validate the results of the concentration-based experiments which rely on the Hindered-Access and SV models, time of flight quenching experiments were also performed. This approach has been used by other researchers to calculate exciton diffusion coefficients.[104] These experiments are performed by spin-coating a series of variable-thickness donor films, on top of which is evaporated an acceptor layer of constant thickness. As the donor layer thickness increases, the exciton lifetime begins to compete with the time necessary to diffuse to the acceptor layer; thus, a variation in donor thickness gives rise to the variation of the exciton quenching. The relationship between donor layer thickness, L, and exciton quenching, Q, is examined as a function of the length of diffusion using Equation 3-6.[104] The exciton quenching can be determined by Equation 3-7. The diffusion coefficient is then calculated using the relationship between D and L_D provided in Equation 3-5.

$$Q(L,L_D)=\frac{L_D}{L}\tanh\left(\frac{L}{L_D}\right) \quad (3\text{-}6)$$

$$Q(L,L_D)=1-\frac{\tau}{\tau_0} \quad (3\text{-}7)$$

The results of TOF experiments employing Ph_{100}|C60 are given in Figure 3-10a. As the film thickness varies from ~25 nm to ~75 nm, the Ph_{100} lifetime rises, as expected. As shown in Figure 3-10b, Equation 3-6 adequately fits the Ph_{100}/C60 TOF data, and the results are given in Table 3-1. The diffusion coefficient and length of diffusion are slightly higher than those values obtained using the concentration-based method but are still valid.

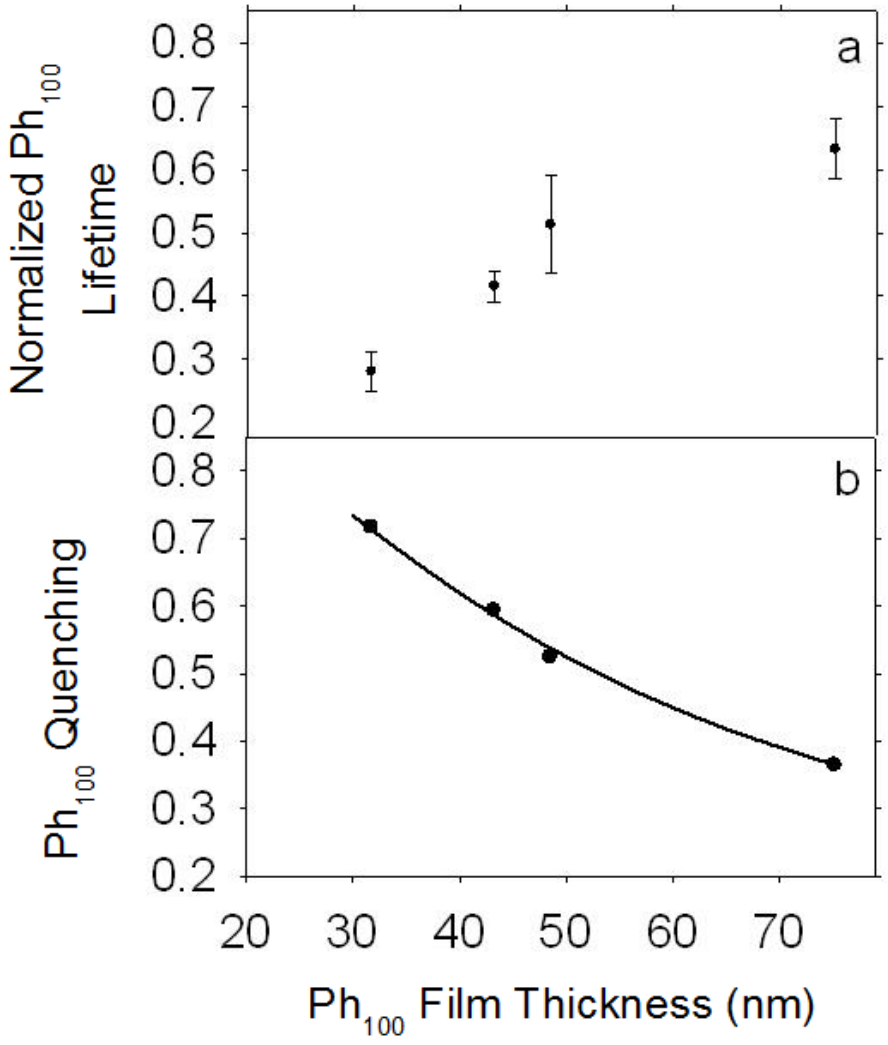

Figure 3-10. Ph_{100}|C60 time-of-flight experiments: a) Triplet lifetime data; b) Triplet lifetime quenching (circles) fitted using Equation 6 (solid line). This was done by Dr. Jarrett H. Vella in Schanze's group and Dr. Jason D. Myers in Xue's group.

Table 3-1. Summary of the concentration- and time of flight (TOF)-based triplet exciton diffusion measurements.

Quencher	Film type[a]	$k_q\tau$ (M^{-1})	k_q (10^9 M^{-1}-s^{-1})[b]	D (10^{-6} cm^2-s^{-1})	L_D (nm)	f_a
PCBM	Blend	1,300	1.26±0.03%	4.2	20.8	0.78
PtOEP	Blend	1,390	1.31±0.04%	4.4	21.5	0.79
$Ph_{95}BTD_5$	Blend	1,500	1.41±0.01%	4.7	22.3	0.90
C60	Bilayer	N/A	N/A	7.7	27.7	N/A

Notes: [a]"Blend" refers to spin-coated films and "Bilayer" refers to TOF experiments. [b]Estimated error in k_q is ±XXX%

Table 3-2. Singlet and triplet exciton diffusion literature data for spin-coated donor films.

Material	Exciton multiplicity[a]	D /10^{-6} cm^2-s^{-1}	L_D (Å)	Reference
PEOPT	S	4500	47	105
MDMO-PPV	S	3200	45	104
PPP	S	4300	110	106
NPD	S	700	51	86
SubPC	S	640	80	86
PTCDA	S	3400	104	86
TnBuPP	S	2500	220	107
Alq_3	S	12	200	86, 108
P3HT	S	220-790	50-200	90,91
C–PCPDTBT	S	1100	110	90
Si–PCPDTBT	S	2600	110	90
Alq_3	T	0.08	140	109
Ph_{100}	T	4.19-7.70	208-277	This work
PtOEP	T	0.06-4.1	130-180	86
BP	T	0.00001-0.5	---	110
PdTPPC	T	0.00008	---	111
CBP	T	0.014	---	112
Eu-DM	T	---	250	113
PTCDA	T	---	880	114
Ir-G1	T	0.40	100	115
Ir-Carb	T	0.060	60	
Ir-G2	T	0.008	20	

Notes: [a]S=singlet, T=triplet; ---, data not reported; PEOPT, poly-3-(trioxaoctylphenyl) thiophenes; MDMO-PPV, poly-(2-methyl-5-(3',7'-dimethyloctyloxy)-p-phenylenevinylene; Alq_3,tris-(8-hydroxyquinoline) aluminum; NPD, N,N'-diphenyl-N,N'-bis(1-naphthyl-1,1'-biphenyl-4,4" diamine; SubPC, boron subphthalyocyanine; PTCDA, 3,4,9.10-perylenetetracarboxylic dianhydride; TnBuPP, tetra-(4-n-butylphenyl)porphyrin; PtOEP, platinum (II) octaethylporphine; BP, benzophenone; Ir-G1 and Ir-G2, dendrimeric tris-(2-phenylpryidine) iridium complexes; Ir-carb, dendrimeric tris(3',3'-dicarbazolyl-2-phenylpryidine) iridium complex; PPP, poly(para-phenylene)

The D and L_D of triplet excitons in the conjugated Ph_{100} polymer are directly determined by measuring the photoluminescence (PL) quenching in well-defined

heterostructures comprising a thin spin-coated polymer layer of variable thickness and a vacuum-deposited fullerene monolayer. From these measurements we infer the values of 7.7×10^{-6} cm^2-s^{-1} and 27.7 nm for the exciton diffusion coefficient (D) and diffusion length (L_D) in the conjugated Ph_{100} polymer. In conjugated Ph_{100} polymer/quenchers blends, quenching of the polymer PL shows a strong concentration-dependence. This is attributed to an efficient electron and energy transfer from the photoexcited conjugated polymer to the quenchers. The D and L_D of Ph_{100} estimated by the concentration-based quenching model are approximately 4×10^{-6} cm^2-s^{-1} and 21.5 nm.

Both procedures afford similar diffusion coefficients that are two to three orders of magnitude higher than other triplet diffusion coefficients in the literature (Table 3-2), in which the diffusion coefficients of most singlets are equal or larger than 10^{-5} cm^2-s^{-1} with L_D < 30 nm; the diffusion coefficients of triplets are equal or lesser than ≤ 10^{-7} cm^2-s^{-1}, and L_D of triplets can approach 100 Å. We can find that delocalization of the triplet exciton along the platinum acetylide polymers backbone greatly increases its length of diffusion and diffusion coefficient, allowing it to overcome the close (< 10 Å) distance needed for intermolecular triplet exciton hopping.

Application of the Quenching Model

Estimation of Diffusion Parameters

The newly-developed model was validated successfully for Pt-acetylide polymers. The next goal was to use the model to estimate the diffusion parameters for a series of polymers, pPtPh, pPtPh(CH_2) and pPtBP, as presented in Figure 3-11. The absorption and emission spectra of the conjugated phenylene-based homo-polymer thin film, pPtPh, was recorded, the absorption spectrum exhibits one broad, featureless band with λ_{max} at 375 nm, as shown in Figure 3-12.[92] This band corresponds to the

long-axis polarized absorption of pPtPh. The emission spectrum of pPtPh exhibits weaker peaks from 390 nm to 450 nm which are assigned as fluorescence according to previous investigations.[59] Additionally, the emission of this polymer at 520 nm is similar to the spectra of analogous materials in earlier studies.[59] Hence, the emission centered at 520 nm is assigned as phosphorescence.

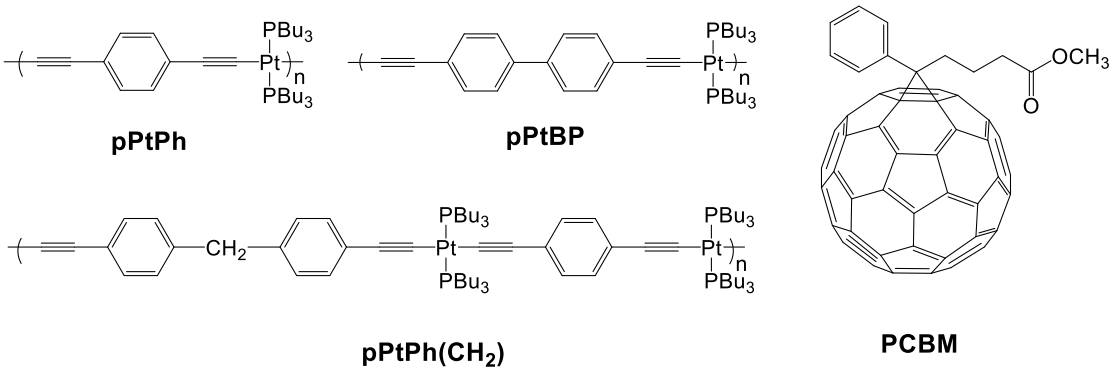

Figure 3-11. The structures of pPtPh, pPtBP and pPtPh(CH_2)with the quencher, PCBM.

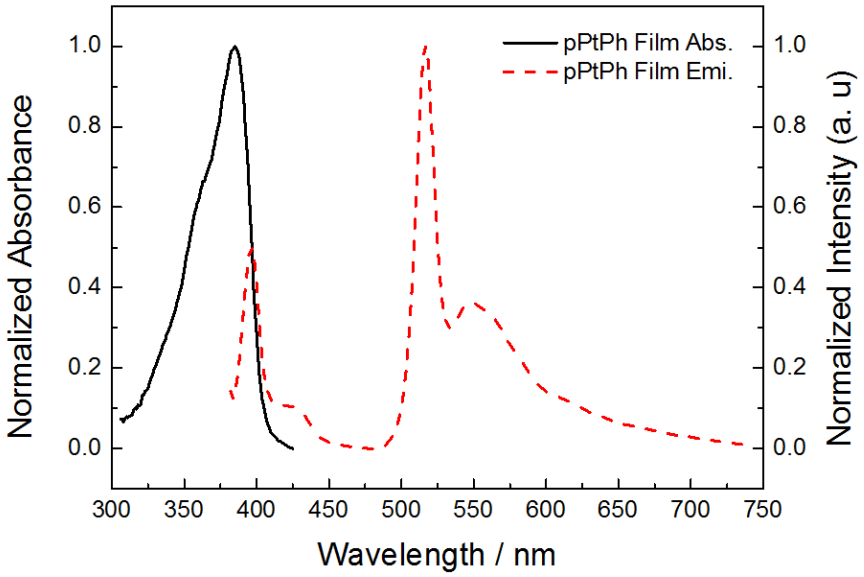

Figure 3-12. Normalized absorption and emission spectra of pPtPh thin film.

The absorption spectra of the conjugation interrupted homo-polymer thin films, pPtPh(CH_2), were recorded and pPtPh(CH_2) displays a strong absorption band at λ_{max} =

357 nm, as presented in Figure 3-13. The photoluminescence of pPtPh(CH_2) films was recorded with the excitation wavelength λ = 357 nm and the spectra are also shown

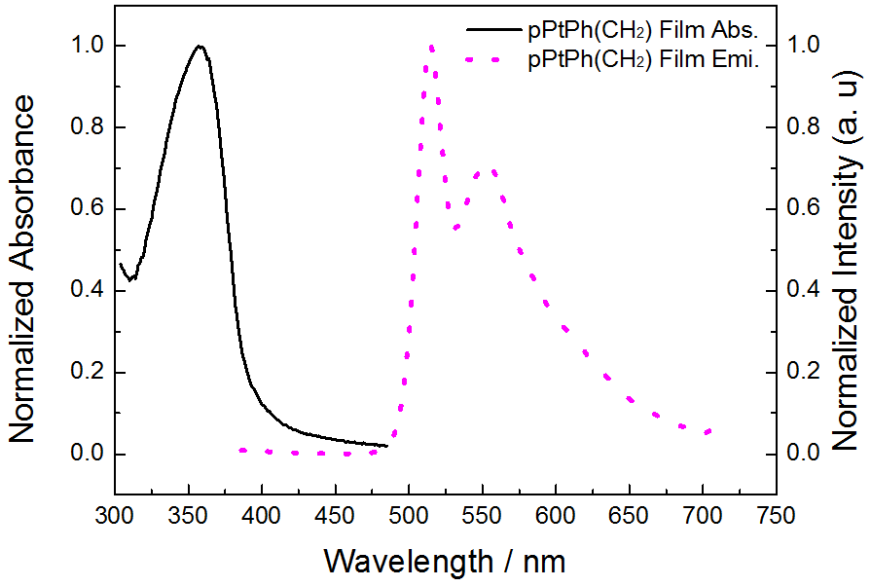

Figure 3-13. Normalized absorption and emission spectra of pPtPh(CH_2) film.

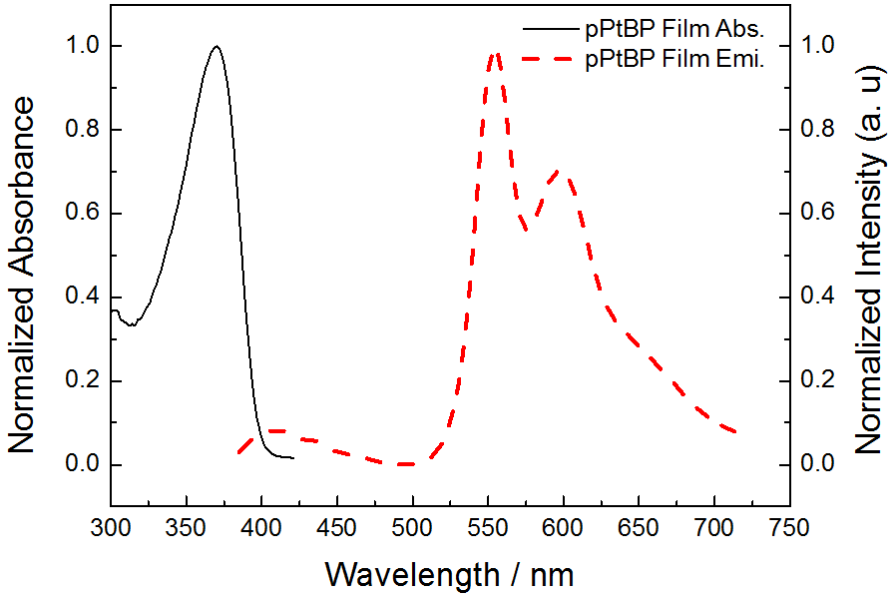

Figure 3-14. Normalized absorption and emission spectra of pPtBP film.

in Figure 3-13. The fluorescence emission band for $Ph_{100}(CH_2)$ thin film is very small at 390 nm and its phosphorescence band is dominated by a sharp band with a maximum

at λ = 520 nm. This sharp band was proved to originate from a phenylene-based triplet excited state.[60] The absorption spectrum of pPtBP was measured, as depicted in Figure 3-14. The strong absorption bands of pPtBP are located at λ_{max} = 370 nm. This 0–0 absorption band is assigned as the $S_0 \rightarrow S_1$ transition from the highest occupied molecular orbital (HOMO) to the lowest unoccupied molecular orbital (LUMO), which are mainly delocalized π and π* orbitals.[11] In Ar-saturated cuvette, the photoluminescence of a pPtBP film was detected with the excitation wavelength λ = 370 nm and the spectra are also presented in Figure 3-14. The pPtBP film emits purple-blue $^1(\pi\pi^*)$ fluorescence ($S_1 \rightarrow S_0$) band near 400 nm that is characterized by the small Stokes shift between the bands in the absorption and the emission spectra. The principal emission bands of the pPtBP film occur at around 550 and 600 nm. The large Stokes shifts of these lower-lying emission bands from the dipole-allowed absorptions, plus the long emission lifetimes (τ_p) in the microsecond regime are indicative of their triplet parentage, and they are thus assigned to the $^3(\pi\pi^*)$ excited states of the 4,4′ –diethynylbiphenyl core (i.e., $T_1 \rightarrow S_0$ emission). [11]

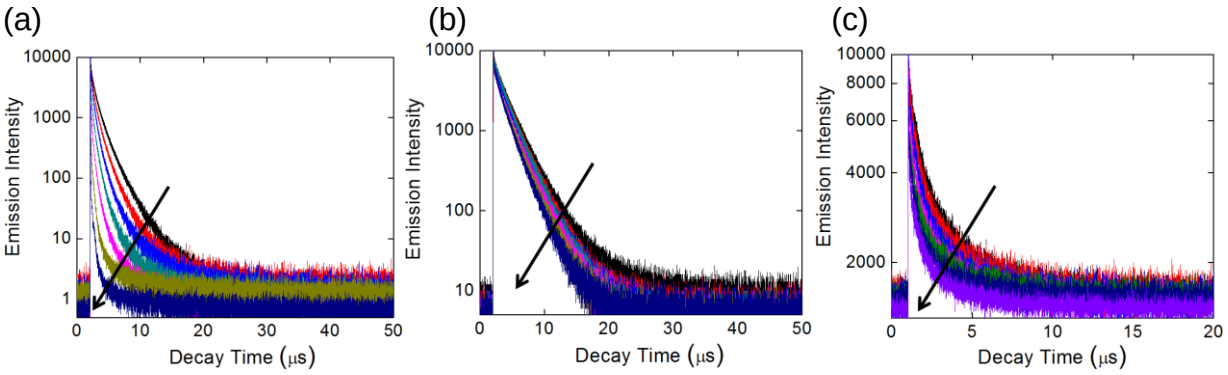

Figure 3-15. Photoluminescence Decay for a) pPtPh/PCBM blended films monitored at 520 nm; b) pPtPh(CH_2)/PCBM blended films monitored at 520 nm; c) pPtBP/PCBM blended films monitored at 550 nm, in order of decreasing decay area: 0.00 wt%, , 0.05 wt%, 0.075 wt%, 0.100 wt%, 0.125 wt%, 0.225 wt%, and 0.525 wt% PCBM.

The photoluminescence of pPtPh, pPtPh$(CH)_2$ and pPtBP films, blended with different amounts of PCBM, decays faster, indicative of the luminescence quenching by efficient energy transfer from the platinum acetylide polymer to the acceptor, shown in Figure 3-15. In the time-resolved measurements of Figure 3-15(a) and 3-15(b), the emissions at 520 nm, corresponding to the phosphorescence maximum of pPtPh and pPtPh$(CH)_2$, were monitored. The time-resolved phosphorescence measurement of pPtBh was collected at 550nm in Figure 3-15(c). All films, both pristine and quenched, were prepared in triplicate. Three separate lifetimes were thus obtained for three separate films at each PCBM concentration. The lifetimes were averaged and are summarized in Figure 3-16. The error bars represent the range of lifetimes measured for each quencher concentration. As the weight percent of PCBM in pPtPh, pPtPh$(CH)_2$ and pPtBP film increases from 0.05-0.525 wt%, the lifetime of the polymers decreases due to triplet exciton quenching in the presence of acceptor molecules. The effect of PCBM concentration on pPtPh lifetime for spin-coated pPtPh/PCBM films is shown in Figure 3-16a. At PCBM concentrations less than 0.225 weight percent (wt%), there is a pronounced effect on the pPtPh lifetime. When the PCBM concentration is larger than 0.225 wt%, the acceptor concentration has a little effect on donor lifetime. As the PCBM concentration increases, the acceptor begins to phase separately from the donor film.[93-95] When a set of pPtPh$(CH)_2$ films are spin-coated with varying amounts of PCBM, the results of Figure 3-16b are obtained. The quenching efficiency for the conjugation-interrupted polymer, pPtPh$(CH)_2$, is lower than the conjugated polymer, pPtPh, because 1,4-phenylene-based structure is interrupted with methylene (CH_2). A pattern similar to pPtPh/PCBM was observed for these films: as acceptor concentration increases, the

lifetime decreases; at higher PCBM concentrations, there is a little change in donor lifetime, suggesting the onset of phase separation. pPtBP is quenched with increasing PCBM concentration, depicted in Figure 3-15c. Due to the intramolecular rotation of biphenyl structure, the quenching efficiency for pPtBP is lower than that of pPtPh. The patterns for pPtBP with PCBM are analogous. The lifetime of pPtBP decreases quickly up to 0.225 wt% PCBM. When the PCBM concentration exceeds 0.225 wt%, the acceptor concentration has a little influence on donor lifetime (Figure 3-16c). As the PCBM concentration increases, phase separation occurs that limits the impact of acceptor concentration on donor lifetime.

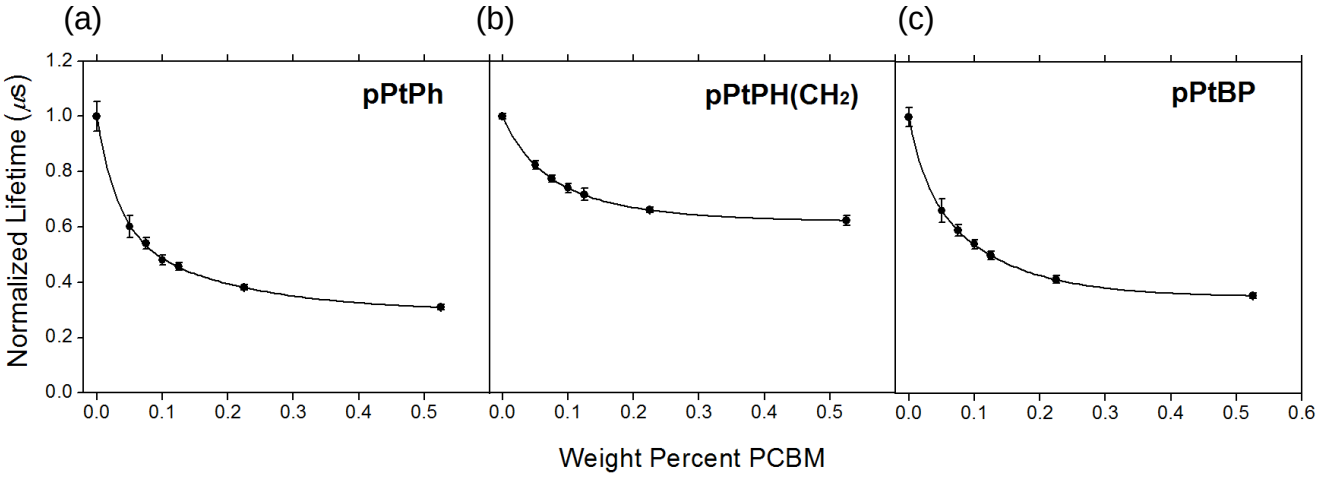

Figure 3-16. Normalized lifetimes for a) pPtPh/PCBM blended films; b) pPtPh(CH_2)/PCBM blended films; c) pPtBP/PCBM blended films. The error bars represent the standard deviation of the average pPtPh triplet lifetime.

Stern-Volmer model was applied to the quenching data, Figure 3-17 is obtained. The donor-acceptor phase separation in the spin-coated films results in a poor fit. To avoid the influence of the donor-acceptor phase separation, the Hindered Access model, Equation 2, was applied to the data.[102] This model still assumes that the donor diffuses to the acceptor before quenching occurs, but it also accounts for f_a, the fraction

of donor able to be quenched by the acceptor. As the spin-coated donor-acceptor films begin to phase separate, the amount of dispersed acceptor molecules remains

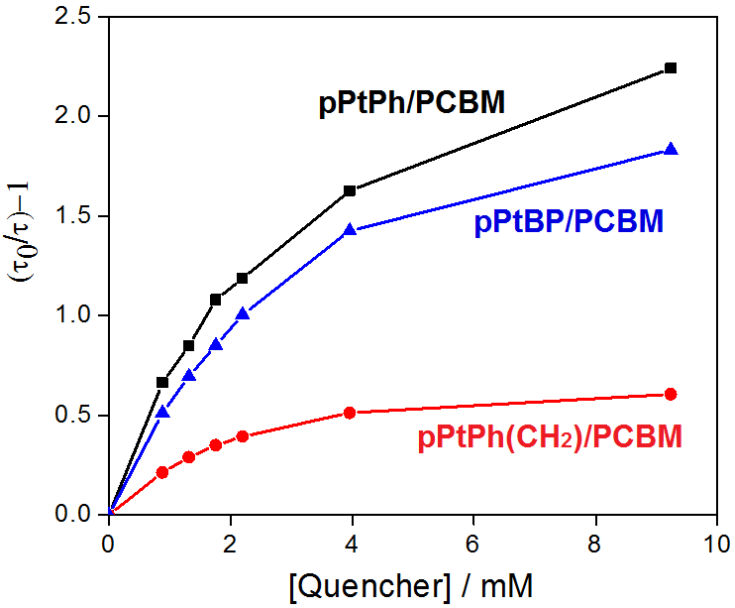

Figure 3-17. Stern-Volmer plots for pPtPh/PCBM (squares), pPtPh(CH_2)/PCBM (circles) and pPtBP/PCBM (triangles) blended films. Error bars have been omitted for clarity.

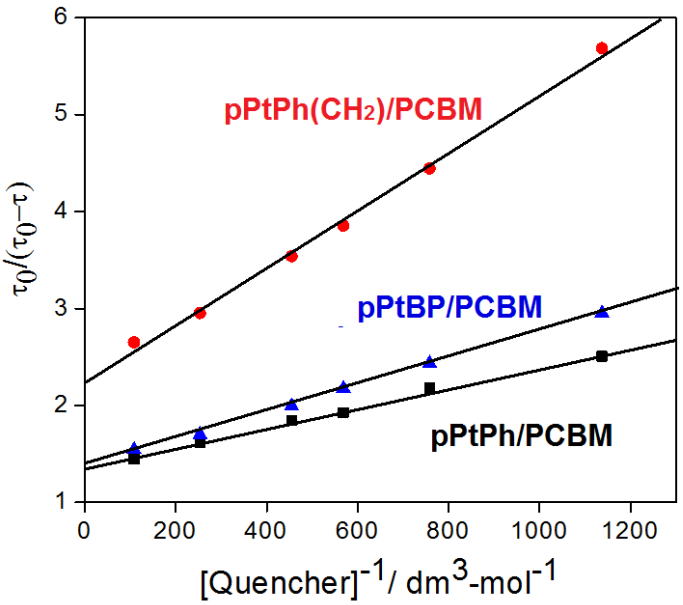

Figure 3-18. Hindered-Access plots for pPtPh/PCBM (squares), pPtPh(CH_2)/PCBM (circles) and pPtBP/PCBM (triangles) blended films. Error bars have been omitted for clarity.

Table 3-3. Summary of the concentration-based triplet exciton diffusion measurements for pPtPh, pPtPh(CH_2) and pPtBP with the PCBM quencher.

Polymer	$k_q\tau$ (M^{-1})	τ_0 (μs)	k_q (10^9 M^{-1}-s^{-1})	D (10^{-6} cm^2-s^{-1})	L_D (nm)	f_a
pPtPh	1,300	1.05	1.30	4.20	21.0	0.80
pPtPh(CH_2)	750	2.15	0.40	1.20	16.0	0.50
pPtBP	1,000	0.95	1.00	3.50	18.0	0.75

constant; the addition of more acceptor molecules results in the growth of pure acceptor domains. This limits the amount of pPtPh, pPtPh(CH_2) and pPtBP that can be quenched by the acceptor. From the Hindered-Access plot in Figure 3-18, the quenching rate constants (k_q) of pPtPh, pPtPh(CH_2) and pPtBP with PCBM can be acquired by Hindered-Access equation. The values of k_q for pPtPh, pPtPh(CH_2) and pPtBP, are 1.3 ×10^9 M^{-1}-s^{-1}, 0.4 ×10^9 M^{-1}-s^{-1} and 1.0 ×10^9 M^{-1}-s^{-1}, respectively (Table 3-3). The k_q of pPtPh/PCBM is approximately one order of magnitude *larger than* k_q of pPtPh(CH_2) with PCBM because of the decreased quenching efficiency of the conjugation interrupted structure. Using the procedure presented above, the values for D and L_D given in Table 3-3 are obtained. The exciton diffusion constants are relatively large for triplets, ~10^{-6} cm^2-s^{-1}, giving a diffusion length of approximately 21 nm, 16 nm and 18 nm for pPtPh, pPtPh(CH_2) and pPtBP, respectively. All of the values calculated using the concentration-based quenching procedure are reproducible. The diffusion coefficient (D) of pPtPh with the PCBM is around four times larger than that of pPtPh(CH_2) /PCBM. Interestingly, the diffusion length (L_D) for pPtPh(CH_2) is only slightly less than L_D of pPtPh since the lifetime of pPtPh(CH_2) (~2.15 μs) is twice that of pPtPh (~1.05 μs). In regards to the fraction of the donor able to be quenched by the acceptor (f_a) for pPtPh and pPtPh(CH_2), the f_a of pPtPh is higher than that of pPtPh(CH_2) since the exciton is trapped in the conjugation-interrupted site of

pPtPh(CH_2). All the diffusion parameters (D, L_D and f_a) of pPtBP are slightly lower than that of pPtPh due to the intrachain rotation in the biphenyl structure

Temperature-Dependent Exciton Dynamics

In order to study the exciton dynamics, the temperature-dependent time-resolved photoluminescence of the pristine polymer thin films, pPtPh, pPtPh(CH_2) and pPtBP, and the quenched polymer thin films with 0.05 % PCBM from – 40 °C to 30 °C were measured, as plotted in Figure 3-19. With the unquenched and quenched lifetime at different temperatures, $\tau_o(T)$ and $\tau(T)$, the quenching rate constants at different temperatures, $k_q(T)$, can be calculated by Equation (3-8).

$$\frac{1}{[Q]}\left(\frac{1}{\tau(T)}-\frac{1}{\tau_o(T)}\right)=k_q(T) \qquad (3\text{-}8)$$

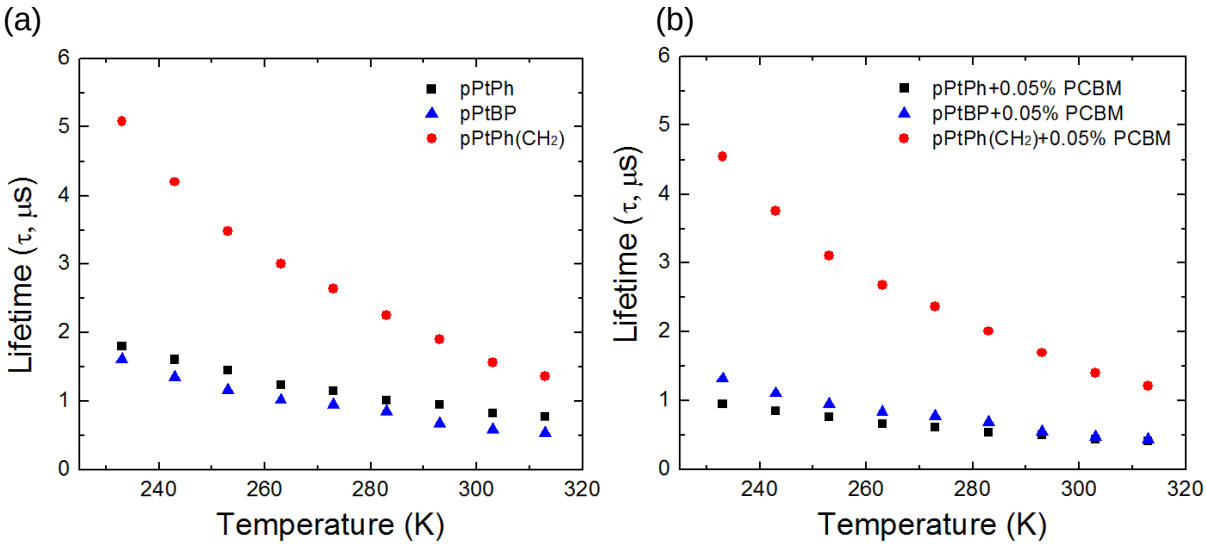

Figure 3-19. Temperature-dependent time-resolved photoluminescence of (a) pPtPh, pPtPh(CH_2) and pPtBP films; (b) pPtPh/0.05% PCBM, pPtPh(CH_2)/0.05% PCBM and pPtBP/0.05% PCBM blended films.

Marcus and Sutin[116] reported an expression for a bimolecular diffusion-controlled system. This mechanism involved in a bimolecular collision between two molecules A and B involves a random diffusion of the molecules toward and away from each other,

becoming an encounter complex, A••B. And then electron transfer occurs with the rate constant k_2, to form the charge separated states A^+ and B^-, as depicted in Equation 3-9.

$$A + B \underset{k_{-1}}{\overset{k_1}{\rightleftharpoons}} A \bullet\bullet B \xrightarrow{k_2} A^+ + B^- \tag{3-9}$$

The bimolecular rate constant k can be written in Equation (3-10),

$$k = K_e A \, exp\left[-\frac{E_a}{k_B T}\right] \tag{3-10}$$

$$K_e = \frac{k_1}{k_{-1}} = \frac{[A \bullet\bullet B]}{[A][B]} \tag{3-11}$$

$$k = A \, exp\left[-\frac{E_a}{k_B T}\right] \tag{3-12}$$

where K_e is an encounter equilibrium constant for the formation of A••B, as shown in Equation (3-11); A is the pre-exponential factor.

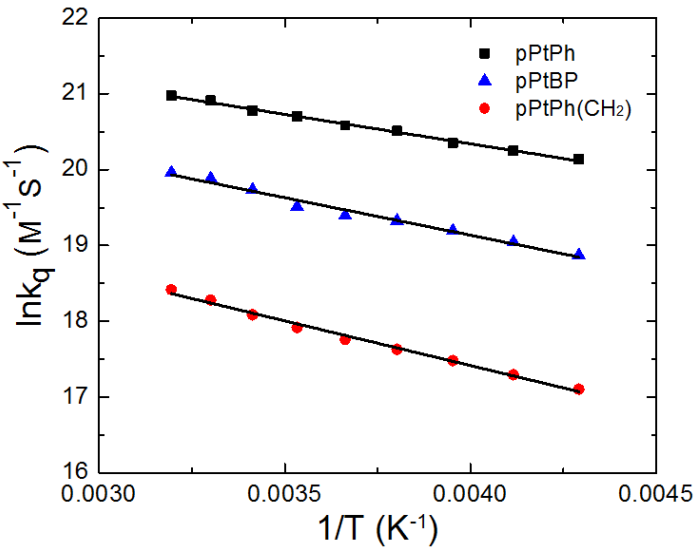

Figure 3-20. Arrhenius plot of pPtPh (squares), pPtBP (triangles) and pPtPh(CH_2) (cycles).

Because the diffusion-controlled process in the exciton quenching system is reversible, we assume the equilibrium rate constant, K_e, is close to unity. Thus, the Arrhenius equation for the second-order reaction can be expressed by Equation (3-12).

Equation (3-8) is applied to calculate the bimolecular rate constants at different temperatures, k(T), which is the quenching rate constants at different temperatures, $k_q(T)$, as shown in Equation (3-13). Using the Equation (3-14), the natural logarithm of k_q versus 1/T for the series of polymers, pPtPh, pPtBP and pPtPh(CH_2), can be displayed as an Arrhenius plot, as shown in Figure 3-20. From the slopes of Arrhenius plots, the activation energies (E_a) of pPtPh, pPtBP and pPtPh(CH_2) can be calculated, which are 65 meV, 85 meV, 100 meV respectively, as listed in Table 3-4.

Triplet exciton motion in the polymers occurs by Dexter energy transfer, which is a process through the HOMO and the LUMO of two molecules or two parts of a molecule exchange an electron simultaneously.[117,118] Köhler group[119] thus demonstrated that Dexter energy transfer can be described using Marcus [25,120] theory. [121] Generally, the rate constant for electron transfer in the quenching process, k_q, given by Marcus [25,120] theory is shown in Equation (3-13).

$$k = k_q = A\ exp\left[-\frac{E_a}{k_B T}\right], \tag{3-13}$$

$$ln\, k_q = \ln A - \frac{E_a}{k_B T} \tag{3-14}$$

where *A* and E_a, in turn, are given by

$$A = \frac{2\pi}{\hbar}|H_{AB}|^2\sqrt{\frac{1}{4\pi k_B T\lambda}}, \tag{3-15}$$

$$E_a = \frac{\lambda}{4}\left[1+\frac{\Delta G^0}{\lambda}\right]^2 \tag{3-16}$$

where $|H_{AB}|$ is the electronic coupling between the initial state *A* and the final state *B* and E_a is the activation energy for the reaction. ΔG^0 is the change of standard Gibb's free energy for energy transfer reaction. When the donor and acceptor molecules are duplicate, the electron transfer reaction is in the isoenergetic situation ($\Delta G^0 = 0$). Thus

the activation energy depends only on the reorganization energy λ for the equilibrium thermodynamic free energy of the donor and acceptor.

$$E_a = \frac{\lambda}{4} \tag{3-17}$$

With the assumption of Equation (3-17), the reorganization energies (λ) of pPtPh, pPtBP and pPtPh(CH_2) are 260 meV, 340 meV, 400 meV, respectively (Table 3-4). The electronic coupling constants (H_{AB}) of pPtPh, pPtBP and pPtPh(CH_2)can be computed by Equation (3-15). The H_{AB} of pPtPh, pPtBP and pPtPh(CH_2) are 5.5 cm^{-1}, 5.0 $cm^{-1}$and 3.0 cm^{-1},respectively. The exchange coupling H_{AB} depends on the overlap of the excited-state wave functions of the initial and final sites. In the conjugated polymers, these wave functions are more delocalized and can overlap to some degree along the chain. In contrast, the overlap of the wave functions of the conjugation interrupted polymer is interrupted by the methylene spacers.

Köhler group[119] has investigated the triplet exciton diffusion of the pPtPh film. The phosphorescence of the pPtPh film is strongly temperature dependent. They attributed the reduction of phosphorescence intensity with increasing temperature to a thermally activated diffusion of the excited state to quenching sites such as chemical defects. The nuclear magnetic resonance data indicated an average of about four missing terbutylphosphine ligands per polymer chain. This corresponds to two defect sites per chain. Thus, a reduced lifetime of the triplets can be demonstrated by a quenching effect. The phosphorescence lifetime, τ, of the pPtPh film can be fitted with a biexponential decay response at all temperatures from 10 to 300 K. A deviation from monoexponential decay is consistent with diffusion to a spatial distribution of quenching sites. The associated phosphorescence decay rate 1/τ for the pPtPh film against

inverse temperature was plotted. This Arrhenius curve of the pPtPh film was fitted by an equation $\frac{1}{\tau} = a \times \sqrt{1/T}\exp\left[-\frac{E_a}{k_B T}\right] + b$, yielding an activation energy (E_a) of 60 meV and an electronic coupling (H_{AB}) of 0.14 cm^{-1}. It is worth noting that the activation energy they acquired (E_a = 60 meV) is closed to the activation energy we measured (E_a = 65 meV), but their electronic coupling (H_{AB} = 0.14 cm^{-1}) is much different from ours (H_{AB} = 5.5 cm^{-1}). The main reason is that we are able to estimate the trap concentration, so we can acquire the more exact value of electronic coupling.

Table 3-4. The activation energies and Electronic Coupling constants of pPtPh, pPtBP and pPtPh(CH_2).

Polymer	E_a (meV)	λ (meV)	H_{AB} (cm^{-1})
pPtPh	65	260	5.5
pPtBP	85	340	5.0
pPtPh(CH_2)	100	400	3.0

Closing Remark

In this work, an acceptor concentration-based method of estimating the exciton diffusion parameters for polymer thin films was developed. In a series of spin-coated, donor-acceptor films, the molar concentration of the acceptor was related to the dynamics of exciton quenching. Assuming the rate constant of exciton quenching is limited by the exciton diffusion coefficient, standard photophysical quenching models were applied to the data to obtain k_q. This rate constant was shown to be equal to the exciton-acceptor collision frequency, allowing the calculation of D. Standard, literature-based exciton time-of-flight experiments validated the newly-developed model, indicating it is a reasonable estimation of the exciton diffusion parameters for optically active thin films.

The conjugated platinum acetylide polymer, Ph_{100}, was designed to quantify the triplet exciton diffusion with a series of quenchers, PCBM, PtOEP or $Ph_{95}BTD_5$, in the

solid state. From the effective concentration-based method, we can determine the exciton diffusion lifetime (τ), exciton diffusion coefficient (D), exciton diffusion length (L_D) and the fraction of donor quenching by the acceptor (f_a) among this series of quenchers. Because the $Ph_{95}BTD_5$ is a homogeneous quencher in this donor-acceptor system, the f_a of $Ph_{100}/Ph_{95}BTD_5$ is close to unity and its Stern-Volmer plot is more linear. In the comparison with the diffusion parameters of the reference methods, the exciton diffusion coefficient and diffusion length depend on chain length of the polymer.

From the results of the dynamics of the triplet exciton diffusion for pPtPh, pPtPh(CH_2) and pPtBP, we can observe that the key parameters of triplet exciton diffusion for pPtPh(CH_2), such as D, L_D and f_a, are smaller than that of pPtPh because the interrupted feature in the polymeric chain hinders exciton transport within polymeric chromophore arrays. This demonstrates triplet diffusion rate in the conjugated polymer is faster than that in the conjugation-interrupted structure since triplet transfer strongly depends on the chain length of the conjugated polymers. This is because the excited-state wave function in the backbone of the polymer is more delocalized that the geometric relaxation energy is lower. Additionally, the diffusion parameters of pPtBP are slightly lower than that of pPtPh due to the intrachain rotation of the biphenyl groups. From the temperature-dependent time-resolved photoluminescence, the activation energy and electronic couping constant were estimated. The activation energy of the conjugation interrupted polymer, pPtPh(CH_2), is highest; by contrast, the electronic coupling of pPtPh(CH_2) is lowest. In addition, the E_a of pPtBP is higher than that of pPtPh and H_{AB} of pPtBP is lower than that of pPtPh, because intrachain rotation can enhance the activation energy and diminish the overlap of π electron wave functions.

Therefore, triplet exciton diffusion in the polymer can be increased by two factors: first, by a lower activation energy due to less geometric distortion along the chain and second, by a strong intrachain electronic coupling. Finally, our method for estimating the electronic coupling is more exact because we know the concentration of the quencher.

Experimental

Materials

Fullerene and PCBM were purchased from Nano-C, and Platinum octaethylporphyrin (PtOEP) was obtained from Frontier Scientific. 4,7-dibromobenzo[1,2,5]thiadiazole, tri-iso-propylsilylacetylene and trimethylsilylacetylene were obtained from either Acros or Aldrich and used as received. Compounds 4-9 were synthesized according to the literature procedures.[93-95,122] All reactions were performed under argon atmosphere in anhydrous solvents, which were dried prior to use following standard procedures. Merck silica gel 60 (particle size 0.04−0.063 mm) was employed for flash chromatography.

^{1}H NMR, ^{13}C NMR, ^{31}P NMR spectra were obtained on a Varian VXR-300 instrument using deuterated chloroform ($CDCl_3$) as the solvent and tetramethylsilane (TMS) as the internal reference. Gel permeation chromatography (GPC) was performed by eluting a tetrahydrofuran (THF) solution of the polymer through two PL-Gel 5 Mixed D columns pressurized by a Rainin Dynamax SD-200 solvent pump. Polymer elution was spectroscopically monitored using a UV detector set to a wavelength where the polymer absorbs, and molecular weight calculations were performed using Polymer Laboratories PL software against a polystyrene standard. All solvents used were of HPLC grade.

Synthesis

4-((triisopropylsilyl)ethynyl)-7-((trimethylsilyl)ethynyl)benzothiadiazole (4). To a flask charged with THF and diisopropylamine (DIPA) (8 mL, 1:1) was added 4,7-dibromobenzo[1,2,5]thiadiazole (582 mg, 2.0 mmol). The resulting solution was degassed for 30 min by purging with argon. This solution was added trimethylsilylacetylene (196.4 mg, 2 mmol), tri-iso-propylsilyl-acetylene (364.1 mg, 2 mmol), $Pd(PPh_3)_4$ (12 mg, 1.6 mmol), and copper iodide (4 mg, 2 mmol). The reaction was then stirred at room temperature for 24 hours. After this time the solvent was removed under reduced pressure. Flash chromatography of the residue with hexanes gave the desired product as a yellow solid. (yield 660 mg, 80%). ^{1}H NMR ($CDCl_3$, 300MHz): δ (ppm) 0.33 (s, 9H), 1.19 (s, 21H), 7.69 (m, 2H). ^{13}C NMR ($CDCl_3$, 300 MHz): δ (ppm) 0.09, 11.5, 18.9, 91.5, 100.2, 100.7, 102.2, 103.4, 117.1, 117.8, 132.8, 133.2, 154.3.

4-Ethynyl-7-((triisopropylsilyl)ethynyl)benzothiadiazole (5). To a deoxy-genated solution of 4 (825 mg, 2.0 mmol) in dichloromethane (DCM, 30 mL) and methanol (MeOH, 30 mL), potassium carbonate (KOH, 0.34 g, 6.0 mmol) was added under argon flow. The mixture was stirred at room temperature for 1 hour. Then deionized water (100 mL) was added to extract unreacted KOH. The organic layer was separated and washed 3 times with brine and deionized water, and was dried over sodium sulfate. The solvent was evaporated to obtain a colorless oil. The crude product was purified by column chromatography on silica gel using hexane as the eluent (Rf = 0.47) to yield a colorless liquid. Yield: 539 mg (99%). ^{1}H NMR (300 MHz, $CDCl_3$): δ (ppm) 1.18 (m, 21H), 3.66 (s, 1H) and 7.71 (m, 2H). ^{13}C NMR (75 MHz, $CDCl_3$): δ (ppm) 11.5, 18.9, 79.4, 85.0, 101.2, 102.0, 115.9, 118.4, 132.8, 133.4, 154.6.

Complex (7). 4-Ethynyl-7-((triisopropylsilyl)ethynyl)benzothiadiazole (5) (126.9 mg, 0.373 mmol) and cis-dichloro-bis-(tri-n-butylphosphine) platinum(II) 6 (250.1 mg, 0.375 mmol) were dissolved in Et_2NH (15 mL) and the solution was degassed with nitrogen. The mixture was stirred under reflux for 8 hours. The solvent was removed and the crude product purified by flash chromatography (silica gel, hexane then 7:3 hexane/CH_2Cl_2) giving the desired product 7 as a yellow solid (146 mg, 40 %). ^{1}H NMR ($CDCl_3$, 300 MHz): δ (ppm) 0.88 (t, 18H), 1.19 (s, 21H), 1.41 (br m, 12H), 1.64 (br m, 12H), 2.29 (br m, 12H), 7.37 (d, 1H), 7.63 (d, 1H). ^{13}C NMR ($CDCl_3$, 75 MHz): δ (ppm) 11.5, 13.9, 18.8, 22.1, 24.5, 26.2, 86.9, 90.9, 107.7, 119.9, 129.1, 130.6, 131.2, 131.8. ^{31}P NMR ($CDCl_3$, 121 MHz) δ 7.95 (J_{Pt-P} = 2360 Hz).

Complex (8). Monomer 7 (146 mg, 0.150 mmol) was dissolved in THF (9 mL) in a 25ml single neck round bottle flask. The solution was degassed with nitrogen and tetrabutylammonium fluoride (86 mg, 0.32 mmol) was added via syringe. A white precipitate immediately formed from the yellow-colored solution. The reaction was stirred at room temperature for about 3.0 hours. The solvent was removed and the crude product purified by flash chromatography (silica gel, hexane then 1:4 hexane/CH_2Cl_2) giving the desired product 8 as a yellow solid (146 mg, 40 %). ^{1}H NMR ($CDCl_3$, 300 MHz): δ (ppm) 0.92 (t, 18H), 1.45 (br m, 12H), 1.60 (br m, 12H), 2.11 (br m, 12H), 3.60 (s, 1H), 7.36 (d, 1H), 7.65 (d, 1H). ^{13}C NMR ($CDCl_3$, 75 MHz): δ (ppm) 14.0, 23.9, 24.5, 26.6, 80.3, 83.2, 106.9, 111.7, 123.9, 129.4, 134.3, 155.1. ^{31}P NMR ($CDCl_3$, 121 MHz): δ (ppm) 7.89 (J_{Pt-P} = 2390.8 Hz).

$Ph_{95}BTD_5$. Monomer 8 (4.9 mg, 0.006 mmol) was added with monomer 9 (90 mg, 0.119 mmol) in a 7:2 mixture of diisopropyamine:THF (9 mL) in a Schlenk flask. The

solution was degassed over 5 freeze-pump-thaw cycles. The flask was backfilled with dry argon and tetrabutylammonium fluoride (73 mg, 0.275 mmol) was added via syringe. A white precipitate immediately formed from the yellow-colored solution. The reaction was stirred at room temperature for about 40 min, at which time a TLC with 1:4 hexanes:DCM revealed total consumption of 9. Copper (I) iodide (1.9 mg, 0.01 mmol) was then added in the Schlenk flask. After stirring overnight at room temperature, it was noticed that the polymerization reaction formed a yellow suspension. The reaction was poured into an excess of methanol, precipitating the polymer as a yellow powder. The precipitate was filtered using a 2.5 µm glass fiber filter pad and redissolved in THF. The solution was reprecipitated into an excess of methanol and filtered using a glass fiber filter pad. The yellow powder was once again redissolved in THF, precipitated from methanol, and filtered for a third and final time. After the final precipitation, the polymer was dried under a vacuum at room temperature overnight to give $Ph_{95}BTD_5$ (62 mg, 65%). The polymer was characterized by GPC, UV-VIS/emission and by NMR. ^{1}H NMR ($CDCl_3$, 300 MHz): δ (ppm) 0.91 (t, 18H), 1.57 (br m, 12H), 1.59 (br m, 12H), 2.13 (br m, 12H), 7.09 (s, 4H), 7.61 (s, 0.04H). ^{31}P NMR ($CDCl_3$, 120 MHz): δ (ppm) 3.96 (t, 2390 Hz). GPC: Mn = 15,600; Mw = 34,400, PDI= 2.20

2-Methyl-4-(4'-((trimethylsilyl)ethynyl)-[1,1'-biphenyl]-4-yl)but-3-yn-2-ol (12). 4,4'-Diiodo-1,1'-biphenyl (5.1 g, 15.16 mmol) was dissolved in THF (60 mL) and *i*-Pr_2NH (40 mL) in a Schlenk flask and the solution was degassed with argon for 30 min. Then, tri-iso-propylsilyl-acetylene (2.76 g, 15.16 mmol), 2-methylbut-3-yn-2-ol (1.28 g, 15.16 mmol), $Pd(PPh_3)_2Cl_2$ (12 mg, 1.6 mmol) and CuI (0.346 g, 1.8 mmol) were added. The mixture was stirred at 70˚C for 3 hours. After cooling down, the mixture was passed

through a bed of Celite, washed with 10% NH_4OH (3 x 50 mL) and water (3 x 50 mL), the organic phase dried on $MgSO_4$, filtered and the solvents were removed. Chromatography on silica (hexane first, then 9:1 hexane/CH_2Cl_2) gave the desired product 12 as a red oil (1.60 g, 65 %). ^{1}H NMR ($CDCl_3$, 300 MHz): δ (ppm) 0.26 (s, 9H), 1.64 (s, 6H), 2.01 (s, 1H), 7.53 (m, 8H); ^{13}C NMR ($CDCl_3$, 75 MHz): δ (ppm) -0.05, 31.4, 81.8, 94.6, 95.2, 104.8, 121.9, 122.3, 126.6, 126.7, 132.1, 132.4, 139.9, 140.1.

4-(4'-ethynyl-[1,1'-biphenyl]-4-yl)-2-methylbut-3-yn-2-ol (13). 2-Methyl-4-(4'-((trimethyl-silyl)ethynyl)-[1,1'-biphenyl]-4-yl)but-3-yn-2-ol 12 (70.8 mg, 0.272 mmol) was dissolved in a 1:1 mixture of methanol:DCM (9 mL) in a round flask. The solution was purged by dry argon for 15 min and potassium carbonate (75.6 mg, 0.54 mmol) was added instantly. And then the reaction was stirred at room temperature for about 3 hours, at which time a TLC with 2:1 hexanes:DCM revealed total consumption of 12. (yield 60 mg, 86%). ^{1}H NMR ($CDCl_3$, 300MHz): δ (ppm) 1.64 (s, 6H), 2.18 (s, 1H), 3.15 (s, 1H), 7.54 (m, 8H); ^{13}C NMR ($CDCl_3$, 300 MHz): δ (ppm) 31.4, 65.6, 78.1, 81.8, 83.4, 94.7, 121.3, 122.1, 126.6, 126.7, 132.0, 132.6, 139.8, 140.5.

trans-Bis(tributylphosphine)chloro{(4'-(3-hydroxy-3-methylbut-1-yn-1-yl)-[1,1'-biphenyl]-4-yl)ethynyl} platinum (II) (14). 4-(4'-Ethynyl-[1,1'-biphenyl]-4-yl)-2-methylbut-3-yn-2-ol (0.33 g, 1.28 mmol) and Et_2NH (30 mL) were added to a round bottom flask with a stir bar. The mixture was stirred and degassed with argon for 10 min, follow by the addition of cis-$Pt(PBu_3)_2Cl_2$ (0.95 g, 1.41 mmol). The reaction was stirred at reflux under argon overnight, then cooled and diluted with CH_2Cl_2. The organic solution was washed with both d.i. water and brine then dried over $NaSO_{4(s)}$. TLC in 5:1 hexane/CH_2Cl_2 gave 4 spots (spot 3 was product). Solvent was evaporated to give a

crude solid that was purified by flash chromatography (silica gel, 9:1 to 3:1 hexane/CH_2Cl_2). Fraction 3 solvent was evaporated to afford a yellow crystalline solid that did not phosphoresce under a long wave UV lamp. Yield 0.90 g (85.0%). ^{1}H NMR (300 MHz, $CDCl_3$): δ (ppm) 0.93 (t, 18H), 1.47 (m, 12H), 1.60 (br m, 12H), 1.63 (s, 6H), 2.01 (br m, 12H), 2.11 (s, 1H), 7.28 (d, 2H), 7.31 (m, 4H), 7.51 (d, 2H); ^{13}C NMR ($CDCl_3$, 300 MHz): δ (ppm) 14.1, 22.3, 24.6, 26.4, 31.9, 66.0, 82.4, 85.5, 94.7, 101.2, 110.3, 121.6, 126.8, 128.8, 131.5, 132.4, 137.0, 141.0; ^{31}P NMR ($CDCl_3$): δ (ppm) 6.9 (J = 2350 Hz).

pPtBP. Monomer 14 (230 mg, 0.272 mmol) was dissolved in a 7:2 mixture of diisopropy-amine:THF (9 mL) in a Schlenk flask. The solution was degassed over 5 freeze-pump-thaw cycles. The flask was backfilled with dry argon and sodium hydroxide (0.025 g, 0.54 mmol) was added, and then reacted at room temperature for 10 hours. A white precipitate immediately formed from the yellow-colored solution. The reaction was stirred at room temperature for about 2 hours, at which time a TLC with 1:4 hexanes:DCM revealed total consumption of 14. Copper (I) iodide (2.8 mg, 0.015 mmol) was then added and the reaction heated to 44 ℃. After stirring overnight, it was noticed that the polymerization reaction formed a neon-yellow suspension. The reaction was poured into an excess of methanol, precipitating the polymer as yellow fibers. The precipitate was filtered using a 2.5 µm glass fiber filter pad and redisolved in THF. The solution was reprecipitated into an excess of methanol and filtered using a glass fiber filter pad. The yellow fibers were once again redissolved in THF, precipitated from methanol, and filtered for a third and final time. After the final precipitation, the polymer was dried under a vacuum at room temperature overnight to give pPtBP (115 mg, 50%).

The polymer was characterized by GPC, UV-VIS/emission and by NMR. ^{1}H NMR ($CDCl_3$, 300 MHz): δ (ppm) 0.94 (t, 18H), 1.47 (m, 12H), 1.62 (m, 12H), 2.16 (m, 12H), 7.30 (s, 4H), 7.46 (s, 4H). ^{31}P NMR ($CDCl_3$, 120 MHz): δ (ppm) 3.96 (t, 2360 Hz). GPC: Mn = 13,100; Mw = 14,800, PDI= 1.13.

Thin Film Preparation

Glass slides were cut into 1.2×2.5 cm rectangles using a glass scribe. Each slide was hand polished using a Kimwipe until no visible contaminant films were visible to the naked eye. The slides were then placed in a custom made slide holder and sonicated for 10 min each in sodium dodecylsulfate (SDS)/water, water, acetone, then isopropanol. All water used was purified to a resistivity of 18.2 MΩ using a Millipore Simplicity water purification system. The slides were dried using filtered, compressed air and then stored in a covered container prior to use.[123]

Glass vials, approximate volume three milliliters, were arranged in seven vertical columns, with each column containing three vials. A tetrahydofuran (THF) solution of Ph_{100} with a concentration of 20.2 g-L^{-1} was dispensed into each vial in 20 µL aliquots using a precision glass syringe. A dilute (<0.02 g-L^{-1}) solution of acceptor in THF was added, using a precision glass syringe, to each vial in pre-determined volume aliquots. Each volume increment was not less than 15 µL to ensure the accuracy and reproducibility of the quencher concentration. To ensure reproducible film thicknesses and complete slide coverage, the solvent in each vial was allowed to evaporate under ambient conditions. Immediately before spin-coating, the solution was redissolved in 100 µL of THF. A slide was placed on a spin-coater programmed to rotate at 1000 RPM for 20 s. After ensuring the slide was properly affixed to the spin-coater, all of the redissolved THF solution was transferred to the slide. The film was spin-coated and

allowed to dry in the dark under vacuum overnight before any measurements were made. Using the method of Albert and Malone, the density of Ph_{100} were calculated to be 1.28 g-cm^{-3}.[96-101] The molar concentrations of PCBM, PtOEP and $Ph_{95}BTD_5$ in the Ph_{100} spin-coated films were thus able to be determined.[100,101]

In order to detect the intense photophysical signals of the polymer thin films, some of the thin films were made by drop coating in the Mbraun glovebox workstation that can attain purity levels of less than one part per million oxygen and moisture. To prepare the drop-coated slides, these polymers are dissolved in THF with a concentration of 20 mg/mL which were stirred for 4 hours. And then the deposited materials on glass slides were fabricated using a pipette. In order to prevent a warped or wavy appearance, the material could be siphoned holding the pipette at approximately 45 degrees during the deposition on the slides, as given in Figure 3-18. Furthermore, air bubbles and particles on the surface can easily be siphoned off in the meantime as well.

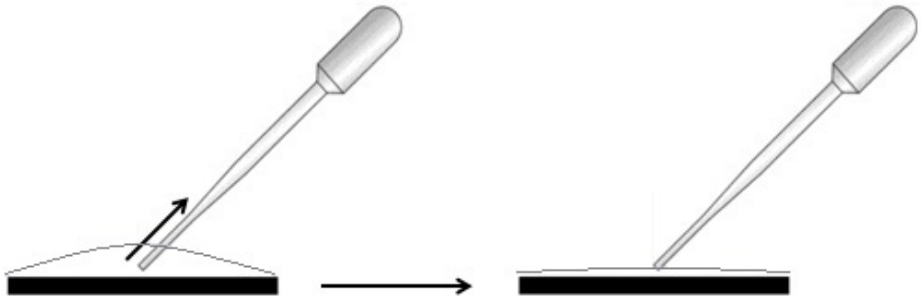

Figure 3-18. Siphoning material to form uniform coat and remove visible film imperfections.

Thin films for TOF measurements were made using a similar technique with anhydrous dichloromethane (DCM) degassed using four cycles of freeze-pump-thaw. The Ph_{100} films were spin-coated inside an argon atmosphere glovebox. Acceptor (C60)

films 40nm thick were deposited in a high vacuum (< 10^{-6} torr) at a rate of 2 Å-s^{-1}. TOF measurements were done by Dr. Jarrett H. Vella of Dr. Kirk Schanze's group ,and by Dr. Jason Myers of Dr. Jiangeng Xue's group in the University of Florida Department of Materials Science and Engineering.

Time-Resolved Photoluminescence

Phosphorescence decay kinetic was obtained with a multichannel scaler/photon counter system with a NanoQuant FluoTime 100 compact phosphorescence lifetime spectrophotometer (PicoQuant Photonics North America, Inc., http://www.picoquant-usa.com/). A CUBE diode laser provided the excitation at 375 nm (< 16 mW). The 100 ns pulsed laser was generated by SRS DG353 Digital Delay/Pulse Generator. The specific narrow bandpass filter was used for each measurements followed by global fit processing (FluoroFit software). Decays were obtained using the biexponential fitting parameters (FluoroFit software, PicoQuant). All films, both pristine and quenched, were prepared in triplicate. Three separate lifetimes were thus obtained for three separate films at each quencher concentration. The lifetimes were averaged and the error bars represent the standard deviation of the average triplet lifetime.

Temperature-Dependent Experiment

In order to study the temperature-dependent time-resolved dynamics, the temperature was controlled using a thermo Neslab RTE-140 Refrigerated Bath/ Circulator, which is designed to provide temperature control for applications requiring a fluid work area or pumping to an external system. Before starting the unit, check all electrical and plumbing connections and make sure the work area has been properly filled with bath fluid. To start the unit press the I/O switch on the side of the controller to the power on position. The pump will start and the POWER LED will light. The

REFRIGERATION switch should be ON for normal operation below 40°C. Because the temperature for the investigation is from – 40 °C to 30 °C, the fluid I chose was the mixture of D.I. water and laboratory grade ethylene glycol (v/v = 50/50).

CHAPTER 4
TRIPLET-TRIPLET ENERGY TRANSFER IN POLYSTYRENE-BASED PLATINUM ACETYLIDE ARRAYS

Introductory Remark

Triplet-triplet energy transfer (TTET) is a fundamental photophysical process which follows the Dexter electron-exchange mechanism and can be considered as two simultaneous electron transfers with different spin.[22,124] This process plays an important role in chemistry (such as photosensitizers[124]), biology (such as photosynthesis, singlet oxygen formation and quenching[125,126]) and material science (such as organic light-emitting diodes, OLEDs[127,128]). The triplet-triplet energy transfer process has been studied in many donor-acceptor systems. A typical example is the multichromophric system containing a Pt(II)-polypyridine-acetylide-pyrene complex, in which TTET occurs from Pt-dimine ^{3}MLCT to Pt-induced pyrene ^{3}IL in around 200 femtoseconds, due to the highly electronically coupled structures.[129,130] The triplet acceptor pyrene moiety can be replaced by other functional moieties, such as different bodipy dyes[131,132] and metal-polypyridine complexes (typically Ru- and Os-complexes).[133,134]

Saturated and π-conjugated bridges can be inserted between donor and acceptor to form donor-bridge-acceptor structures. Ru complexes, Os complexes and porphyrins are often used in the donor-bridge-acceptor systems as triplet energy donor or acceptor. In these systems, superexchange mechanism (insulating bridge)[135-137] and injection mechanism (conducting bridge)[138] are applied to explain the triplet-triplet energy transfer. The triplet-triplet energy transfer depends on the donor-acceptor

---

This Chapter is considered for publication in the Journal of the American Chemical Society.

distance, the donor-bridge energy gap and the influence of the distance dependence by the donor-bridge energy gap.[139]

Platinum-acetylide complexes, which structurally feature a four-coordinated square planar platinum(II) center with the general formula *trans*-$PtL_2(C{\equiv}CAr)_2$ (where L is typically a phosphine ligand (e.g., PBu_3) and Ar is a π-conjugated aryrene unit), are a versatile platform for triplet exited states and related photophysical processes. The long-lived and phosphorescent $^3\pi,\pi^*$ triplet excited states caused by heavy atom-induced spin-orbital coupling and the electronic delocalization in Pt-acetylide based π-conjugated oligomers and polymers have been studied extensively. The intramolecular triplet-triplet energy transfer in Pt-acetylide oligomers and polymers has been explored in our group. In the Pt-acetylide oligomers (with 2 or 4 repeat units) with anthracene moiety, triplet-triplet energy transfer from Pt-acetylide segment (^{3}Pt) to anthracene segment (^{3}Ar) is observed from steady-state and time-resolved photoluminescence spectroscopies.[140] A series of monodisperse Pt-acetylide oligomers have been prepared, which consist of different number of $Pt(PBu_3)_2$-C≡C-Ph-C≡C- repeat units and naphthalene diimide (NDI) as end groups. Near-UV excitation produces triplet excitons localized on the Pt-acetylide chains; then the excitons transport to the chain ends and are trapped by the NDI end group. The excitons transports rapidly with an average moving distance of ~3 nm within 200 ps; and the exciton transport follows a site-to-site hopping mechanism with a hopping time of ~27 ps each step.[141] Intrachain triplet-triplet energy transfer has also been investigated in Pt-acetylide based donor-acceptor copolymers. In the copolymers, [$Pt(PBu_3)_2$-C≡C-Ph-C≡C-)] repeat units (Ph-Pt) are randomly incorporated with [$Pt(PBu_3)_2$-C≡C-T-C≡C-)] repeat units (T-Pt, where Ph =

1,4-phenylene and T = 2,5-thienylene). Rapid and efficient triplet-triplet energy transfer from ^{3}(Ph-Pt) to ^{3}(T-Ph) is observed with a rate constant larger than 10^8 s^{-1} at room temperature.[58,142]

In this chapter we expand the intrachain triplet-triplet energy transfer to a Pt-acetylide based non-conjugated macromolecular system, which consists of a well-defined non-conjugated polystyrene backbone and different platinum acetylide side groups. Triplet-triplet energy transfer between platinum acetylide side groups with different excited state energies is highly efficient. The dynamics of energy transfer was studied by nanosecond (ns) scale time-resolved transient absorption, and it was proved that triplet energy transport along the non-conjugated polymer chain occurs by site-to-site hopping process.

The Design of Polymer

A series of well-defined polystyrene-based macromolecular structure (poly-Pt-Ar) were designed and prepared to study the triplet-triplet energy transfer in platinum acetylide arrays. These poly-Pt-Ar feature a well-defined polystyrene backbone, and two different pendent platinum acetylide side groups. The two platinum acetylides designed for triplet energy transfer have a PE2 unit and pyrene unit attached to platinum, respectively (referred as PE2-Pt and Py-Pt in this chapter). After excitation, the platinum atom will induce strong spin-orbit coupling, which makes fast intersystem crossing (ISC) to produce triplet state of the platinum acetylides. The triplet of PE2-Pt has a higher energy than that of Py-Pt (2.35 eV vs. 1.88 eV, calculated from phosphorescence emission peak wavelengths), thus in the polymer PE2-Pt units act as triplet energy donor and the Py-Pt units act as the acceptor. The structures of the designed polymers are depicted in Figure 4-1. Poly-Pt-Ar with different PE2-Pt/Py-Pt ratios are identified as

P-x, where x represents the percentage of Py-Pt in the polymer. P-0 is the homopolymer of PE2-Pt and P-100 is the homopolymer of Py-Pt. In addition, triplet donor and acceptor model compounds (M1 and M2) were also prepared.

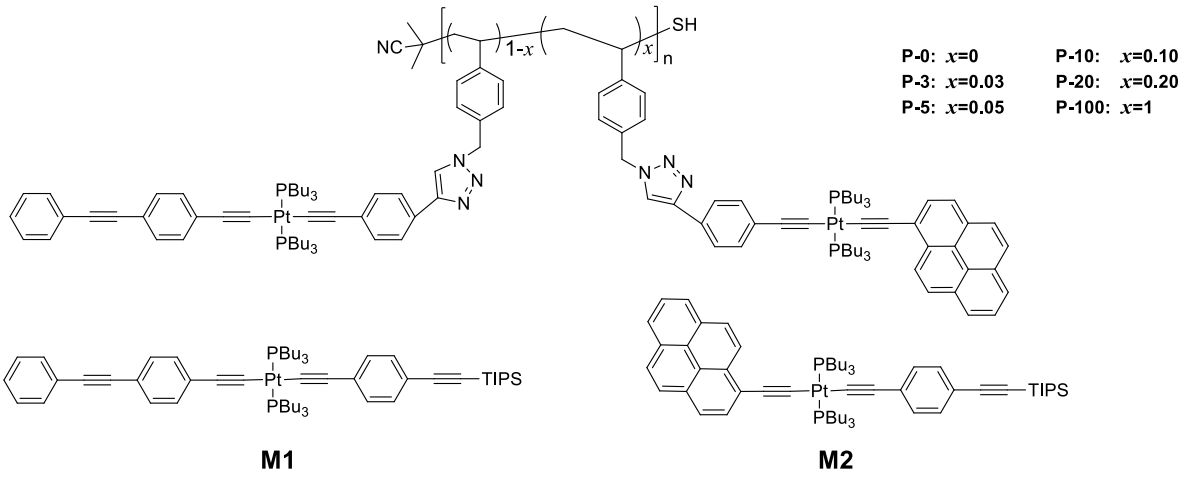

Figure 4-1. Structures of poly-Pt-Ar (P-0 to P-100) and model compounds.

Result and Discussion

UV-Visible Absorption

The absorption spectra of poly-Pt-Ar (P-0 to P-100) and two model compounds (M1 and M2) were measured in THF solution at room temperature, as presented in Figure 4-2. The energy donor (PE2-Pt)-only polymer P-0 has similar absorption spectrum as the PE2-Pt model compound M1. Both have two near-UV peaks around 302 nm and 350 nm, which arise from π- π* transitions of PE2-Pt moieties. Likewise, the acceptor (Py-Pt)-only polymer P-100 and the Py-Pt model compound M2 also have similar absorption spectra. Both have a near-UV absorption band at 292 nm (π- π* transition of -Ph-≡-Pt-) and three visible absorption bands at 368 nm, 387 nm and 398 nm (-Pt-≡-Py), and also has a moderately broad absorption from 300 nm to 350 nm. The comparison of extinction coefficients between model compound and corresponding polymer (i.e., M1 vs. P-0 and M2 vs. P-100) indicate the quantitative grafting ratio during

the “click” reaction, as the difference between extinction coefficients are less than 5% (summarized in Table 4-1).

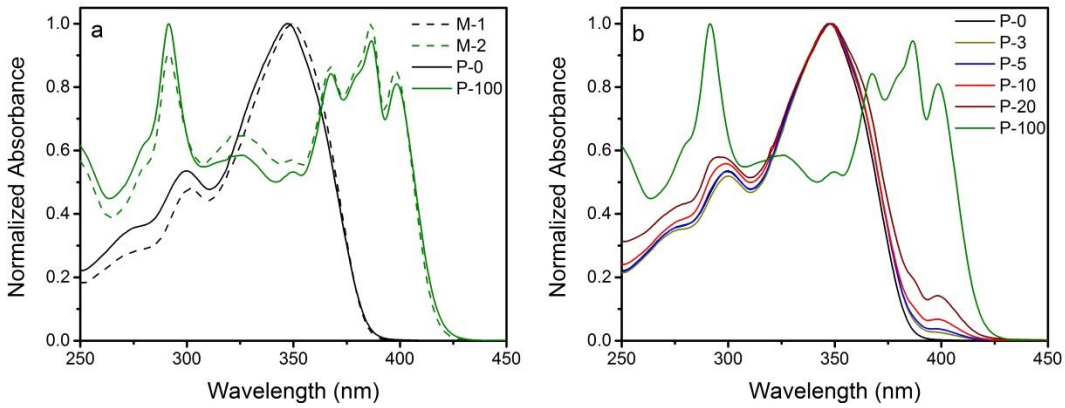

Figure 4-2. (a) Comparison of ground-state absorption of model compounds (M1 and M2), donor-only and acceptor only polymers (P-0 and P-100); (b) Ground-state absorption of poly-Pt-Ar in THF solution.

As for the absorption of the donor-acceptor copolymers P-3 to P-20, the spectra are a combination of PE2-Pt and Py-Pt based transitions, but dominated by the PE2-Pt based transitions (especially at around 350 nm); however, they show increasing Py-Pt character, which features the absorption at 398 nm, as the loading of the lower energy chromophores in the click grafting increases. This feature allows straightforward determination of the Py-Pt loading in the copolymer from the ratio of the absorbance at 350 and 398 nm. The calculation results (summarized in Table 4-1) indicate that the fractional loading of PE2-Pt and Py-Pt corresponds closely to the stoichiometry used in the click reaction. In addition, we simulated the absorption spectrum of a polymer containing 80% of PE2-Pt and 20% of Py-Pt using the absorption spectra and extinction coefficients of P-0 and P-100, which corresponds nicely with the measured P-20 absorption (Figure 4-3).

To summarize, the absorption data for the model compounds and polymers allow several conclusions. First, the fractional loading of PE2-Pt and Py-Pt units in the polymers closely corresponds to the stoichiometry used in the feed for the click reactions, which indicates that the “click” reaction rates of the two platinum acetylids are similar. Second, the absorption at 348 nm is due almost exclusively to PE2-Pt (donor), making it possible to selectively excite this chromophore in the energy transfer studies. Finally, the polymer spectra are accurately simulated as a linear combination of the spectra of the PE2-Pt and Py-Pt chromophores, indicating that there is not a strong ground state interaction among the individual units in the polymers.

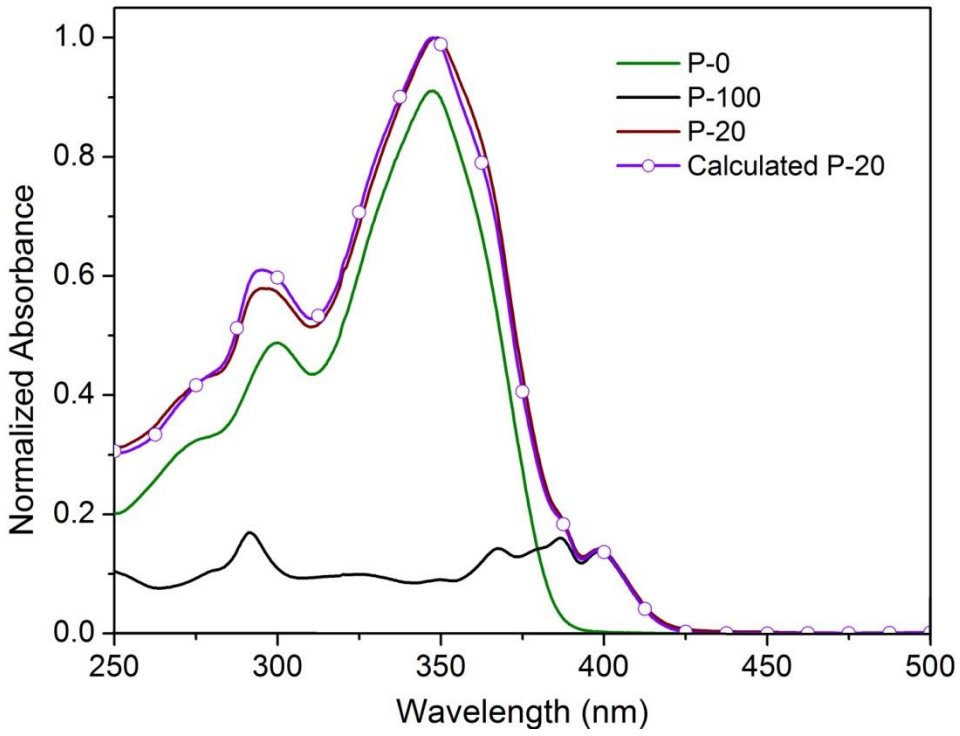

Figure 4-3. Comparison of measured (brown) and simulated (violet circle) absorption spectra of P-20. The calculated spectrum was derived from the absorption spectra and extinction coefficients of P-0 and P-100 based on the equation ε(Calculated P-20) = 0.8 x ε(P-0) + 0.2 x ε(P-100). The results were then normalized to obtain the spectrum (violet circle) above. The spectra of P-0 and P-100 in this figure are normalized based on their relative molar absorptivities and relative PE2-Pt/Py-Pt content in P-20 copolymer

Table 4-1. Photophysical characteristics of model compounds and poly-platinums.

Compound/ Polymer	Py-Pt Content[a] /%	Abs_{max} /nm[b]	Extinction Coefficient / M^{-1}•cm^{-1}	FL_{max} /nm[b]	ϕ_{FL}[c]	Ph_{max} /nm[b]	ϕ_{ph}[c]			Energy Transfer Efficiency /%
							ϕ_{PE2-Pt} (480-628 nm)	ϕ_{Py-Pt} (628-850 nm)	ϕ_{total} (480-850 nm)	
M1	--	350	84,700	--	--	527	0.18	--	0.18	--
M2	--	292 368 387 398	60,900 58,000 66,800 57,100	412	0.002	660 737	--	0.015	0.015	--
P-0	0	348	89,700	388	<0.0001	527	0.12	--	0.12	--
P-1	3.2	348	--	388	<0.0001	527 660 737	0.016	0.023	0.039	86.3
P-5	5.3	348	--	388	<0.0001	527 660 737	0.0065	0.021	0.028	94.6
P-10	10.3	348	--	388	<0.0001	527 660 737	0.0025	0.018	0.021	97.9
P-20	21.1	348	--	388	<0.0001	527 660 737	0.00072	0.015	0.016	99.4
P-100	100	292 368 387 398	66,800 56,100 63,500 54,100	412	0.0013	660 737	--	0.014	0.014	--

[a] Determined by UV-visible absorption

[b] Abs_{max}: Ground state absorption maxima; FL_{max}: Fluorescence emission maxima; Ph_{max}: Phosphorescence emission maxima

[c] With anthracene as quantum yield standard, ϕ = 0.27 in ethanol at room temperature

Steady-State Photoluminescence

The photoluminescence spectra of poly-Pt-Ar, P-0 to P-100, and model compounds, M1 and M2, were recorded in deoxygenated THF solution at room temperature (Figure 4-4a). The donor model M1 and poly-Pt-Ar P-0 to P-20 were excited with λex = 350 nm (PE2-Pt absorption), while the acceptor model M2 and the acceptor-only P-100 were excited with λex = 398 nm (Py-Pt absorption). The photoluminescence spectrum of M1 has an intense phosphorescence peak centered at λmax = 527 nm along with a vibronic peak at λ = 570 nm. P-0 has nearly identical spectrum as M1, except lower phosphorescent quantum yield (Table 4-1) likely due to self-quenching.143 The acceptor model M2 has a phosphorescence peak at 660 nm and vibronic peaks at 675 nm, 718 nm and 735 nm. The emission spectrum of P-100 exhibits the same peaks as those of M2.

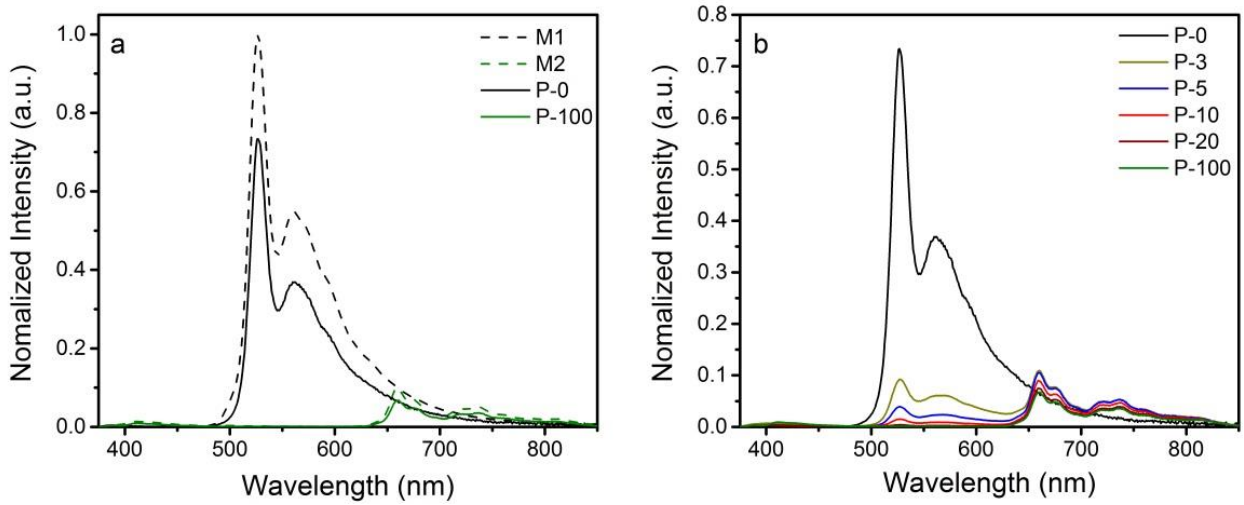

Figure 4-4. (a) Comparison of emission of model compounds (M1 and M2), donor only and acceptor-only polymers (P-0 and P-100). (b) Emission of poly-Pt-Ar in THF. The solutions had OD around 0.8 and were deoxygenated by bubbling argon for 45 minutes. The excitation wavelength was set at 350 nm for P-0 to P-20 and M1, and 385 nm for P-100 and M2.

Selective excitation of donor-acceptor copolymers (P-3 to P-20) with PE2-Pt donor absorption wavelength (λex = 350 nm) allows us to study energy transfer in the copolymers. When 3% of Py-Pt acceptor is doped in the polymer (P-3), the phosphorescence from the PE2-Pt donor is quenched ~ 85% relative to the intensity of P-0, and emission from Py-Pt acceptor aroused, indicating the PE2-Pt* to Py-Pt energy transfer is efficient. The energy transfer efficiency (ηEnT) can be calculated with the quantum yields according to equation ηEnT = 1 – $\phi_{\text{PE2-Pt}}/\phi_{\text{P-0}}$,144 in which $\phi_{\text{P-0}}$ is the phosphorescence quantum yield of P-0, and $\phi_{\text{PE2-Pt}}$ is quantum yield of phosphorescence emission from PE2-Pt* (480 to 628 nm) in the copolymers. The quantum yields of the poly-Pt-Ar are listed in Table 4-1. According to the equation, the energy transfer efficiency in P-3 is ~ 86%. In P-5, where the acceptor content increases to 5%, the PE2-Pt emission is quenched to a greater extent, and the energy transfer efficiency from PE2-Pt* to Py-Pt approaches 95%. When Py-Pt content increased to 20% (P-20), the PE2-Pt emission is quenched almost completely, with η_{EnT} ~ 100%.

Figure 4-5 shows the quantum yields from PE2-Pt and Py-Pt emission, respectively, as well as the energy transfer efficiencies in the polymers P-0 to P-20. The quantum yield of PE2-Pt emission decreases sharply from P-0 to P-3, followed by a more gradual decline from P-5 to P-20. By contrast, the quantum yield of Py-Pt emission increases sharply from P-0 to P-3; however, it then decreases slightly from P-5 to P-20. The latter trend is likely due to self-quenching of the Py-Pt chromophores as the concentration increasing in the polymers. The energy transfer efficiency increased sharply from P-0 to P-3 (86.3%), and then increased gradually to approach 100% in P-20. The quantum yield and energy transfer efficiency data are also listed in Table 4-1.

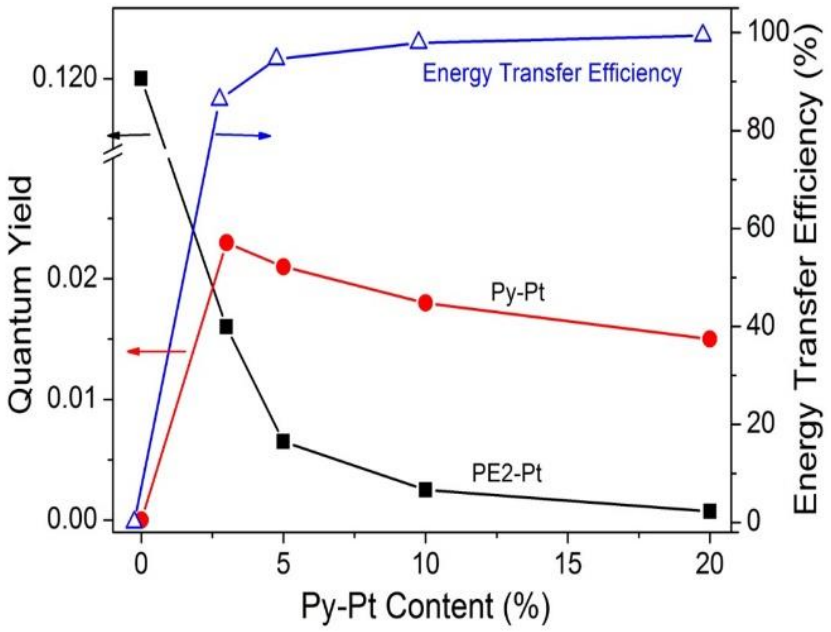

Figure 4-5. Quantum yields and energy transfer efficiency for Poly-Pt-Ar copolymers.

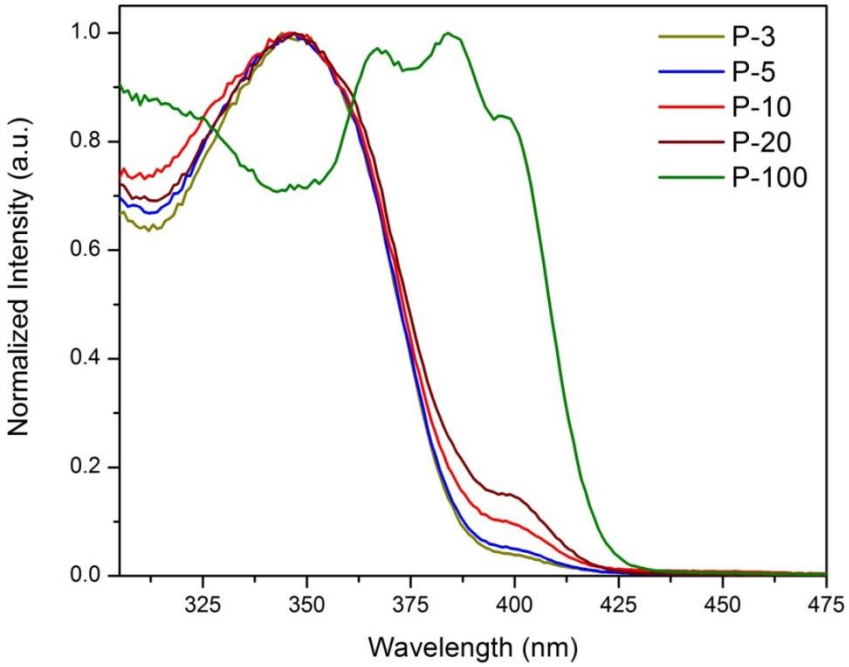

Figure 4-6. Excitation spectra of Poly-Pt-Ar. $\lambda_{emission}$ = 660 nm.

The phosphorescence emissions clearly demonstrate the triplet-triplet energy transfer from PE2-Pt (donor) chromophore to Py-Pt (acceptor) chromophore. Additional evidence for PE2-Pt to Py-Pt energy transfer in from P-3 to P-20 is provided by

excitation spectra, as presented in Figure 4-6, which were collected while monitoring the Py-Pt phosphorescent emission maximum at 660 nm. The spectrum of the Py-Pt only polymer P-100 shows that the phosphorescence of 660 nm comes from the three visible absorption bands of Py-Pt, 368 nm, 387nm and 398 nm. However, emission at 660 nm of polymers bearing both PE2-Pt and Py-Pt side groups (P-3 to P-20) are originate mainly from excitation of PE2-Pt (~ 347 nm). The excitation spectra of P-3 to P-20 match the absorption spectra of these polymers. These data clearly show that the Py-Pt emissions are coming from excitation of the PE2-Pt chromophores.

Time-Resolved Photoluminescence

Time-resolved photoluminescence spectra of PE2-Pt containing polymer P-0 to P-20 were recorded to study the kinetics of energy transfer from PE2-Pt* to Py-Pt. Figure 4-7 (a) shows emission decays monitored at 520 nm (emission wavelength of PE2-Pt phosphorescence) for PE2-Pt containing polymer P-0 to P-20. The decay of PE2-Pt only polymer P-0 is biexponential with a fast decay (τ_1 = 1.89 μs) and a slow decay (τ_2 = 62 μs); the two components have nearly equal amplitude. As 3% of Py-Pt is loaded, the time constant of the fast decay decreases by 30% (τ_1 = 1.29 μs) and the amplitude increases up to 0.90. As the loading of the acceptor increases, the time constants for both decay components decrease; and the time constant of the fast decay (τ_1) of P-20 deceases to 360 ns, with an amplitude of 0.96. The trend is more obvious at a 10 μs time scale, as displaced in Figure 4-7(b). The lifetimes and amplitudes obtained from the time-resolved photoluminescence are listed in Table 4-2. The decrease of the time constant of the fast decay and the increase of its amplitude clearly demonstrate the energy transfer from PE2-Pt* to Py-Pt, and this quenching process is a dynamic

process. The increase of Py-Pt (acceptor) in the copolymer can enhance the quenching process.

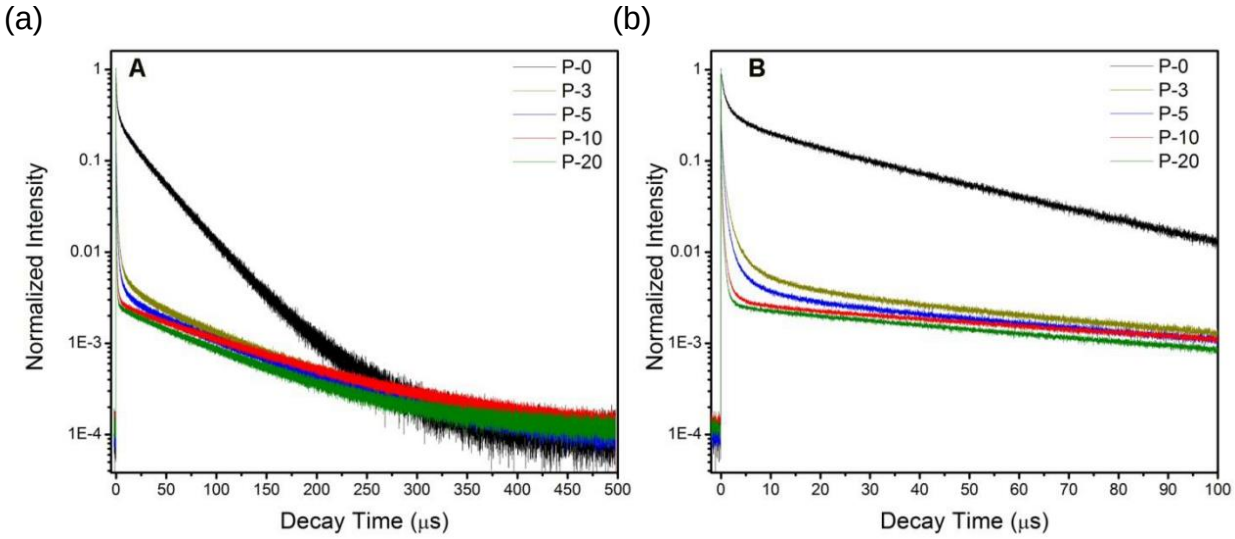

Figure 4-7. Phosphorescence decay of copolymers(P-0 to P-20) at 520 nm. a) Complete decay from 0 to 500 μs. b) Decay from 0 to 100 μs. Excitation wavelength was set at 375 nm

At a 10 μs time scale, the decay of P-0 exhibits a fast component (τ_1 = 92.7 ns and A_1 = 0.43) and an intermediate component (τ_2 = 817 ns and A_2 = 0.57). As the loading of Py-Pt increases from 3% to 20%, the time constants of fast components (τ_1) decreases from 53.0 ns to 15.9 ns, with the amplitude increased from 0.76 to 0.86. At the same time, time constants of the second component (τ_2) decrease from 395 ns to 222 ns, with a decreased amplitude from 0.15 to 0.13. The first component (τ_1) can be assigned to the direct energy transfer from nearest neighbor PE2-Pt* to Py-Pt, with a timescale from 10 to 50 ns. The second component (τ_2) is attributed to energy migration through a random walk, site-to-site hopping process of PE2-Pt exited energy to a position along the chain that is in close proximity to an acceptor.

Increasing the loading of acceptor chromophores in the copolymer has two effects. First, the probability of photoexcitation producing excited states next to an

acceptor increases. Second, for those excitons created far from an acceptor, the number of steps necessary to migrate near enough for quenching to occur decreases. Both of these effects will result in qualitatively faster quenching of the excited state, which agrees with the amplitude change for the direct energy transfer and energy migration processes.

Table 4-2. Time-resolved photoluminescence lifetimes of poly-platinums.

Polymer	τ_1 /ns (A_1)	τ_2 /ns (A_2)	τ_3 /ns (A_3)
P-0	454 (0.09)	3600 (0.53)	52350 (0.38)
P-3	37 (0.68)	885 (0.30)	18190 (0.03)
P-5	30 (0.70)	651 (0.28)	18050 (0.02)
P-10	22 (0.82)	375 (0.17)	17810 (0.01)
P-20	17 (0.86)	235 (0.13)	17650 (0.01)

Transient Absorption

Nanosecond transient absorption (ns-TA) data were acquired for poly-Pt-Ar across a wide range of probe wavelengths in order to provide the exhaustive information relating to the dynamics of the energy transfer processes. A comparison of nanosecond transient absorption among the donor only polymer (P-0), acceptor only polymer (P-100) and the donor-acceptor co-polymers (P-3 to P-20) is depicted in Figure 4-8. The spectra of P-0 (Figure 4-8, black) and P-100 (Figure 4-8, green) are similar to those of model compounds M1 and M2 (Figure 4-9), respectively. The spectrum of P-0 shows negative bleach at 360 nm that results from ground state bleach, as well as an intense excited state absorption centered near 600 nm. For P-100, the absorptions

centered near 440 nm and 550 nm can be attributed to the triplet-triplet absorption and excimer formation, whereas the bleach at ~ 390 nm reflects the loss of the ground-state absorption.145

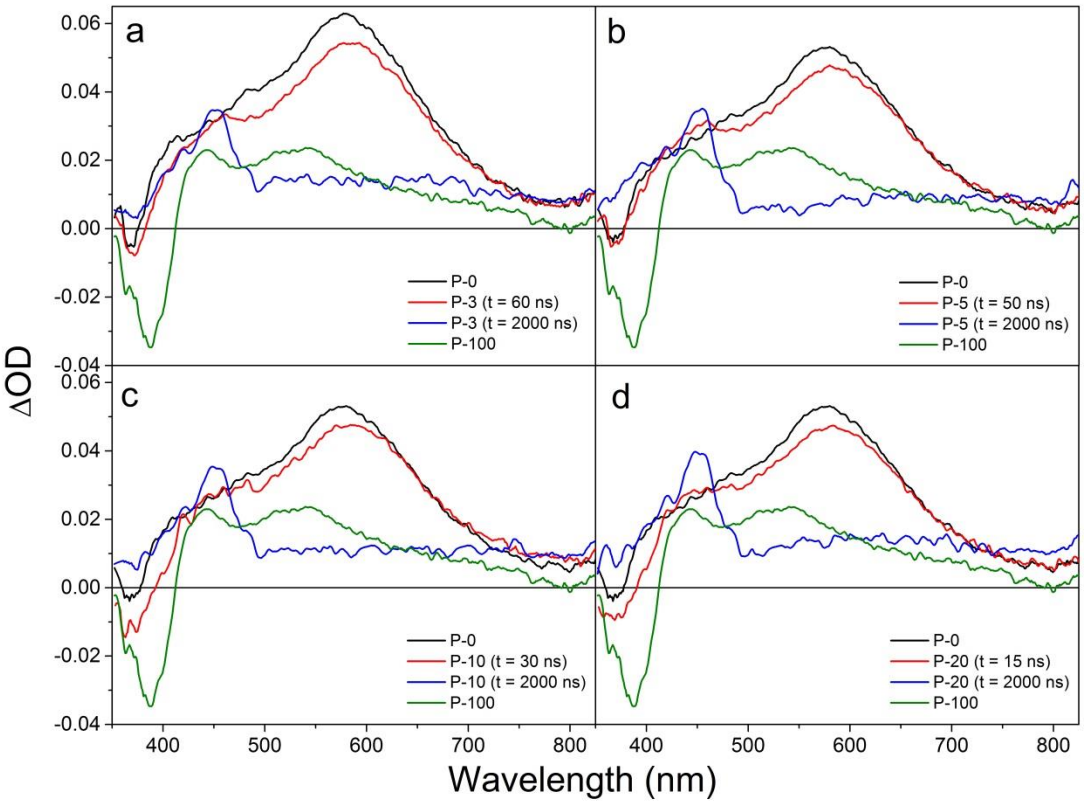

Figure 4-8. Transient absorption spectra of copolymers (P-3 to P-20) and homopolymers (P-0 and P-100) at different delay time.

Investigation of the transient absorption of copolymers P-3 to P-20 clearly reveals dynamic significance of energy transfer from PE2-Pt donor to Py-Pt acceptor moieties on a single chain. As shown in Figure 4-8a, the ns-TA spectrum of P-3 at the early time (60 ns) is nearly identical to that of the donor-only polymer, P-0 (black), indicating that photoexcitation at 355 nm predominantly creates the PE2-Pt triplet state (PE2-Pt*); however, a small peak around 460 nm arises, which is coming from Py-Pt excited states (Py-Pt*), suggesting certain amount of triplet energy have transferred from PE2-Pt* to

Py-Pt within 60 ns. At the longer delay time (2000 ns) the absorption peak at 600 nm has decayed, and it is replaced by narrow, weak visible peak at λ_{max} =450 nm. The visible absorption at this wavelength is clearly due to T_1-T_n absorption of the excited Py-Pt*. Investigations of P-5 to P-20 copolymers reveal similar phenomena as P-3. It is worth noting that the delay time for the appearance of a small shoulder at 460 nm is getting shorter from P-3 to P-20, which means the energy transfer from donor to acceptor becomes faster as the content of Py-Pt increases. The observation of these intermediates provides the straightforward evidence for photoinduced energy transfer from PE2-Pt to Py-Pt.

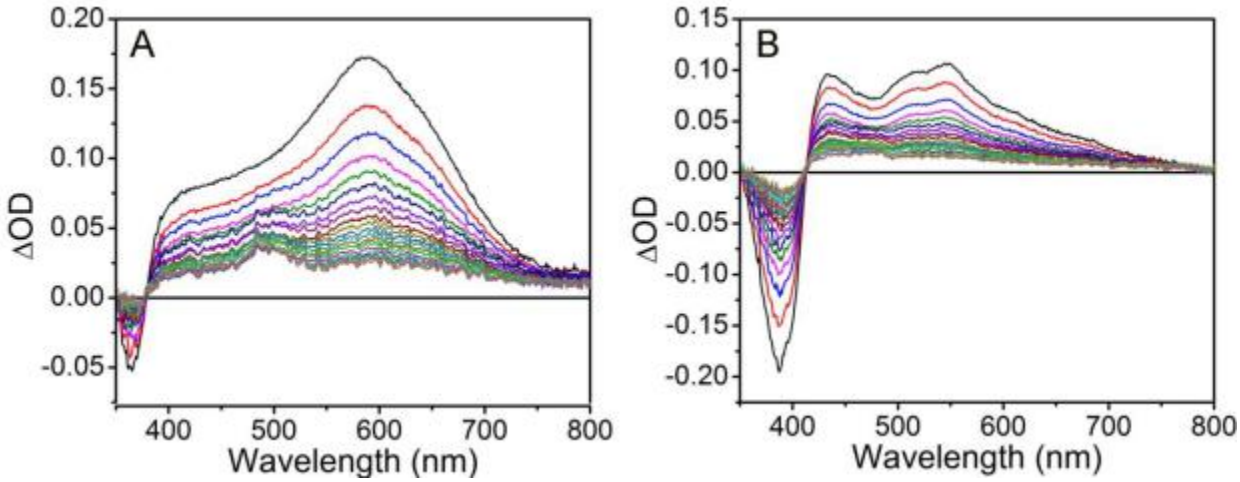

Figure 4-9. Transient absorption spectra of model compounds. A) M1 and B) M2.

Dynamics of Triplet-Triplet Energy Transfer

The rate of energy transfer can in principle be followed either through the disappearance of the PE2-Pt excited state (i.e. quenching) or appearance of the Py-Pt excited state species. However, monitoring the appearance of Py-Pt* via its ground state bleach at λ = 390 nm is problematic due to the PE2-Pt emission in this spectral region. We have instead focused our analysis on the decay of the PE2-Pt excited state

absorption of the donor-containing polymers (P-0 to P-20) at 600 nm, where the PE2-Pt emission and Py-Pt* contributions are minimized. As the laser power is increased above 15 mJ/pulse, the excited state absorption begins to exhibit intensity dependent kinetics, presumably due to triplet-triplet annihilation events that occur when more than one triplet state is created on each chain. The transient data reported here were collected at pulse energies below this threshold (10 mJ/pulse), thus avoiding the triplet-triplet processes.

The single wavelength kinetic traces recorded at 600 nm for P-0 to P-20 polymers on different time scales (1 μs to 10 μs) show biphasic decays, as presented in Figure 4-10a and Figure 4-10b. Time constants and normalized amplitudes recovered from the biexponential modeling of the 5 polymers (P-0 to P-20) between short and long timescale are summarized in Table 4-3. The slow decay can be assigned to the relaxation of PE2-Pt exciton to its ground state, and the fast decay can be assigned to quenching of PE2-Pt exciton. In P-0, PE2-Pt* exciton may be quenched by conformation-originated low-energy sites in the donor-only polymer (such as excimer site).[143] For P-3 to P-20, the fast component contributes almost exclusively for the decay, indicating PE2-Pt* exciton is quenched by Py-Pt acceptor efficiently.

A closer look at the quenching process of the copolymers (P-3 to P-20) on a short time scale of 1 μs, shown in Figure 4-10b, reveals there are two kinds of photophysical processes in these donor-acceptor systems. The faster decays are primarily caused by the first components (14-19 ns), which are assigned to the direct energy transfer from nearest neighbor PE2-Pt* to Py-Pt. As the loading increases from 3% to 20%, the amplitude of the fast component increases from 0.72 to 0.83 with little

change in the time constant itself, consistent with PE2-Pt* to Py-Pt energy transfer assignment. The intermediate components (130 - 260 ns) are attributed to energy migration through a random walk, site-to-site hopping process to a position along the chain that is in close proximity to a Py-Pt acceptor. The time constant associated with the intermediate processes trend downward as loading increases, reflecting the shorter amount of time necessary for an excited state to migrate to the Py-Pt trap (Table 4-3).

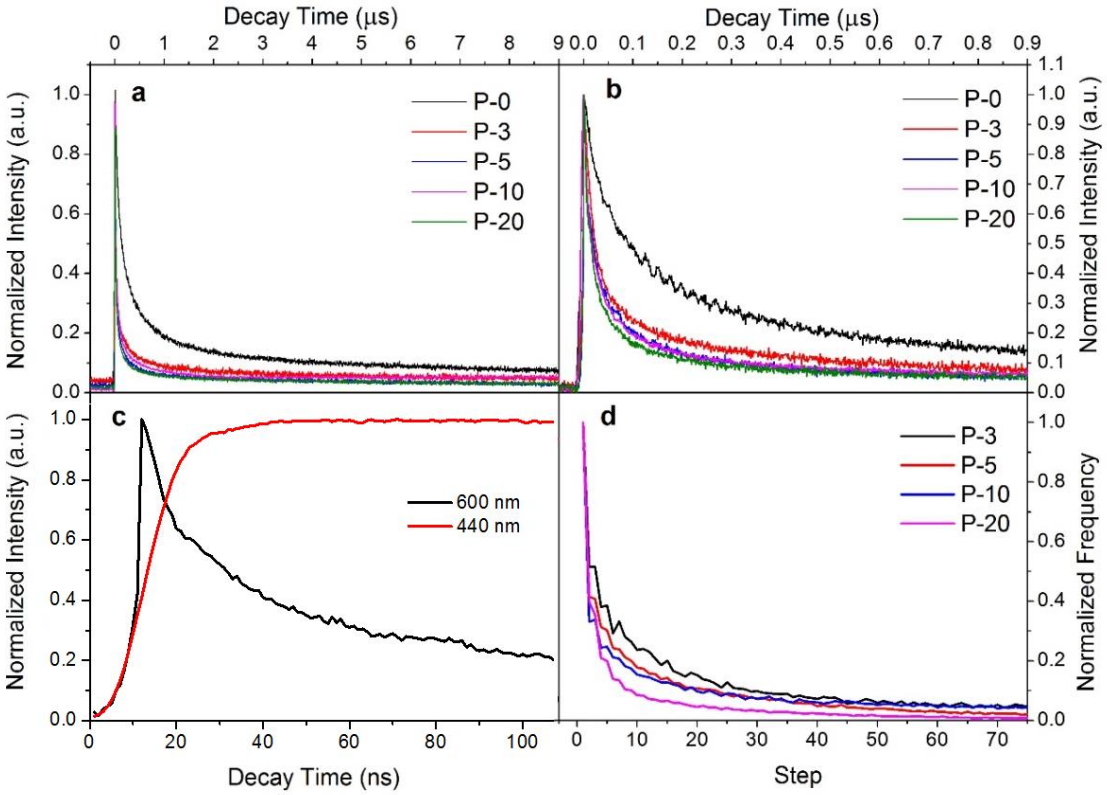

Figure 4-10. (a) Transient absorption kinetics decays of P-0 to P-100 at 600 nm on a long-time scale (10 μs). (b) Transient absorption kinetics decays of P-0 to P-100 at 600 nm on a short-time scale (1 μs). (c) Transient absorption kinetic traces of P-5 at 600 nm (PE2-Pt tiplet signal) and 440 nm (Py-Pt triplet signal). Excitation wavelength was set at 355 nm. (d) Random-walk simulation of the triplet exciton decay profile in P-3 to P-20. Simulation results placed on time axis by assuming 12 ns per step.

Both effects are originated from the increasing loading of acceptors in the copolymer series. First, the probability of photoexcitation producing excited states at the

neighboring sites of an acceptor increases. Second, for those excited states created far from an acceptor, the number of steps necessary to migrate near enough for quenching to occur decreases. Both of these effects will result in qualitatively faster quenching of the excited state (i.e., increasing contribution from fast decay and decreasing time constant values for slower decay component.)

Table 4-3. Lifetimes of poly-Pt-Ar measured by nanosecond transient absorption.

Polymer	τ_1 /ns (A_1)	τ_2 /ns (A_2)	τ_3 /ns (A_3)
P-0	36 (0.34)	259 (0.48)	6850 (0.18)
P-3	19 (0.72)	227 (0.17)	6450 (0.11)
P-5	17 (0.77)	180 (0.17)	6015 (0.06)
P-10	16 (0.80)	165 (0.17)	5655 (0.03)
P-20	14 (0.83)	136 (0.15)	5295 (0.02)

Mechanism of Energy Transfer

In the system with triplet state, the energy transfer may have two distinct pathways after the donor in the copolymer is excited selectively to produce ^{1}(PE2-Pt). The first pathway involves rapid singlet energy transfer from ^{1}(PE2-Pt) to ^{1}(Py-Pt); and following singlet transfer, ^{1}(Py-Pt) can relax either radioactively (fluorescence) or via intersystem crossing to produce ^{3}(Py-Pt) triplet excited state. The second pathway, which is triplet energy transfer, involves intersystem crossing on PE2-Pt unit to produce ^{3}(PE2-Pt) first, followed by intrachain triplet energy transfer from ^{3}(PE2-Pt) to ^{3}(Py-Pt). Radiative decay of ^{3}(Py-Pt) emits phosphorescent photons.

From spectroscopic data, we cannot rule out intrachain singlet-singlet energy transfer mechanism (the first pathway) completely, however, we can demonstrate that intrachain triplet-triplet energy transfer (the second pathway) dominates the energy transfer mechanisms. Evidence is the triplet decay of copolymers, as shown in Figure 4-10a and 4-10b. Triplet lifetime decreases as the acceptor loading increases, indicating the triplet quenching of donor is dynamic quenching. This suggests that ^{3}(PE2-Pt) is created prior to excited energy transferring from PE2-Pt moieties to Py-Pt moieties. Another direct evidence of triplet-triplet energy transfer is the comprehensive insight in the excited-state dynamics of P-5 copolymer was obtained by time-resolved transient absorption with nanoseconds time resolution at 440 nm and 600 nm, respectively (shown in Figure 4-10c). The kinetic traces show that the rise of the 440 nm absorption (Py-Pt acceptor absorption) correlates with the decay of PE2-Pt donor absorption at 600 nm, indicating that the growth of Py-Pt excited states arises from PE2-Pt* to Py-Pt energy transfer.

As we confirmed the intrachain energy transfer is dominated by triplet-triplet energy transfer, we believe the energy transport along the polymer chain occurs by site-to-site hopping process. Specifically, when a PE2-Pt site is selectively excited and ^{3}(PE2-Pt) is created, the triplet exciton moves in a random direction to an adjacent site, until it is “trapped” by a Py-Pt side group. Figure 4-10d shows the random-walk simulation results for triplet exciton decay in P-3 to P-20. These histograms are placed on a time scale in comparison with the experimental decay kinetics of triplet exiton (Figure 4-10b) by assuming a hopping step time of 12 ns. As shown in the figure, the simulation reproduces the experimental data relatively well.

Closing Remark

In summary, a series of polymeric arrays consisting of ~ 60 platinum acetylide chromophores have been synthesized with RAFT-S_N2-"click" strategy. We present an extensive analysis of the photoinduced dynamics for a donor-acceptor system in an effort to understand the mechanism of excited state energy migration that occurs following selective-photoexcitation of PE2-Pt in the copolymers containing PE2-Pt triplet donor and Py-Pt triplet acceptor. These results demonstrate that the PE2-Pt moieties in the copolymers act as efficient "antennas" for collecting visible light and transferring its energy along the polymer backbone. The energy transfer and energy migration of this series of poly-Pt-Ar occur with time constants of 14 - 19 ns and 130 - 220 ns, respectively. In addition, the heavy atom effect can enhance intersystem crossing due to spin-orbit coupling and the intersystem crossing rate becomes a fast process and competes favorably with higher singlet excitation and fluorescence or other relaxation pathways. Hence, this series of these poly-Pt-Ar shows prominent phosphorescent emission with the longer lifetime in the nanosecond range. This feature combined with its broad absorption throughout the visible makes it a candidate for use in molecular scale electronic devices and solar energy conversion applications.

Experimental

Photophysical Measurements

The UV-visible absorption measurements were recorded in THF and were carried out on a Shimadzu UV-1800 dual beam absorption spectrophotometer using 1 cm quartz cells. Photoluminescence measurements were obtained on a fluorimeter from QuantaMaster 300 of Photon Technology International (PTI) using 1 cm quartz cells.

For phosphorescence measurement the sample solutions were degassed via bubbling argon for 45 minutes.

Phosphorescence decay kinetics was obtained with a multichannel scaler/photon counter system with a NanoQuant FluoTime 100 Compact phosphorescence lifetime spectrophotometer (PicoQuant Photonics North America, Inc., http://www.picoquant-usa.com/). A CUBE diode laser provided the excitation at 375 nm (< 16 mW). The 100 ns pulsed laser was generated by SRS DG353 Digital Delay/Pulse Generator. The specific narrow bandpass filter was used for each measurements followed by global fit processing (FluoroFit software). Decays were obtained using the multi-exponential fitting parameters (FluoroFit software).

Nanosecond triplet-triplet transient absorption measurements were acquired with excitation at 355 nm (10 mJ/pulse) using the third harmonic of a Continuum Surelite II-10 Nd:YAG laser. Perkin-Elmer LS1130-3 pulsed xenon lamp was used as a probe source and the transient absorption signal was detected with a gated–intensified CCD mounted on a 0.18 M spectrograph (Princetor PiMax/Acton Pro 180). Samples were prepared to an optical density of 0.7 at the excitation wavelength in a continuously circulating 1 cm pathlength flow cell (volume = 9 mL). Triplet lifetimes were calculated with a single-exponential global fitting of the transient absorption decay data using SpecFit analysis software.

Single-wavelength kinetics measurements were done in a home-built system, with the same laser source and xenon lamp described above. The detected wavelength was controlled by a monochromator (Instruments SA, H-20) and the intensity of the monitoring light is detected by a photomultiplier tube (Humamatsu, R928).[146]

To simulate the random-walk process numerically, a program was written with MatLab.[141] Briefly, the triplet exciton was assumed to travel one-dimensionally along the polymer backbone, as the fully-conjugated polymer. The polymer chain was modeled and the polymer length was defined as *m*. Then the desired number of Py-Pt acceptors *n* (e.g., in P-10, $n = 0.1 \times m$) was selected, and acceptors were doped along the polymer chain. The initial position of the exciton was randomly selected along the oligomer chain at a donor site; and the exciton can randomly move to either left or right. In either case, the counter for the number of random-walk steps taken (Steps) is increased by 1 (Steps + 1). When the exciton reached the position of an acceptor, the random-walk stopped and the counter for the number of steps taken (Steps) was recorded. The same procedure is repeated for the desired number of repetition times (Rep), and the obtained number of random-walk steps (Steps) are subjected to histogram analysis.

CHAPTER 5
ULTRAFAST PHOTOPHYSICS IN POLY PLATINUM ACETYLIDE THIOPHENE POLYMERS

Introductory remark

The performance of organic electronic devices such as light emitting diodes [147,148], photovoltaic cells [149-151], and field effect transistors [152,153] depends on the optical and electronic properties of π-conjugated oligomers or polymers. The efficiency of optoelectronic devices makes a significant progress with phosphorescent organometallic complexes, which has attracted considerable attention in the development of advanced optoelectronic materials. The phosphorescence can be enhanced by the heavy atom effect, which will promote singlet → triplet (S - T) intersystem crossing due to spin-orbit coupling.[76,154] Platinum containing poly(phenylene ethynylene)s are a noticeable category of conjugated polymers. Their photophysics are dominated by long-lived triplet excited states[3] and phosphorescent emission since platinum has a large spin - orbit coupling constant. This appealing property makes them promising candidate materials for the fabrication of electroluminescent devices, [4] and for applications in optical limiting.[155]

The optoelectronic properties of platinum-acetylide oligomers and polymers have been studied in organometallic π-conjugated electronic systems, in order to define the structure and dynamics of triplet excitons and charge carriers. [7,59,156] In our previous study, we explored electronic and geometric structures of the ground and triplet excited states, and observed that triplets are localized in Pt – acetylide oligomers [157], and that

---

This Chapter is considered for publication in the Journal of the American Chemical Society.

absorption and emission of light arise from π, π* transitions based on orbitals that are mainly localized on the organic chromophores (pπ) but contain contributions from Pt-based (dπ) orbitals. The photoluminescence and absorption spectra for a series of Pt-containing conjugated polymers and monomers were collected by Wilson and co-workers[92], and found that high-energy triplet states intrinsically have the most efficient phosphorescence. Although the triplet excited states in organic and organometallic conjugated oligomers and polymers has been explored in a number of investigations, [66,158] we still concerned about the ultrafast dynamics of platinum-acetylide polymers.

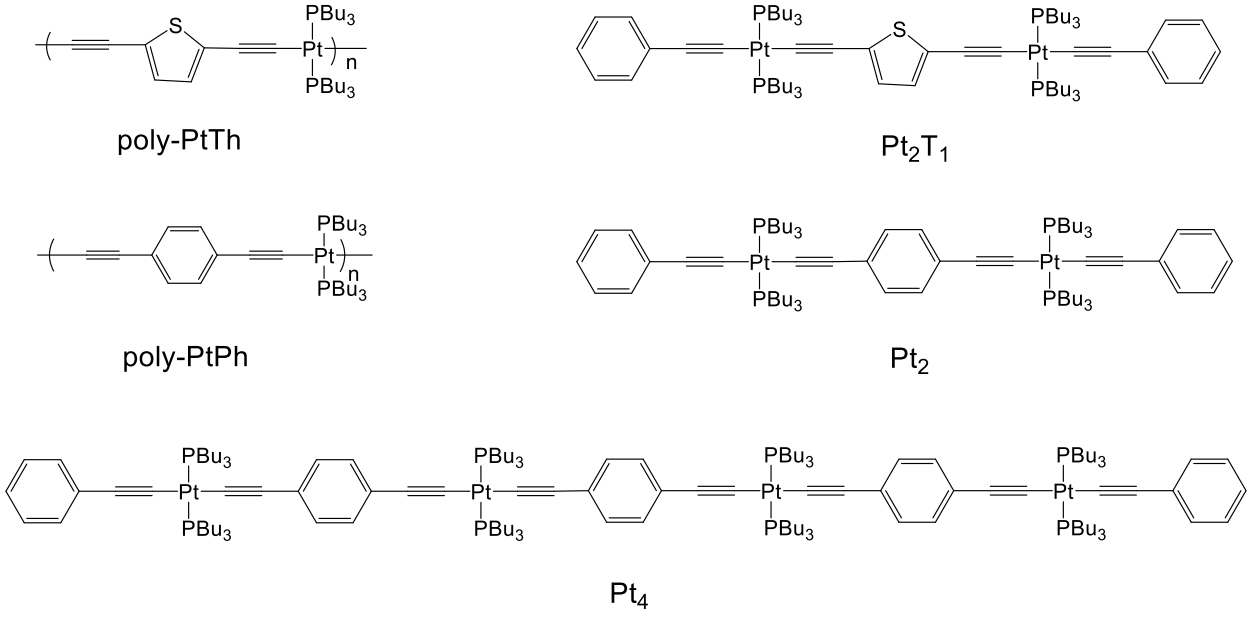

Figure 5-1. Structures of poly-PtTh, poly-PtPh and model compounds.

In this chapter, we present a systematic spectroscopic study of 2,5-thienylene-based conjugated platinum acetylide homopolymer (poly-PtTh) and 1,4-phenylene-based conjugated platinum acetylide homopolymer (poly-PtPh) with three platinum model complexes (Pt_2, Pt_2T_1 and Pt_4), shown in Figure 5-1. Singlet and triplet excited-state dynamics were recorded by femtosecond pump-probe transient absorption spectroscopy. For poly-PtTh and poly-PtPh, we found that intersystem crossing, which

is a radiationless process involving a transition between two electronic states with different spin multiplicity, occurs on a sub-picosecond time scale, and transient absorption spectrum reveals the mechanism for the relaxation from the excited states to singlet ground state. Since the photophysical properties of poly-PtTh in solution and thin film are identical, it means that they have the same photophysical mechanisms. Ultrafast excited-state dynamics of model complexes, Pt_2, Pt_2T_1 and Pt_4, are also detected, and their results are consistent with that of poly-PtTh and poly-PtPh.

Synthesis

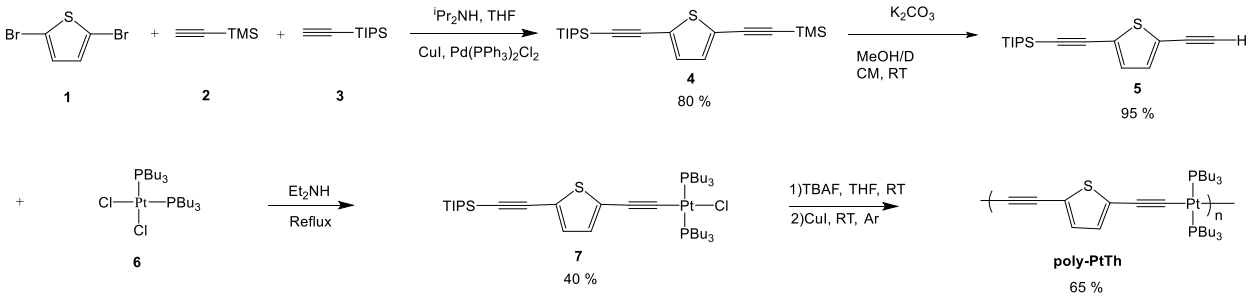

Figure 5-2. Synthesis of conjugated polymer poly-PtTh using an AB asymmetric monomer.

The defects present in the polymer backbone can be avoided by the polymerization of asymmetric AB monomers.[56,57] Figure 5-2 illustrates this strategy for poly-PtTh synthesis. In the beginning, 2,5-dibromothiophene, 1, was subjected to a one pot Sonogashira coupling between (trimethylsilyl)-acetylene (TMS-acetylene) 2 and (triisopropylsilyl) acetylene (TIPS-acetylene), 3, giving asymmetrically protected triisopropyl((5-((trimethylsilyl)ethynyl)thiophen-2-yl)ethynyl)silane, 4, in 80% yield. The TMS-acetylene protecting group was selectively removed through reaction with potassium hydroxide in the mixture of methanol (MeOH) and dichloromethane (DCM) at room temperature to give 5 in 95% yield. Following a Hagihara reaction with platinum

complex 6, the TIPS-protected monomer 7 were then deprotected in situ with TBAF and polymerized overnight to give conjugated co-polymers, poly-PtTh, in 65% yield.

Results and Discussion

UV-Visible Absorption and Steady-State Photoluminescence

The UV-vis absorption and steady-state emission spectra of the platinum-acetylide polymers, poly-PtTh and poly-PtPh, in a 1:1 mixed solution of dichloromethane (DCM) : acetonitrile (ACN) are presented in Figure 5-3. The absorption spectra of the two homopolymers, poly-PtTh and poly-PtPh, appear as broad bands, with λ_{max} = 400 and 375nm, for poly-PtTh and poly-PtPh, respectively.[55] In each case, the absorption is due to the long-axis polarized π,π* transition of the platinum - acetylide backbone.[59] The photoluminescence spectra of poly-PtTh and poly-PtPh were obtained in DCM/ACN (1:1, v/v) at room temperature (Figure 5-3).[55]

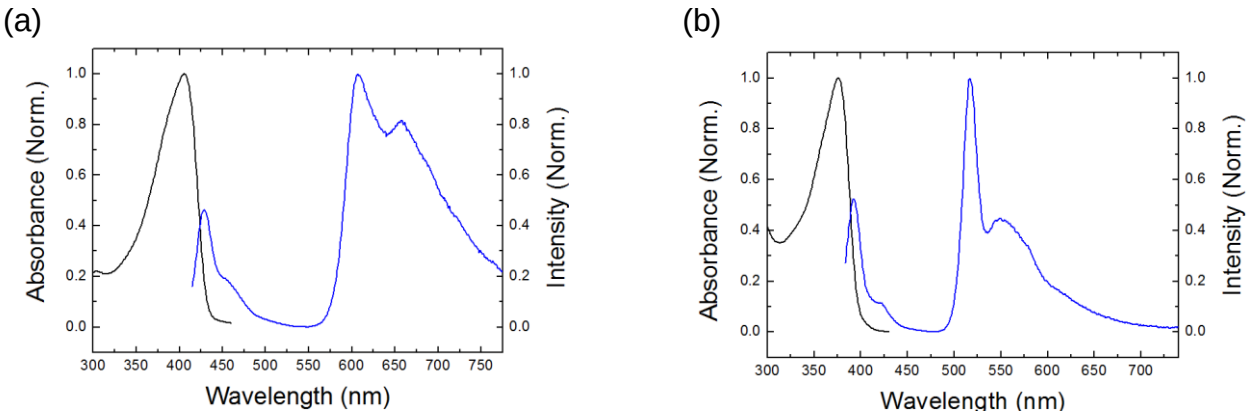

Figure 5-3. Normalized absorption and emission spectra of a) poly-PtTh; b) poly-PtPh in DCM/ ACN (1;1, v/v).

The luminescence from poly-PtTh features two broad bands with λ_{max} = 425 and 600 nm. The high energy band is due to fluorescence from ^{1}π,π*, whereas the low energy band is phosphorescence from the ^{3}π,π* manifold.[55] The phosphorescence assignment is supported by a lifetime of 5.0 μs. The emission spectrum of poly-PtPh

exhibits weaker peaks from 390 nm to 450 nm which are assigned as fluorescence in view of previous studies.[59] Besides, the emission of this polymer at 520 nm is completely quenched in the presence of oxygen, and this peak is similar to the spectra of similar materials in earlier investigations.[59] Therefore, the emission centered at 520 nm is assigned as phosphorescence.

Transient Absorption and Fluorescence Upconversion

Femtosecond time-resolved transient absorption (fs-TA) spectra were obtained on poly-PtTh in solution and thin film to provide information regarding the electronic properties and dynamic profiles of transient states produced by photoexcitation. These experiments were conducted with 395nm excitation, and the absorption spectra obtained immediately following the 100 fs laser excitation pulse are shown for comparison in Figure 5-4.

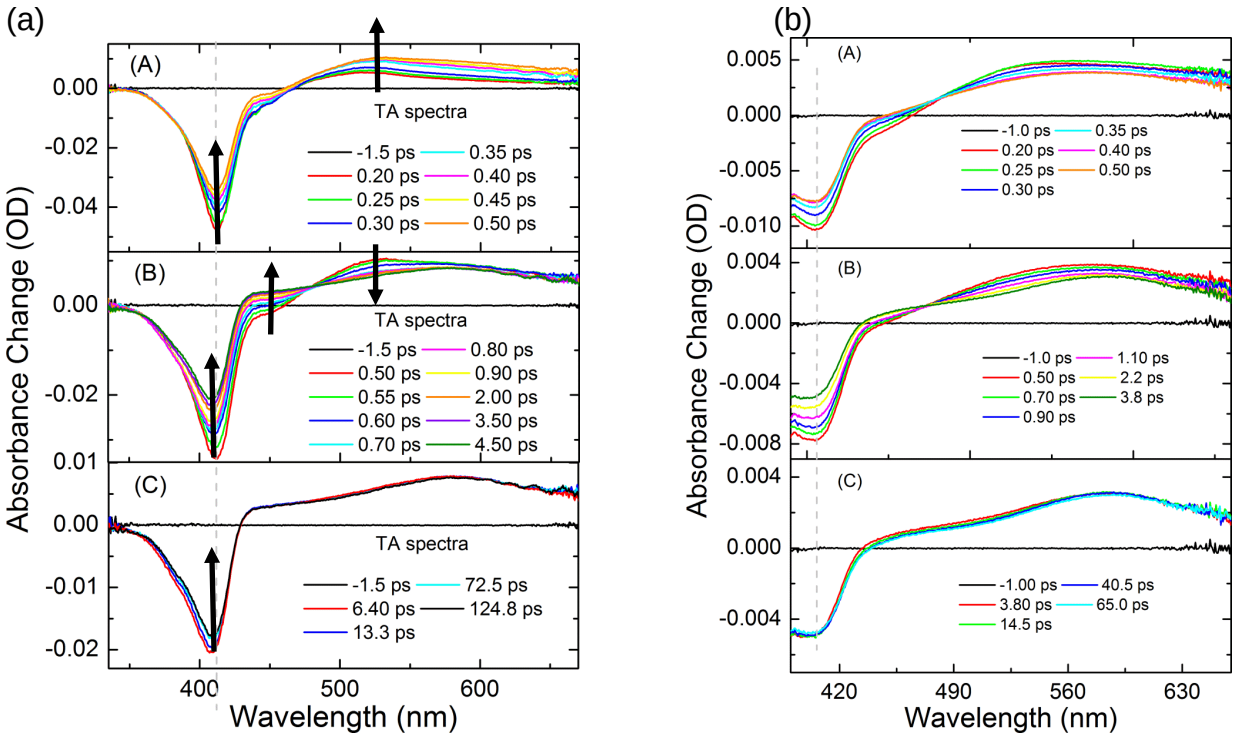

Figure 5-4. Femtosecond transient absorption spectra of a) poly-PtTh in solution ; b) poly-PtTh in thin film. Excitation wavelength is 395 nm.

All of the fs-TA spectra are characterized by strong bleaching in the near-UV or blue region due to ground-state depletion, along with broad, moderately intense excited-state absorption extending throughout the visible region with a maximum between 500 and 600 nm. At initial time delay of 200 fs, transient absorption spectrum is broad with a shoulder around 440 nm and a maximum around 520 nm. This decays as the time delay is increased with a concomitant growth at the ESA maximum at 440 nm. This can be ascribed to ISC.[159] The photophysical mechanisms of poly-PtTh for solution and thin films are the same since their ultrafast transient absorption spectra are remarkably similar.

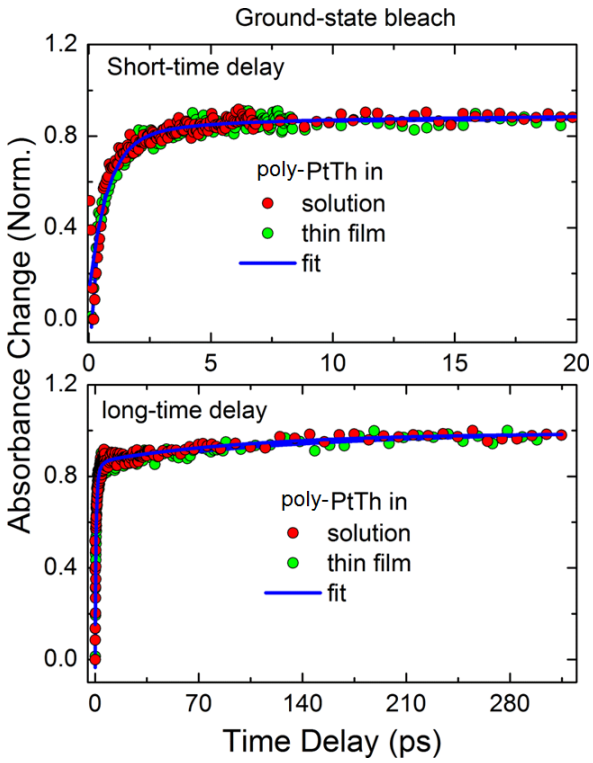

Figure 5-5. Femtosecond time-resolved kinetic traces for ground sate bleach of poly-PtTh at short-time. Excitation wavelength is 395 nm. The spectrum was recorded at 408 nm.

As shown in Figure 5-5, femtosecond time-resolved kinetic traces for ground state bleaching of poly-PtTh were obtained at short-time delay and long-time delay. We

found that solvent relaxation/organization does not play any role here since the dynamics of the ground state bleach is identical in solution and thin film.

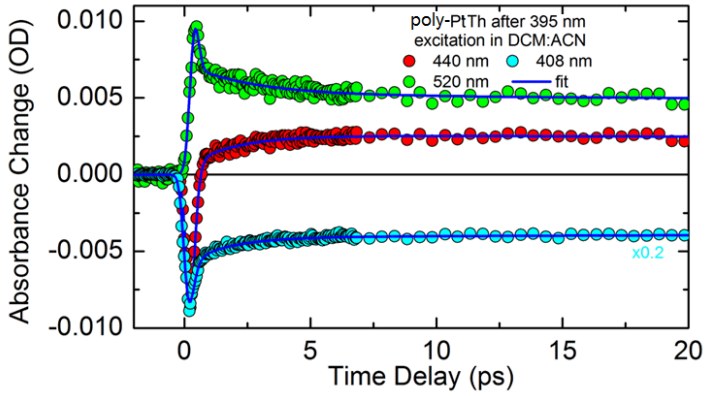

Figure 5-6. Kinetic growth and decay traces of poly-PtTh in DCM/ACN (1:1, v/v) probed at 408, 440 and 520 nm. Excitation wavelength is 395 nm.

The kinetic decay trace at 520 nm shows a faster decay with a time constant of 260 fs and a slower decay, while the transients at 408 and 440 nm shows growths with time constants of 280 fs and 300 fs and slower decays with a time constant of 2.4 ps (Figure 5-6)(Table 5-1). The fluorescence upconversion measurement was carried out on poly-PtTh in DCM/ACN (1:1,v/v) after excitation at 450 nm, and the corresponding decay of fluorescence with a time constant of 2.5 ps are shown in Figure 5-7. On the basis of the kinetic information, we can clarify that the apparent ground state bleach recovery is caused by the relaxation from the excited states to singlet ground state. The fs-TA of poly-PtPh was measured in DCM/ACN (1:1, v/v), displayed in Figure 5-8. The kinetic trace at 371 nm shows a growth for poly-PtPh, which dynamics is similar to that of poly-PtTh. This gives clear evidence that the fast relaxation to ground state occurs in poly-PtPh as well.

The excited state dynamics of the platinum model complexes, Pt_2, Pt_2T_1 and Pt_4, were also studied using femtosecond transient absorption spectra, depicted in Figure 5-

9a. We also observed the ground state bleach recovery in the visible region and intersystem crossing on a sub-picosecond time scale. In Figure 5-9b, the corresponding femtosecond time-resolved kinetic traces describe the response of the ground state bleaching and the excited state absorption after photoexcitation. In the comparison with the ultrafast photophysical data of poly-PtTh and poly-PtPh, the similar photophysical behaviors were found in platinum model complexes. The lifetimes of platinum acetylide polymers and the corresponding model complexes are listed in Table 5-1.

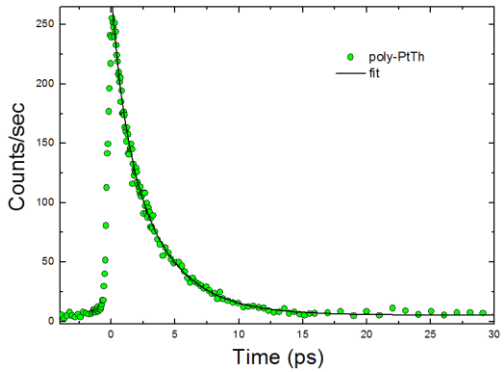

Figure 5-7**.** Fluorescence upconversion of poy-PtTh at 450 nm in DCM/ACN (1:1, v/v).

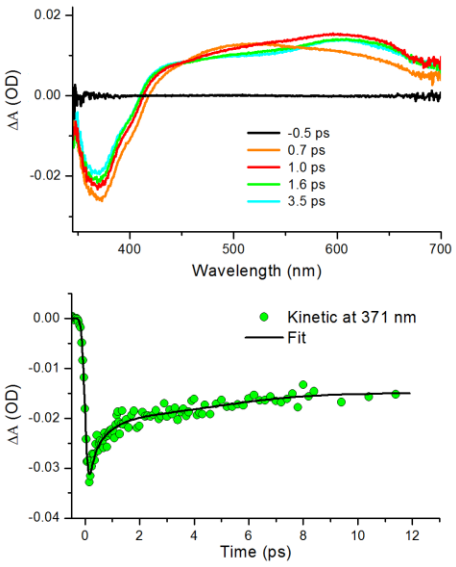

Figure 5-8**.** Ultrafast transient absorption and the kinetic trace at 371 nm of poly-PtPh in DCM/ACN (1:1, v/v).

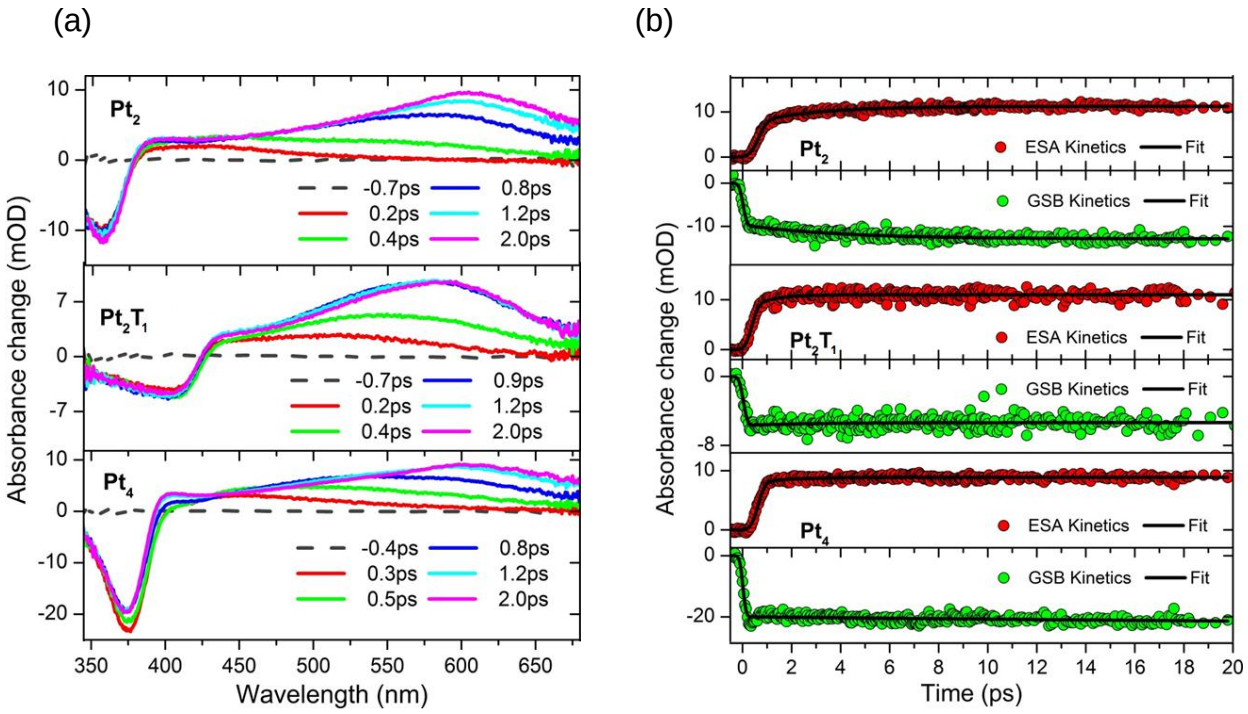

Figure 5-9. (a)Ultrafast transient absorption spectra and (b) Kinetic traces of Pt_2, Pt_2T_1 and Pt_4.

Table 5-1.Time-resolved measurements of platinum acetylide polymers and the corresponding model complexes by fluorescence upconversion and transient absorption

	FL[a]	TA[b]					
Molecule	τ/ps	τ_1/ps (A_1) (GSA)[c]	τ_2/ps (A_2) (GSA)	τ_1/ps (A_1) (ESA)[d]	τ_2/ps (A_2) (ESA)	τ_1/ps (A_1) (ESA)	τ_2/ps (A_2) (ESA)
Poly-PtTh	2.5 (100%)	0.28 (86%) (407 nm)	2.40 (14%) (407 nm)	0.30 (93%) (440 nm)	2.40 (7%) (440 nm)	0.26 (90%) (520 nm)	3.60 (10%) (520 nm)
Poly-PtPh	-	0.50 (52%) (371 nm)	3.40 (48%) (371 nm)	-	-	-	-
Pt_2	-	4.0 (100%) (360 nm)	-	2.5 (100%) (610 nm)	-	-	-
Pt_2T_1	-	2.9 (100%) (403 nm)	-	0.8 (100%) (585 nm)	-	-	-
Pt_4	-	50.9 (100%) (374 nm)	-	1.3 (100%) (606 nm)	-	-	-

[a] From fluorescence upconversion. [b] From transient absorption. [c] GSA:ground state absorption. [d] ESA:excited state absorption

Closing Remark

In order to probe the mechanism and dynamics of platinum acetylide homopolymers, poly-PtTh and poly-PtPh were synthesized according to the AB asymmetric polymerization procedure, outlined in Figure 5-2 and Figure 2-2. Ultrafast transient absorption studies carried out in the presence of platinum acetylide polymers, poly-PtTh and poly-PtPh, provide evidence that intersystem crossing processes take place on a sub-picosecond time scale, and the exicted states are deactivated by the relaxation from the excited states to singlet ground state. Analysis of the model complexes (Pt_2, Pt_2T_1 and Pt_4), using photoluminescence and femtosecond transient absorption spectra indicates the photophysical properties and ultrafast excited-state dynamics of platinum acetylide polymers are very similar to that of corresponding model complexes.

Experimental

Materials

2,5-dibromothiophene, tri-isopropylsilylacetylene and trimethylsilylacetylene were obtained from either Acros or Aldrich and used as received. Compounds 4-7 were synthesized according to the literature procedures.[93-95,122] All reactions were performed under argon atmosphere in anhydrous solvents, which were dried prior to use following standard procedures. Merck silica gel 60 (particle size 0.04−0.063 mm) was employed for flash chromatography.

^{1}H NMR, ^{13}C NMR, ^{31}P NMR spectra were obtained on a VXR-300 instrument using deuterated chloroform ($CDCl_3$) as the solvent and tetramethylsilane (TMS) as the internal reference. Gel permeation chromatography (GPC) was performed by eluting a tetrahydrofuran (THF) solution of the polymer through two PL-Gel 5 Mixed D columns

pressurized by a Rainin Dynamax SD-200 solvent pump. Polymer elution was spectroscopically monitored using a UV detector set to a wavelength where the polymer absorbs, and molecular weight calculations were performed using Polymer Laboratories PL software against a polystyrene standard. All solvents used were of HPLC grade.

Synthesis

Triisopropyl((5-((trimethylsilyl)ethynyl)thiophen-2-yl)ethynyl)silane (4). To a flask charged with THF and diiospropylamine (DIPA) (8 mL, 1:1) was added 2,5-dibromothiophene (480 mg, 2.0 mmol). The resulting solution was degassed for 30 min by purging with argon. This solution was added trimethylsilylacetylene (196.4 mg, 2 mmol), triisopropylsilylacetylene (364.1 mg, 2 mmol), $Pd(PPh_3)_4$ (12 mg, 1.6 mmol), and copper iodide (4 mg, 2 mmol). The reaction was then stirred at room temperature for 24 hours. After this time the solvent was removed under reduced pressure. Flash chromatography of the residue with hexanes gave the desired product as a yellow solid. (yield 580 mg, 80%). ^{1}H NMR ($CDCl_3$, 300MHz): δ (ppm) 0.33 (s, 9H), 1.19 (s, 21H), 7.03 (m, 2H). ^{13}C NMR ($CDCl_3$, 300 MHz): δ (ppm) 0.22, 11.3, 18.7, 96.6, 96.9, 98.8, 99.9, 124.5, 124.9, 131.8, 132.3.

((5-Ethynylthiophen-2-yl)ethynyl)triisopropylsilane (5). To a deoxygenated solution of 4 (720 mg, 2.0 mmol) in dichloromethane (DCM, 30 mL) and methanol (MeOH, 30 mL), potassium carbonate (KOH, 0.34 g, 6.0 mmol) was added under argon flow. The mixture was stirring at room temperature for 1 hour. Then deionized water (100 mL) was added to extract unreacted KOH. The organic layer was separated and washed 3 times with brine and deionized water, and was dried over sodium sulfate. The solvent was evaporated to obtain colorless oil. The crude product was purified by column chromatography on silica gel using hexane as the eluent (Rf = 0.47) to yield

colorless liquid. Yield: 550 mg (95%). ^{1}H NMR (300 MHz, $CDCl_3$): δ (ppm) 1.12 (m, 21H), 3.33 (s, 1H) and 7.05 (m, 2H). ^{13}C NMR (75 MHz, $CDCl_3$): δ (ppm) 11.2, 18.6, 81.8, 96.8, 98.4, 114.0, 122.9, 125.2, 131.8, 132.6.

Complex (7). ((5-Ethynylthiophen-2-yl)ethynyl)triisopropylsilane (5) (107.4 mg, 0.373 mmol) and cis-dichloro-bis-(tri-n-butylphosphine) platinum(II) 6 (250.1 mg, 0.375 mmol) were dissolved in Et_2NH (15 mL) and the solution was degassed with nitrogen. The mixture was stirred under reflux for 8 hours. The solvent was removed and the crude product purified by flash chromatography (silica gel, hexane then 7:3 hexane/CH_2Cl_2) giving the desired product 7 as a yellow solid (136 mg, 40 %). ^{1}H-NMR ($CDCl_3$, 300 MHz): δ (ppm) 0.93 (t, 18H), 1.11 (s, 21H), 1.46 (br m, 12H), 1.56 (br m, 12H), 1.99 (br m, 12H), 6.63 (d, 1H), 6.97 (d, 1H). ^{13}C NMR ($CDCl_3$, 75 MHz): δ (ppm) 11.3, 13.8, 18.7, 22.0, 24.3, 26.1, 92.0, 93.2, 94.2, 100.1, 120.0, 126.8, 131.3, 132.1. ^{31}P NMR ($CDCl_3$, 121 MHz): δ (ppm) 7.95 (J_{Pt-P} = 2360 Hz).

poly-PtTh. Monomer 7 (85 mg, 0.119 mmol) was added in a 7:2 mixture of diiso-propyamine:THF (9 mL) in a Schlenk flask. The solution was degassed over 5 freeze-pump-thaw cycles. The flask was backfilled with dry argon and tetrabutylammonium fluoride (73 mg, 0.275 mmol) was added via syringe. A white precipitate immediately formed from the yellow-colored solution. The reaction was stirred at room temperature for about 40 min, at which time a TLC with 1:4 hexanes:DCM revealed total consumption of 7. Copper (I) iodide (1.9 mg, 0.01 mmol) was then added in the Schlenk flask. After stirring overnight at room temperature, it was noticed that the polymerization reaction formed a yellow suspension. The reaction was poured into an excess of methanol, precipitating the polymer as yellow powders. The precipitate was filtered

using a 2.5 µm glass fiber filter pad and redissolved in THF. The solution was reprecipitated into an excess of methanol and filtered using a glass fiber filter pad. The yellow powders were once again redissolved in THF, precipitated from methanol, and filtered for a third and final time. After the final precipitation, the polymer was dried under a vacuum at room temperature overnight to give poly-PtTh (60 mg, 65%). The polymer was characterized by GPC, UV-VIS/emission and by NMR. ^{1}H NMR ($CDCl_3$, 300 MHz): δ (ppm) 0.91 (t, 18H), 1.57 (br m, 12H), 1.59 (br m, 12H), 2.13 (br m, 12H), 6.58 (s, 2H). ^{31}P NMR ($CDCl_3$, 120 MHz): δ (ppm) 3.96 (t, 2400 Hz). GPC: Mn = 9,800; Mw = 18,600, PDI= 1.90

Photophysical Measurements

UV-vis absorption spectra were obtained with samples contained in 1 cm quartz cuvettes using a Varian Cary 100 dual-beam spectrophotometer. Corrected, steady-state photoluminescence spectra were recorded on a Photon Technology International (PTI) photon counting fluorescence spectrophotometer. Samples were contained in 1 cm × 1 cm quartz cuvettes, and the optical density was adjusted to approximately 0.1 at the excitation wavelength. All photophysical measurements were carried out in argon degassed DCM/ACN (1:1. v/v) solutions. Femtosecond time-resolved transient absorption spectra were measured by Prof. Omar F. Mohammed Abdelsaboor at King Abdullah University of Science and Technology (KAUST). The fluorescence upconversion spectrum was collected by Dr. Allen Ricks at Ultrafast Systems LLC using a 1W 1KHz 100femtosecond Libra system to generate the second harmonic and gate pulse.

CHAPTER 6
CONCLUSION

In the previous chapters, several series of organometallic polymers have been synthesized and characterized. The basic photophysical properties of polymers in solution and in the solid state, such as triplet exciton transfer, exciton migration, reverse energy transfer, excited state dynamics, were investigated in detail by UV/Visible absorption, steady-state photoluminescence spectroscopy, time-resolved photolumine-scence spectroscopy, time-resolved transient absorption spectroscopy. A fundamental photophysics is built for the application of these materials or their analogues in electronic or optoelectronic devices.

The conjugated and conjugation interrupted polymers were designed for the photophysical studies. I found that the conjugated polymers are more red-shifted than conjugation interrupted polymers because of longer conjugation length. These results demonstrated the singlet state of conjugated polymers is more highly delocalized than the corresponding conjugation interrupted polymers. By contrast, the triplet states are highly localized between two Pt centers. Additionally, triplet energy transfer occurs at room temperature in the conjugated copolymers. In contrast to conjugated system, the exciton can transport to a lower energy trap less effectively while the π-conjugation structure is interrupted with methylene spacer. It is worth noting that reversible energy transfer may happen in the solid state of $Ph_{95}Th_5$ copolymer in comparison to $Ph_{95}BTD_5$ from the photophysical results of temperature-dependent time-resolved photoluminescence measurements.

This Chapter is considered for publication in the Journal of the American Chemical Society.

There are various types of techniques to calculate exciton diffusion coefficients and lengths of diffusion in the literatures, but they necessitate expensive instrumentation and complicated mathematical modeling. Hence, we developed a new method of exciton diffusion. The accurate methods are applied to calculate the polymer density and the concentration of acceptor molecules in the film. We then use Hindered Access model, a standard exciton quenching method, to estimate quenching rate constant. The relationship between estimate quenching rate constant and exciton diffusion coefficient can be derived from Fick's Law of Diffusion. Thus, we calculated the diffusion coefficient and diffusion length of pPtPh films, which are around $4.5X10^{-6}$ cm^2-s^{-1} and 21.5 nm respectively. These diffusion parameters were confirmed using by literature-based time-of-flight experiments with the bilayer structure of pPtPh|C60 films. We then studies a series of polymers, pPtPh, pPtPh(CH_2) and pPtBP, using this newly developed model. The diffusion parameters of pPtPh(CH_2) are smaller than that of pPtPh because the conjugation structure is interrupted by methylene spacers. Also, the diffuusion parameters of pPtBP are slightly lower than that of pPtPh due to the higher activation energy, which is enhanced by intrachain rotation.

Triplet exciton transfer and exciton migration along a non-conjugated polymer chain have been investigated with graft copolymers having different platinum acetylide side groups as energy donor (PE2-Pt, Ph-C≡C-Ph-C≡C-Pt(PBu_3)$_2$-C≡C-) and acceptor (Py-Pt, Pyrene-C≡C- Pt(PBu_3)$_2$-C≡C-). The graft copolymers were prepared from the reversible addition-fragmentation transfer polymerization (RAFT)-S_N2-"click" route. The triplet energy transfer from donor to acceptor was characterized employing both time-resolved and steady-state phosphorescence spectroscopy, as well as nanosecond time-

resolved transient absorption spectroscopy. Near unity energy transfer from PE2-Pt triplet state to the Py-Pt moiety occurs on multiple timescales (10 - 220 ns) depending on where the initial exciton is formed on the polymer.

The platinum acetylide-based polymers, poly-PtTh and poly-PtPh, that contain with 2,5-thienylene (Th) and 1,4-phenylene(Ph) units in the polymer backbone has been synthesized. A series of platinum model complexes (Pt_2, Pt_2T_1 and Pt_4) has also been prepared that features the same structure as a single polymer repeat unit. UV/vis, fluorescence, and phosphorescence spectra, fluorescence upconversion, and transient absorption spectra on the fs - ps time scale were collected. The ultrafast absorption spectra in solution and thin films have broad absorption bands from 450 to 700 nm and long wavelength contribution, which is shown in the flash photolysis measurements, from the intersystem crossing (ISC) ($S_1 \rightarrow T_1$) with a record ISC time of < 1.0 ps in poly-PtTh and poly-PtPh. We observe that the fast relaxation occurs from excited states to ground state, and dynamics of the ground state bleach is identical in solution and thin film which means that the solvent relaxation/ organization has no influence on the photophysical behavior in this polymer system.

APPENDIX
KINETIC TRACES OF POLYMERS

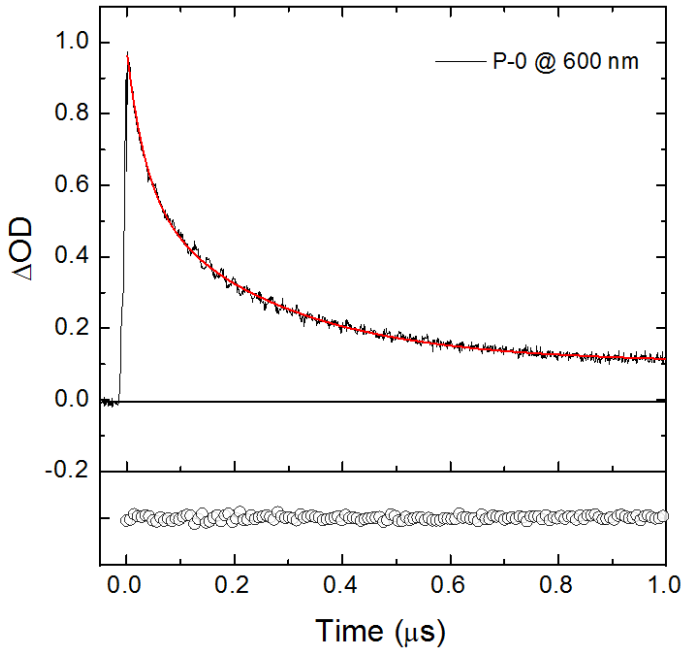

Figure A-1. Transient absorption kinetics decays of P-0 at 600 nm on a short-time scale (1 μs).

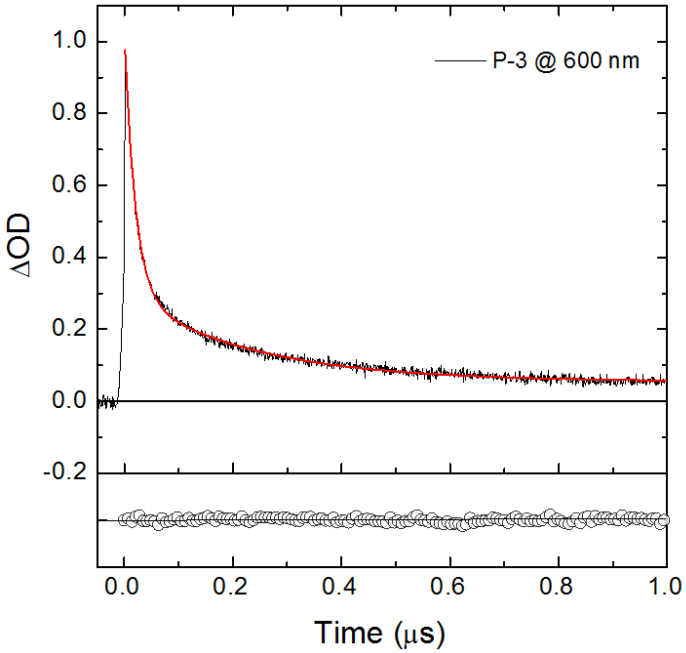

Figure A-2. Transient absorption kinetics decays of P-3 at 600 nm on a short-time scale (1 μs).

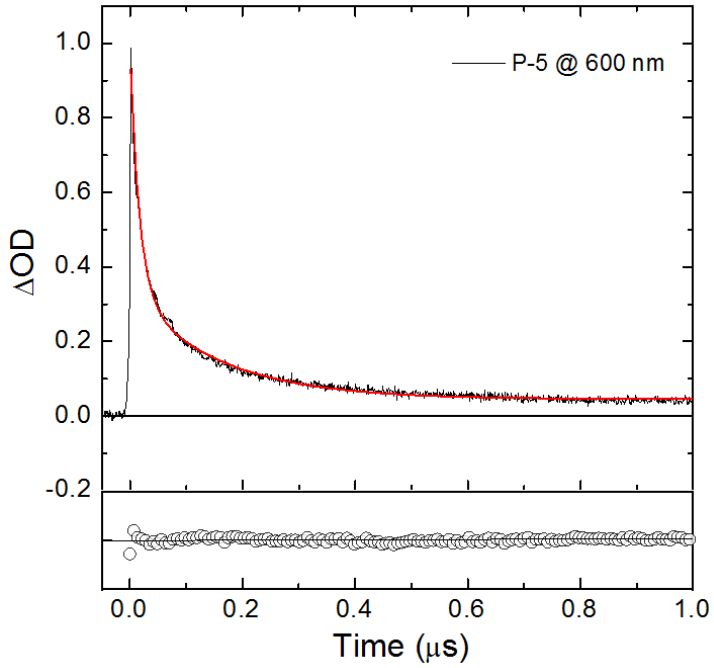

Figure A-3. Transient absorption kinetics decays of P-5 at 600 nm on a short-time scale (1 μs).

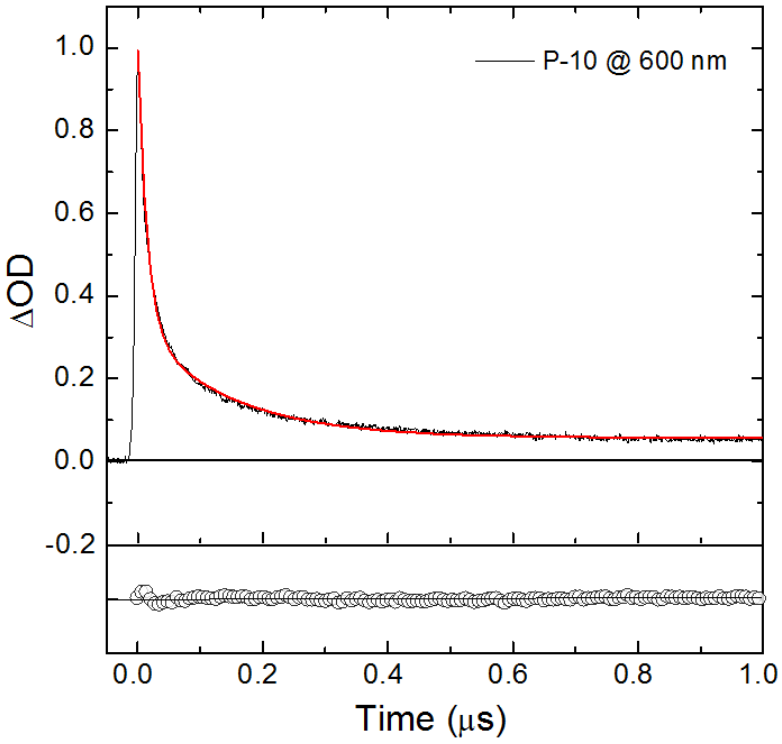

Figure A-4. Transient absorption kinetics decays of P-10 at 600 nm on a short-time scale (1 μs).

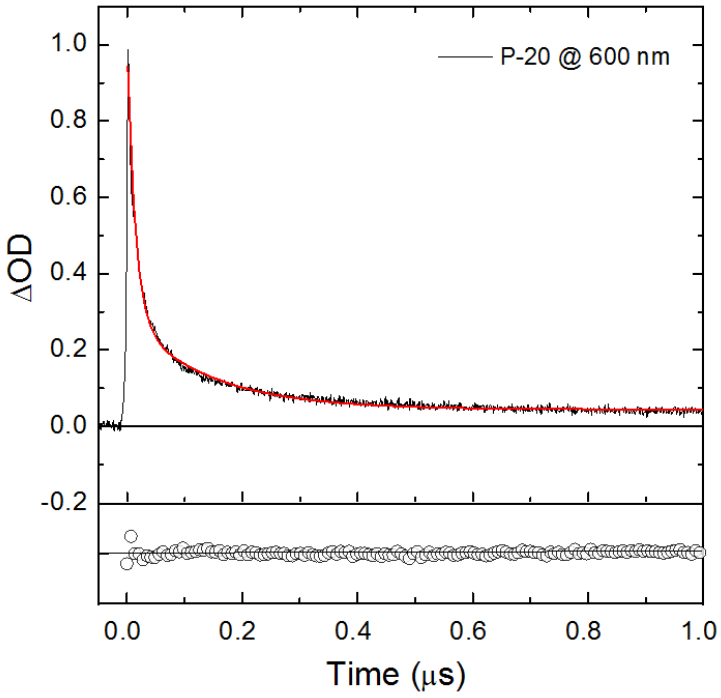

Figure A-5. Transient absorption kinetics decays of P-20 at 600 nm on a short-time scale (1 μs).

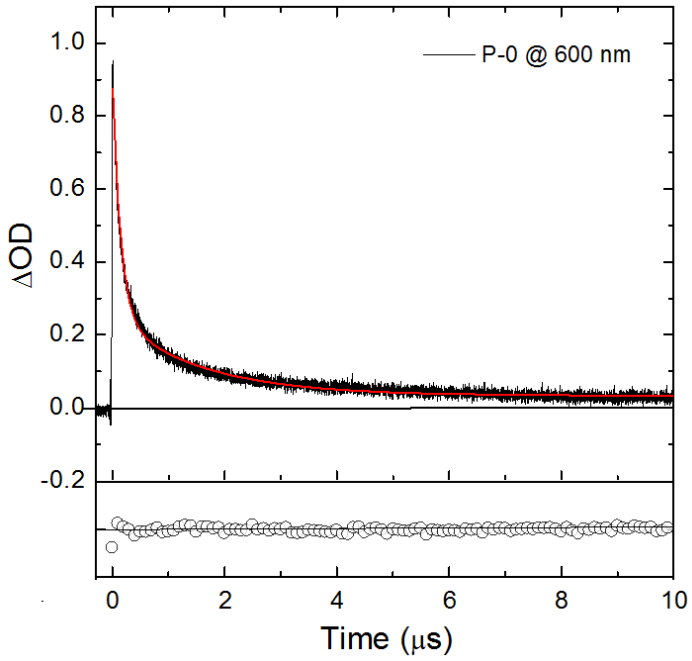

Figure A-6. Transient absorption kinetics decays of P-0 at 600 nm on a long-time scale (10 μs).

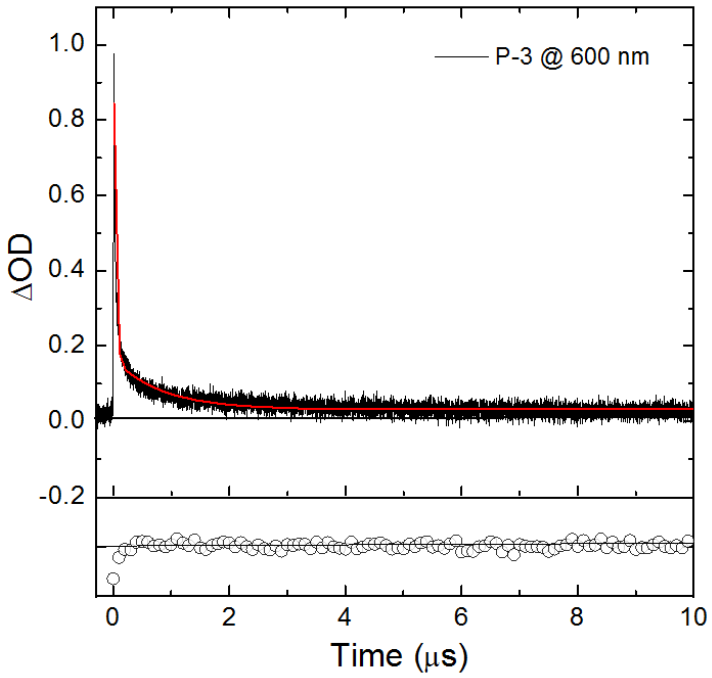

Figure A-7. Transient absorption kinetics decays of P-3 at 600 nm on a long-time scale (10 μs).

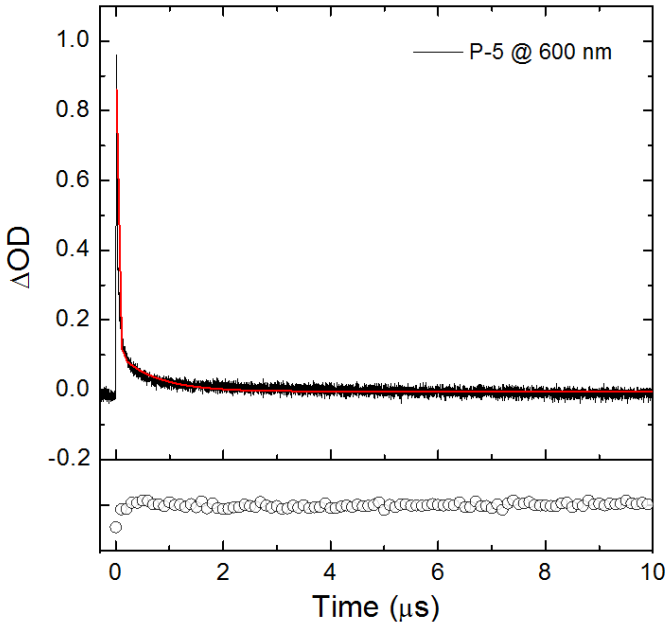

Figure A-8. Transient absorption kinetics decays of P-5 at 600 nm on a long-time scale (10 μs).

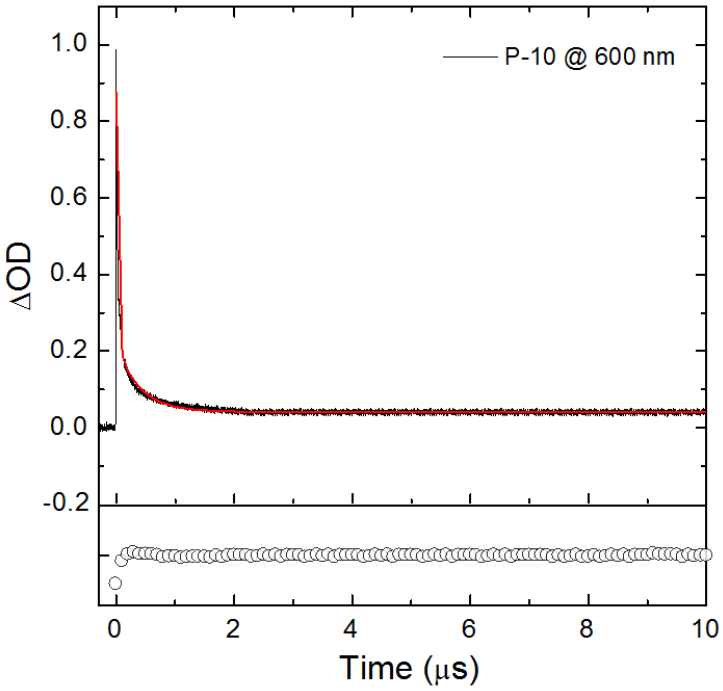

Figure A-9. Transient absorption kinetics decays of P-10 at 600 nm on a long-time scale (10 μs).

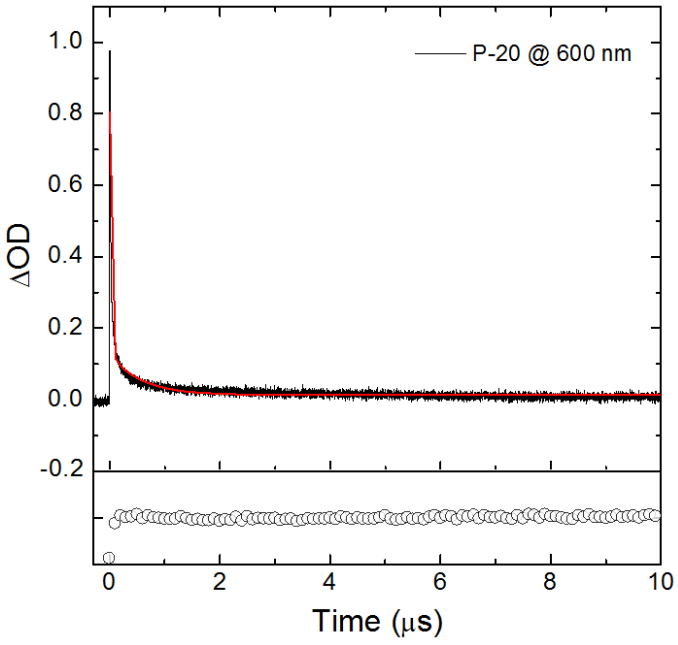

Figure A-10. Transient absorption kinetics decays of P-20 at 600 nm on a long-time scale (10 μs).

LIST OF REFERENCES

(1) Shirakawa, H.; Louis, E. J.; MacDiarmid, A. G.; Chiang, C. K.; Heeger, A. J. *Journal of the Chemical Society, Chemical Communications* **1977**, 578.

(2) Bunz, U. H. F. *Chemical Reviews* **2000**, *100*, 1605.

(3) Beljonne, D.; Wittmann, H.; Köhler, A.; Graham, S.; Younus, M.; Lewis, J.; Raithby, P.; Khan, M.; Friend, R.; Bredas, J. *The Journal of chemical physics* **1996**, *105*, 3868.

(4) Wilson, J.; Dhoot, A.; Seeley, A.; Khan, M.; Köhler, A.; Friend, R. *Nature* **2001**, *413*, 828.

(5) Staromlynska, J.; McKay, T.; Bolger, J.; Davy, J. *JOSA B* **1998**, *15*, 1731.

(6) Sonogashira, K.; Fujikura, Y.; Yatake, T.; Toyoshima, N.; Takahashi, S.; Hagihara, N. *Journal of Organometallic Chemistry* **1978**, *145*, 101.

(7) Silverman, E. E.; Cardolaccia, T.; Zhao, X. M.; Kim, K. Y.; Haskins-Glusac, K.; Schanze, K. S. *Coordin Chem Rev* **2005**, *249*, 1491.

(8) Mei, J.; Ogawa, K.; Kim, Y.-G.; Heston, N. C.; Arenas, D. J.; Nasrollahi, Z.; McCarley, T. D.; Tanner, D. B.; Reynolds, J. R.; Schanze, K. S. *ACS Applied Materials & Interfaces* **2009**, *1*, 150.

(9) Wittmann, H. F.; Friend, R. H.; Khan, M. S.; Lewis, J. *The Journal of Chemical Physics* **1994**, *101*, 2693.

(10) Guha, S.; Frazier, C. C.; Porter, P. L.; Kang, K.; Finberg, S. E. *Optics letters* **1989**, *14*, 952.

(11) Liu, L.; Poon, S.-Y.; Wong, W.-Y. *Journal of Organometallic Chemistry* **2005**, *690*, 5036.

(12) Khan, M. S.; Al-Mandhary, M. R. A.; Al-Suti, M. K.; Corcoran, T. C.; Al-Mahrooqi, Y.; Attfield, J. P.; Feeder, N.; David, W. I. F.; Shankland, K.; Friend, R. H.; Kohler, A.; Marseglia, E. A.; Tedesco, E.; Tang, C. C.; Raithby, P. R.; Collings, J. C.; Roscoe, K. P.; Batsanov, A. S.; Stimson, L. M.; Marder, T. B. *New J Chem* **2003**, *27*, 140.

(13) Khan, M. S.; Al-Mandhary, M. R. A.; Al-Suti, M. K.; Al-Battashi, F. R.; Al-Saadi, S.; Ahrens, B.; Bjernemose, J. K.; Mahon, M. F.; Raithby, P.

R.; Younus, M.; Chawdhury, N.; Kohler, A.; Marseglia, E. A.; Tedesco, E.; Feeder, N.; Teat, S. J. *Dalton Transactions* **2004**, 2377.

(14) Zhao, X.; Cardolaccia, T.; Farley, R. T.; Abboud, K. A.; Schanze, K. S. *Inorg Chem* **2005**, *44*, 2619.

(15) Wittmann, H.; Friend, R.; Khan, M.; Lewis, J. *The Journal of chemical physics* **1994**, *101*, 2693.

(16) Wittmann, H. F. *Ph.D. Thesis* **1993**, University of Cambridge.

(17) Fratoddi, I.; Gohlke, C.; Cametti, C.; Diociaiuti, M.; Russo, M. V. *Polymer* **2008**, *49*, 3211.

(18) Penza, M.; Cassano, G.; Sergi, A.; Lo Sterzo, C.; Russo, M. V. *Sensors and Actuators B: Chemical* **2001**, *81*, 88.

(19) Wong, W. Y.; Harvey, P. D. *Macromolecular rapid communications* **2010**, *31*, 671.

(20) Zhao, X. Y.; Pinto, M. R.; Hardison, L. M.; Mwaura, J.; Muller, J.; Jiang, H.; Witker, D.; Kleiman, V. D.; Reynolds, J. R.; Schanze, K. S. *Macromolecules* **2006**, *39*, 6355.

(21) Smith, K. C. *Stanford University School of Medicine* **Vol. 2013.** .

(22) Turro, N. J.; Ramamurthy, V.; Scaiano, J. C. *Principles of Molecular Photochemistry: An Introduction*; Univ Science Books, 2009.

(23) Praveen, V. K.; Ranjith, C.; Bandini, E.; Ajayaghosh, A.; Armaroli, N. *Chemical Society Reviews* **2014**.

(24) Misra, A.; Kumar, P.; Kamalasanan, M.; Chandra, S. *Semiconductor science and Technology* **2006**, *21*, R35.

(25) Marcus, R. A. *The Journal of Chemical Physics* **1956**, *24*, 966.

(26) Landau, L. D. *Phys. Z. SSR.* **1932**, *2*, 46.

(27) Miller, J. R.; Calcaterra, L. T.; Closs, G. L. *Journal of the American Chemical Society* **1984**, *106*, 3047.

(28) Peng, K.-Y.; Chen, S.-A.; Fann, W.-S. *Journal of the American Chemical Society* **2001**, *123*, 11388.

(29) Aly, S. M.; Ho, C. L.; Fortin, D.; Wong, W. Y.; Abd-El-Aziz, A. S.; Harvey, P. D. *Chem-Eur J* **2008**, *14*, 8341.

(30) Aly, S. M.; Ho, C.-L.; Wong, W.-Y.; Fortin, D.; Harvey, P. D. *Macromolecules* **2009**, *42*, 6902.

(31) Duncan, T. V.; Susumu, K.; Sinks, L. E.; Therien, M. J. *Journal of the American Chemical Society* **2006**, *128*, 9000.

(32) Sedghi, G.; Sawada, K.; Esdaile, L. J.; Hoffmann, M.; Anderson, H. L.; Bethell, D.; Haiss, W.; Higgins, S. J.; Nichols, R. J. *Journal of the American Chemical Society* **2008**, *130*, 8582.

(33) Meier, H. *Angewandte Chemie International Edition* **2009**, *48*, 3911.

(34) Jiang, B.; Yang, S.-W.; Jones, W. E. *Chem Mater* **1997**, *9*, 2031.

(35) Li, B.; Fu, Y.; Han, Y.; Bo, Z. *Macromolecular Rapid Communications* **2006**, *27*, 1355.

(36) Frapper, G.; Kertesz, M. *Inorg Chem* **1993**, *32*, 732.

(37) Jiang, F.-L.; Fortin, D.; Harvey, P. D. *Inorg Chem* **2010**, *49*, 2614.

(38) Liu, L.; Fortin, D.; Harvey, P. D. *Inorg Chem* **2009**, *48*, 5891.

(39) *Physical Chemistry*; Atkins, P. W., Ed.; W. H. Freeman and Co.: New York, 1940.

(40) Turro, N. J. *Modern Molecular Photochemistry*, University Science Books.

(41) Lakowicz, J. R. *Principles of Fluorescence Spectroscopy, Third edition* **2006**.

(42) Norrish, R.; Porter, G. *Nature* **1949**, *164*, 658.

(43) Swager, T. M. *Accounts of Chemical Research* **1998**, *31*, 201.

(44) Swager, T. M.; Gil, C. J.; Wrighton, M. S. *The Journal of Physical Chemistry* **1995**, *99*, 4886.

(45) Chen, L. X.; Jäger, W. J. H.; Niemczyk, M. P.; Wasielewski, M. R. *The Journal of Physical Chemistry A* **1999**, *103*, 4341.

(46) Harrison, B. S.; Ramey, M. B.; Reynolds, J. R.; Schanze, K. S. *Journal of the American Chemical Society* **2000**, *122*, 8561.

(47) Funston, A. M.; Silverman, E. E.; Miller, J. R.; Schanze, K. S. *J Phys Chem B* **2004**, *108*, 1544.

(48) Wang, J.; Wang, D.; Miller, E. K.; Moses, D.; Bazan, G. C.; Heeger, A. J. *Macromolecules* **2000**, *33*, 5153.

(49) Liu, Y.; Jiang, S.; Schanze, K. S. *Chem Commun* **2003**, 650.

(50) Tan, C.; Pinto, M. R.; Schanze, K. S. *Chem Commun* **2002**, 446.

(51) Martin, R. E.; Diederich, F. *Angewandte Chemie International Edition* **1999**, *38*, 1350.

(52) Haskins-Glusac, K.; Pinto, M. R.; Tan, C.; Schanze, K. S. *Journal of the American Chemical Society* **2004**, *126*, 14964.

(53) Kokil, A.; Shiyanovskaya, I.; Singer, K. D.; Weder, C. *Journal of the American Chemical Society* **2002**, *124*, 9978.

(54) Tour, J. M. *Chemical Reviews* **1996**, *96*, 537.

(55) Chawdhury, N.; Köhler, A.; Friend, R. H.; Wong, W.-Y.; Lewis, J.; Younus, M.; Raithby, P. R.; Corcoran, T. C.; Al-Mandhary, M. R. A.; Khan, M. S. *The Journal of Chemical Physics* **1999**, *110*, 4963.

(56) Mei, J.; Ogawa, K.; Kim, Y. G.; Heston, N. C.; Arenas, D. J.; Nasrollahi, Z.; McCarley, T. D.; Tanner, D. B.; Reynolds, J. R.; Schanze, K. S. *Acs Applied Materials & Interfaces* **2009**, *1*, 150.

(57) Wilson, J.; Köhler, A.; Friend, R.; Al-Suti, M.; Al-Mandhary, M.; Khan, M.; Raithby, P. *The Journal of Chemical Physics* **2000**, *113*, 7627.

(58) Schanze, K. S.; Silverman, E. E.; Zhao, X. *The Journal of Physical Chemistry B* **2005**, *109*, 18451.

(59) Liu, Y.; Jiang, S. J.; Glusac, K.; Powell, D. H.; Anderson, D. F.; Schanze, K. S. *Journal of the American Chemical Society* **2002**, *124*, 12412.

(60) Liu, Y.; Jiang, S.; Glusac, K.; Powell, D. H.; Anderson, D. F.; Schanze, K. S. *Journal of the American Chemical Society* **2002**, *124*, 12412.

(61) Uoyama, H.; Goushi, K.; Shizu, K.; Nomura, H.; Adachi, C. *Nature* **2012**, *492*, 234.

(62) Dias, F. B.; Bourdakos, K. N.; Jankus, V.; Moss, K. C.; Kamtekar, K. T.; Bhalla, V.; Santos, J.; Bryce, M. R.; Monkman, A. P. *Adv Mater* **2013**, *25*, 3707.

(63) Lapprand, A.; Khiri, N.; Fortin, D.; Jugé, S.; Harvey, P. D. *Inorg Chem* **2013**, *52*, 2361.

(64) Zimmerman, H. E.; Goldman, T. D.; Hirzel, T. K.; Schmidt, S. P. *The Journal of Organic Chemistry* **1980**, *45*, 3933.

(65) Evans, R. W. *Integrated forms of certain differential rate expressions in chemical kinetics* **1950**, *M. S. Thesis, University of Wisconsin*.

(66) Köhler, A.; Wilson, J.; Friend, R.; Al-Suti, M.; Khan, M.; Gerhard, A.; Bässler, H. *The Journal of chemical physics* **2002**, *116*, 9457.

(67) Kauffman, G. B. T., L. A. *Inorg. Syn.* **1963**, *7*, 9.

(68) Cardolaccia, T.; Funston, A. M.; Kose, M. E.; Keller, J. M.; Miller, J. R.; Schanze, K. S. *J Phys Chem B* **2007**, *111*, 10871.

(69) Xie, D. P.; Parthasarathy, A.; Schanze, K. S. *Langmuir* **2011**, *27*, 11732.

(70) Materials Research Society Symposium Proceedings: Materials for Optical Limiting;Materials Research Society: Pittsburgh, P. **1995**, Vol. 374.

(71) Friend, R.; Gymer, R.; Holmes, A.; Burroughes, J.; Marks, R.; Taliani, C.; Bradley, D.; Dos Santos, D.; Bredas, J.; Lögdlund, M. *Nature* **1999**, *397*, 121.

(72) Holmes, R. J.; Forrest, S. R.; Sajoto, T.; Tamayo, A.; Djurovich, P. I.; Thompson, M. E. *Organic Electronics* **2006**, *7*, 163.

(73) Kalinowski, J.; Stampor, W.; Mezyk, J.; Cocchi, M.; Virgili, D.; Fattori, V.; Di Marco, P. *Physical Review B* **2002**, *66*, 235321.

(74) Baldo, M. A.; Adachi, C.; Forrest, S. R. *Physical Review B* **2000**, *62*, 10967.

(75) Kalinowski, J.; Mezyk, J.; Meinardi, F.; Tubino, R.; Cocchi, M.; Virgili, D. *J Appl Phys* **2005**, *98*, 063532.

(76) Baldo, M.; Thompson, M.; Forrest, S. *Nature* **2000**, *403*, 750.

(77) Adachi, C.; Baldo, M. A.; Thompson, M. E.; Forrest, S. R. *J Appl Phys* **2001**, *90*, 5048.

(78) Ikai, M.; Tokito, S.; Sakamoto, Y.; Suzuki, T.; Taga, Y. *Appl Phys Lett* **2001**, *79*, 156.

(79) Lupton, J. M.; Pogantsch, A.; Piok, T.; List, E. J.; Patil, S.; Scherf, U. *Phys Rev Lett* **2002**, *89*, 167401.

(80) Arif, M.; Yang, K.; Li, L.; Yu, P.; Guha, S.; Gangopadhyay, S.; Förster, M.; Scherf, U. *Appl Phys Lett* **2009**, *94*, 063307.

(81) Luhman, W. A.; Holmes, R. J. *Appl Phys Lett* **2009**, *94*, 153304.

(82) Ghosh, A. K.; Feng, T. *J Appl Phys* **1978**, *49*, 5982.

(83) Banerjee, S.; Parhi, A. P.; Iyer, S. S. K.; Kumar, S. *Appl Phys Lett* **2009**, *94*, 223303.

(84) Gommans, H.; Schols, S.; Kadashchuk, A.; Heremans, P.; Meskers, S. C. J. *The Journal of Physical Chemistry C* **2009**, *113*, 2974.

(85) Kalinowski, J.; Szybowska, K. *Organic Electronics* **2008**, *9*, 1032.

(86) Lunt, R. R.; Giebink, N. C.; Belak, A. A.; Benziger, J. B.; Forrest, S. R. *J Appl Phys* **2009**, *105*, 053711.

(87) Scully, S. R.; McGehee, M. D. *J Appl Phys* **2006**, *100*, 034907.

(88) Holzhey, A.; Uhrich, C.; Brier, E.; Reinhold, E.; Bäuerle, P.; Leo, K.; Hoffmann, M. *J Appl Phys* **2008**, *104*, 064510.

(89) Kalinowski, J.; Fattori, V.; Di Marco, P. *Chem Phys* **2001**, *266*, 85.

(90) Mikhnenko, O. V.; Azimi, H.; Scharber, M.; Morana, M.; Blom, P. W. M.; Loi, M. A. *Energy & Environmental Science* **2012**, *5*, 6960.

(91) Tamai, Y.; Matsuura, Y.; Ohkita, H.; Benten, H.; Ito, S. *The Journal of Physical Chemistry Letters* **2014**, 399.

(92) Wilson, J. S.; Chawdhury, N.; Al-Mandhary, M. R. A.; Younus, M.; Khan, M. S.; Raithby, P. R.; Köhler, A.; Friend, R. H. *Journal of the American Chemical Society* **2001**, *123*, 9412.

(93) Zhong, H.; Yang, X.; deWith, B.; Loos, J. *Macromolecules* **2006**, *39*, 218.

(94) Bull, T. A.; Pingree, L. S. C.; Jenekhe, S. A.; Ginger, D. S.; Luscombe, C. K. *ACS Nano* **2009**, *3*, 627.

(95) Nilsson, S.; Bernasik, A.; Budkowski, A.; Moons, E. *Macromolecules* **2007**, *40*, 8291.

(96) Malone, W. M.; Albert, R. *Journal of Applied Polymer Science* **1973**, *17*, 2457.

(97) Quayle, O. R. *Chemical Reviews* **1953**, *53*, 439.

(98) Edward, J. T. *Chem. Ind. (London)* **1956**, *52*, 774.

(99) Durchschlag, H. Z., P. *Prog. Colloid Polym. Sci.* **1994**, *94*, 20.

(100) Lu, H. M. W., Z.; Jiang, Q. *Colloids. Surf., A: Physiochem. Eng. Aspects* **2006**, *278*, 160.

(101) Ishikawa, T. P., P. F.; Koike, N. *Jpn. J. Appl. Phys., Part 1* **2006**, *45*, 1719.

(102) Clements, J. H. W., S. E. *J. Phys. Chem. A* **1999**, *103*, 2513.

(103) Benson, S. W. *The Foundations of Chemical Kinetics*, McGraw.

(104) Mikhnenko, O. V. C., F.; Sieval, A. B.; Hummelen, J. C.; Blom, P. W. M.; Loi, M. A. *J. Phys. Chem. B* **2008**, *112*, 11601.

(105) Theander, M.; Yartsev, A.; Zigmantas, D.; Sundström, V.; Mammo, W.; Andersson, M. R.; Inganäs, O. *Physical Review B* **2000**, *61*, 12957.

(106) Gulbinas, V.; Minevičiūtė, I.; Hertel, D.; Wellander, R.; Yartsev, A.; Sundström, V. *The Journal of Chemical Physics* **2007**, *127*, 144907.

(107) Huijser, A.; Savenije, T. J.; Meskers, S. C. J.; Vermeulen, M. J. W.; Siebbeles, L. D. A. *J. Am. Chem. Soc.* **2008**, *130*, 12496.

(108) Sokolik, I.; Walser, A. D.; Priestley, R.; Tang, C. W.; Dorsinville, R. *Synth. Met.* **1997**, *84*, 921.

(109) Baldo, M. A.; Forrest, S. R. *Phys. Rev. B.* **2000**, *62*, 10958.

(110) Tsuchida, A.; Yamamoto, M.; Liebe, W. R.; Burkhart, R. D.; Tsubakiyama, K. *Macromolecules* **1996**, *29*, 1589.

(111) Kroeze, J. E.; Savenije, T. J.; Candeias, L. P.; Warman, J. M.; Siebbeles, L. D. *Solar energy materials and solar cells* **2005**, *85*, 189.

(112) Giebink, N. C.; Sun, Y.; Forrest, S. R. *Organic Electronics* **2006**, *7*, 375.

(113) Black, M. R.; Chavez, C.; Brosha, E. *Org. Electron.* **2007**, *8*, 601.

(114) Bulovic, V.; Forrest, S. R. *Chem. Phys.* **1996**, *210*, 13.

(115) Namdas, E. B.; Ruseckas, A.; Samuel, I. D. W.; Lo, S.-C.; Burn, P. L. *Appl Phys Lett* **2005**, *86*, 091104.

(116) Marcus, R. A.; Sutin, N. *Biochimica et Biophysica Acta (BBA)-Reviews on Bioenergetics* **1985**, *811*, 265.

(117) Closs, G. L.; Johnson, M. D.; Miller, J. R.; Piotrowiak, P. *Journal of the American Chemical Society* **1989**, *111*, 3751.

(118) M. Klessinger and J. Michl *Excited States and Photochemistry of Organic Molecules*, VCH.

(119) Devi, L. S.; Al-Suti, M. K.; Dosche, C.; Khan, M. S.; Friend, R. H.; Köhler, A. *Physical Review B* **2008**, *78*, 045210.

(120) Marcus, R. A. *Reviews of Modern Physics* **1993**, *65*, 599.

(121) Brédas, J.-L.; Beljonne, D.; Coropceanu, V.; Cornil, J. *Chemical Reviews* **2004**, *104*, 4971.

(122) Mwaura, J. K.; Pinto, M. R.; Witker, D.; Ananthakrishnan, N.; Schanze, K. S.; Jr, R. *Langmuir* **2005**, *21*, 10119.

(123) Mwaura, J. K.; Pinto, M. R.; Witker, D.; Ananthakrishnan, N.; Schanze, K. S.; Reynolds, J. R. *Langmuir* **2005**, *21*, 10119.

(124) Anslyn, E. V.; Dougherty, D. A. *Modern Physical Organic Chemistry*; University Science Books, 2006.

(125) Corbitt, T. S.; Ding, L.; Ji, E.; Ista, L. K.; Ogawa, K.; Lopez, G. P.; Schanze, K. S.; Whitten, D. G. *Photochem. Photobiol. Sci.* **2009**, *8*, 998.

(126) Xing, C.; Xu, Q.; Tang, H.; Liu, L.; Wang, S. *J. Am. Chem. Soc.* **2009**, *131*, 13117.

(127) Poulsen, D. A.; Kim, B. J.; Ma, B.; Zonte, C. S.; Fréchet, J. M. J. *Adv. Mater.* **2010**, *22*, 77.

(128) Furuta, P. T.; Deng, L.; Garon, S.; Thompson, M. E.; Fréchet, J. M. J. *J. Am. Chem. Soc.* **2004**, *126*, 15388.

(129) Pomestchenko, I. E.; Luman, C. R.; Hissler, M.; Ziessel, R.; Castellano, F. N. *Inorg. Chem.* **2003**, *42*, 1394.

(130) Danilov, E. O.; Pomestchenko, I. E.; Kinayyigit, S.; Gentili, P. L.; Hissler, M.; Ziessel, R.; Castellano, F. N. *J. Phys. Chem. A* **2005**, *109*, 2465.

(131) Nastasi, F.; Puntoriero, F.; Campagna, S.; Diring, S.; Ziessel, R. *Phys. Chem. Chem. Phys.* **2008**, *10*, 3982.

(132) Nastasi, F.; Puntoriero, F.; Campagna, S.; Olivier, J.-H.; Ziessel, R. *Phys. Chem. Chem. Phys.* **2010**, *12*, 7392.

(133) Ziessel, R.; Seneclauze, J. B.; Ventura, B.; Barbieri, A.; Barigelletti, F. *Dalton Trans.* **2008**, 1686.

(134) Ventura, B.; Barbieri, A.; Barigelletti, F.; Batcha Seneclauze, J.; Retailleau, P.; Ziessel, R. *Inorg. Chem.* **2008**, *47*, 7048.

(135) Jensen, K. K.; van Berlekom, S. B.; Kajanus, J.; Mårtensson, J.; Albinsson, B. *The Journal of Physical Chemistry A* **1997**, *101*, 2218.

(136) McConnell, H. M. *The Journal of Chemical Physics* **1961**, *35*, 508.

(137) Wenger, O. S. *CHIMIA International Journal for Chemistry* **2007**, *61*, 823.

(138) Barigelletti, F.; Flamigni, L. *Chem. Soc. Rev.* **2000**, *29*, 1.

(139) Barbieri, A.; Ventura, B.; Ziessel, R. *Coord. Chem. Rev.* **2012**, *256*, 1732.

(140) Li, Y.; Köse, M. E.; Schanze, K. S. *J. Phys. Chem. B* **2013**, *117*, 9025.

(141) Keller, J. M.; Glusac, K. D.; Danilov, E. O.; McIlroy, S.; Sreearuothai, P.; R. Cook, A.; Jiang, H.; Miller, J. R.; Schanze, K. S. *Journal of the American Chemical Society* **2011**, *133*, 11289.

(142) Silverman, E. E.; Cardolaccia, T.; Zhao, X.; Kim, K.-Y.; Haskins-Glusac, K.; Schanze, K. S. *Coord. Chem. Rev.* **2005**, *249*, 1491.

(143) Slagle, J. E.; Cooper, T. M.; Krein, D. M.; Rogers, J. E.; McLean, D. G.; Urbas, A. M. *Chem. Phys. Lett.* **2007**, *447*, 65.

(144) Fleming, C. N.; Dupray, L. M.; Papanikolas, J. M.; Meyer, T. J. *The Journal of Physical Chemistry A* **2002**, *106*, 2328.

(145) Rogers, J. E.; Cooper, T. M.; Fleitz, P. A.; Glass, D. J.; McLean, D. G. *The Journal of Physical Chemistry A* **2002**, *106*, 10108.

(146) Wang, Y.; Schanze, K. S. *Chem. Phys.* **1993**, *176*, 305.

(147) Kraft, A.; Grimsdale, A. C.; Holmes, A. B. *Angew. Chem. Int. End Engl* **1998**, *37*, 402.

(148) Veinot, J. G. C.; Marks, T. J. *Accounts of Chemical Research* **2005**, *38*, 632.

(149) Winder, C.; Sariciftci, N. S. *Journal of Materials Chemistry* **2004**, *14*, 1077.

(150) Coakley, K. M.; McGehee, M. D. *Chem Mater* **2004**, *16*, 4533.

(151) Günes, S.; Neugebauer, H.; Sariciftci, N. S. *Chemical Reviews* **2007**, *107*, 1324.

(152) Dodabalapur, A.; Torsi, L.; Katz, H. E. *Science* **1995**, *268*, 270.

(153) Horowitz, G.; Deloffre, F.; Garnier, F.; Hajlaoui, R.; Hmyene, M.; Yassar, A. *Synthetic Met* **1993**, *54*, 435.

(154) Lamansky, S.; Djurovich, P.; Murphy, D.; Abdel-Razzaq, F.; Lee, H.-E.; Adachi, C.; Burrows, P. E.; Forrest, S. R.; Thompson, M. E. *Journal of the American Chemical Society* **2001**, *123*, 4304.

(155) Wong, W.-Y.; Ho, C.-L. *Coordin Chem Rev* **2006**, *250*, 2627.

(156) Haskins-Glusac, K.; Ghiviriga, I.; Abboud, K. A.; Schanze, K. S. *J Phys Chem B* **2004**, *108*, 4969.

(157) Glusac, K.; Kose, M. E.; Jiang, H.; Schanze, K. S. *J Phys Chem B* **2007**, *111*, 929.

(158) Wasserberg, D.; Dudek, S. P.; Meskers, S. C. J.; Janssen, R. A. J. *Chem Phys Lett* **2005**, *411*, 273.

(159) Ramakrishna, G.; Goodson, T.; Rogers-Haley, J. E.; Cooper, T. M.; McLean, D. G.; Urbas, A. *The Journal of Physical Chemistry C* **2008**, *113*, 1060.

BIOGRAPHICAL SKETCH

Hsien-Yi Hsu grew up in Hsinchu, Taiwan. In July of 2002, he graduated from National Chung Hsing University with a B.S. in chemistry. He then attended the National Taiwan University for graduate school, where he got his Master of Science degree in 2004. While at the National Taiwan University, he worked with Professor Tong-Ing Ho studying electrogenerated chemiluminescence (ECL) for the Intramolecular charge transfer of polycyclic aromatic compound system. During this time, his interest in physical chemistry began to develop. Opting to attend the doctoral program at University of Florida, Hsien-Yi decided to obtain his Ph.D. in chemistry with Professor Kirk S. Schanze and eventually concentrated on photophysical chemistry.